FINAL REPORT

THE EFFECTS OF HIGH INTENSITY ELECTRICAL CURRENTS ON ADVANCED COMPOSITE MATERIALS

N00019-71-C-0063

21 MARCH 1972

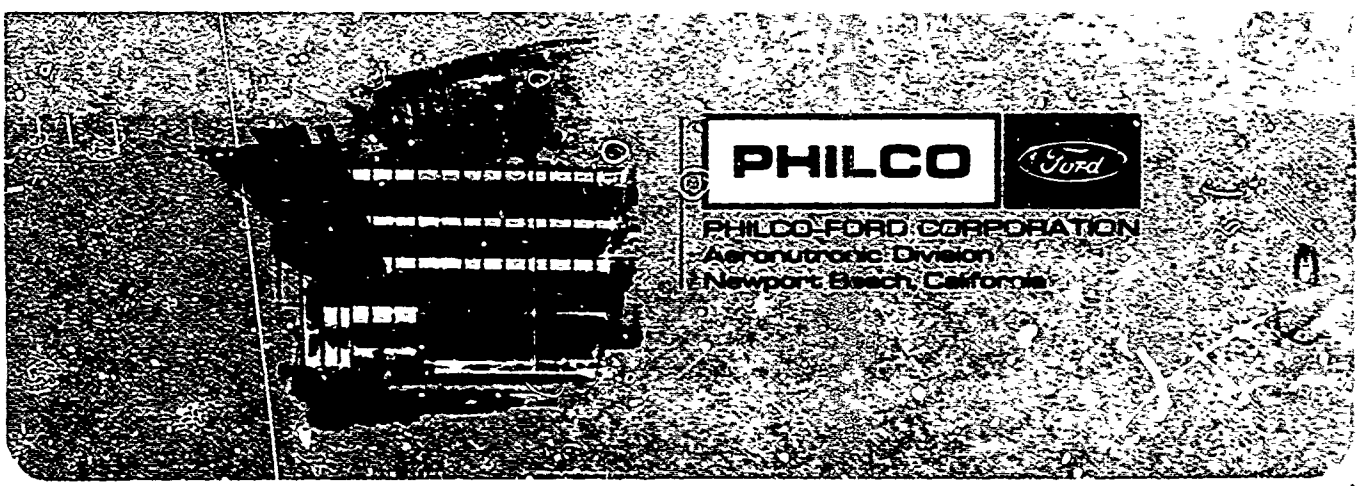

REPORT NO. U-5018

THE EFFECTS OF HIGH INTENSITY ELECTRICAL CURRENTS ON ADVANCED COMPOSITE MATERIALS

FINAL REPORT

21 March 1972

by

A. P. Penton and J. L. Perry of Philco-Ford Corporation

K. J. Lloyd of General Electric Company

Prepared Under Contract
N00019-71-C-0063

for

Naval Air Systems Command
Department of the Navy

PHILCO-FORD CORPORATION
Aeronutronic Division
Newport Beach, Calif. • 92663

CONTENTS

ILLUSTRATIONS

ILLUSTRATIONS (Continued)

ILLUSTRATIONS (Continued)

ILLUSTRATIONS (Continued)

(Appendix Illustrations)

TABLES

(APPENDIX TABLES)

TABLES (Continued)

ACKNOWLEDGEMENTS

This program was performed under the sponsorship of the Naval Air Systems Command, Contract N00019-71-C-0063, with J. W. Willis as the project engineer. The authors also wish to acknowledge the valuable participation of Mr. T. M. Place of Philco-Ford and Mr. J. A. Plumer of the General Electric Company.

SECTION 1

SUMMARY

The objective of this program was to perform a research study to investigate high intensity electric current flow of such magnitude and waveform as might result from lightning strikes, and to characterize the resulting degradation in advanced composites and to investigate means of providing internal protection from such damage. The work being performed closely parallels that work conducted in the N00019-70-C-0073 program and is an extension and continuation of the effort accomplished therein.[1] The approach followed in the program essentially involved the selection of representative high modulus boron and graphite filaments and composites and the exposure of those filaments and composites to precisely controlled electrical current flow. Necessary electrical, physical, chemical, microstructure, and mechanical analyses and tests were performed to permit modeling of electrical current flow processes and damage mechanisms. The laboratory analyses and tests performed included photomicrographic analysis, electron microprobe, scanning electron microscope, X-ray diffraction, tensile tests, and physical property measurements. The electrical properties measured included resistivity, dielectric strength, and impedance.

In the performance of this program specimen fabrication, physical testing, mechanical testing, specimen inspection and degradation mechanism analyses were performed by Philco-Ford Corporation. Current injection tests, electrical property measurements and current flow process analyses were performed by the General Electric Company High Voltage Laboratory.

In this program, boron and graphite filaments and epoxy resin composites were studied. The boron filaments were of the 0.004 in. diameter high modulus variety that are manufactured by the chemical vapor deposition of boron onto a substrate wire. Such filaments typically have a 55×10^6 psi

modulus of elasticity. High modulus graphite filaments were included, such as are manufactured from polyacrylonitrile precursor fiber.

In this program, the types of high intensity electric current investigated for their effect on advanced boron and graphite filaments and composites are such as might result from lightning strikes to the surface of an aircraft. The program did not include studies of the highly severe type damage that might result at the point of lightning stroke attachment. Instead, the program studied the effects of and current flow processes involved when the electric current from such a strike disperses throughout surrounding structures of advanced boron or graphite filament reinforced plastic composites, such as are planned for use in advanced Navy aircraft.

The work in this current program was divided into nine tasks, as listed below:

Task I - Evaluation of Carbon Core Boron Filaments

Task II - Energy Relationship Studies of Boron and Graphite Composites

Task III - Visual Observations of Damage Mechanisms

Task IV - Investigations into Variations in Boron Filament Electrical Conductivity

Task V - Variations in Graphite Filament Chemistry and Crystallite Structure as Related to Electrical Conductivity

Task VI - Damage Thresholds of Additional Types of Graphite Filament Composites

Task VII - Acoustic Emission as an Indicator of Electrical Current Produced Degradation

Task VIII - Investigation of Degradation Limiting Techniques

Task IX - Electrical Current Flow Paths in Multi-oriented Boron and Graphite Filament Composites

SECTION 2

INVESTIGATION OF CURRENT FLOW PROCESSES, DAMAGE MECHANISMS AND INTERNAL PROTECTION TECHNIQUES

The overall objective of this program was to continue the research into the effects of high intensity electric current on advanced filament reinforced plastic composites as initiated in the N00019-70-C-0073 program. Specifically, the work was to be directed toward those current high strength and modulus filament types that have been developed for use in structural composites for advanced aircraft. Also, the electric currents to be used in the study were to be representative of those that might occur as the result of a lightning strike to the surface of an aircraft. Following this overall approach, the program was oriented to study the processes involved in electric flow through filaments and composites and in the determination of the mechanisms of any damage resulting from the current flow. In addition, the approach includes investigations of approaches to prevention or minimization of damage due to high intensity electric current flow. The work during the past 12 months of program activity was divided into several tasks, discussed as follows:

2.1 TASK I - EVALUATION OF CARBON CORE BORON FILAMENTS

During the previous program[1] it was discovered and reported that the degradation of boron filaments is due to thermal stresses resulting from the electric current flow through the center core of the filaments. Standard 0.004 in. diameter boron filaments are manufactured by the chemical vapor deposition of boron onto 0.0005 in. diameter tungsten wire. In the process the tungsten wire is converted to tungsten boride, which has a much higher electrical conductivity than does the outer shell of boron. As a result, the electric current flows through the tungsten boride core. In the process electric energy is resistively converted to heat. At

threshold current intensities the energy that is dissipated within the core results in a thermal expansion to a degree that stresses the outer boron shell to failure. At this threshold the boron filament is severely cracked and loses its structural integrity.

Work is proceeding to develop boron filaments in which the boron is vapor deposited on a substrate wire other than tungsten. For instance, the use of carbon monofilaments for this purpose offers promise to reduce boron filament cost. It was then decided that this task would be directed to a determination of whether the carbon substrate core boron filament process would produce filaments that were more or less susceptible to degradation due to high intensity electric current flow.

The Air Force Materials Laboratory is sponsoring the development of boron filaments in which the boron is chemically vapor deposited onto a substrate carbon core filament of 0.002 in. diameter instead of the conventional tungsten wire substrate of 0.0005 in. diameter. A small quantity of these filaments was obtained through the Air Force Materials Laboratory, Wright-Patterson AFB, Ohio. Longitudinal and cross section photomicrographic views of the boron-carbon core filaments are presented in Figure 1. The most striking difference between the carbon core filament and the tungsten core filament (other than core diameter) is the relatively smooth external surface of the boron-carbon core filament and the relative absence of linked boron "cone growth" which is seen on the boron-tungsten core filament external surface.[1]

The manufacturer's data for the boron-carbon core filaments list a resistivity of 28.1×10^{-3} ohm-cm. This compares favorably to the 22×10^{-3} ohm-cm average resistivity data obtained for the boron-carbon core filaments on this program. The dynamic resistivity of boron-carbon core filaments at two current injection levels (3.71 and 8.04×10^{4} amps/cm^2) is plotted in Figure 2.

The results of the current injection tests are listed in the Appendix Table I. Filament specimens were exposed to injection current intensity levels from 3.7×10^4 to 16.0×10^4 amps/cm^2 of filament cross-sectional area with a waveform front time of 3μ sec. and tail time of 24μ sec. Resistance measurements were made before and after current injection. Tensile strengths of the exposed specimens were determined, but the results were too erratic and inconclusive due to the apparent tensile strength variation between individual specimens and the minimal number of specimens available for testing.

Scanning electron microscope (SEM) pictures were made of the boron-carbon core filaments which were exposed to the various injection current levels. The SEM pictures revealed that the same type of degradation (cracking) exists with the boron-carbon core filament type as was previously determined[1]

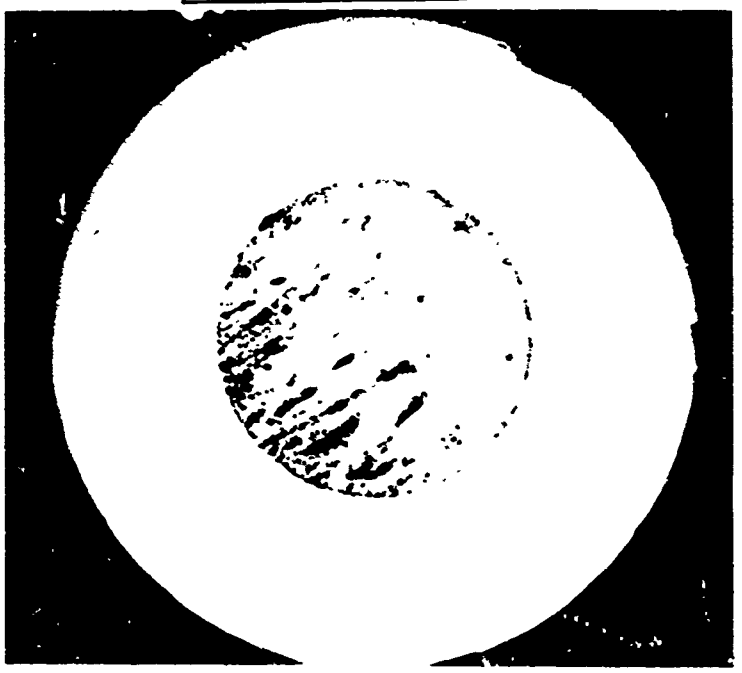

FIGURE 1A. BORON-CARBON CORE FILAMENT CROSS-SECTIONAL VIEW (800X) OF UNEXPOSED SPECIMEN

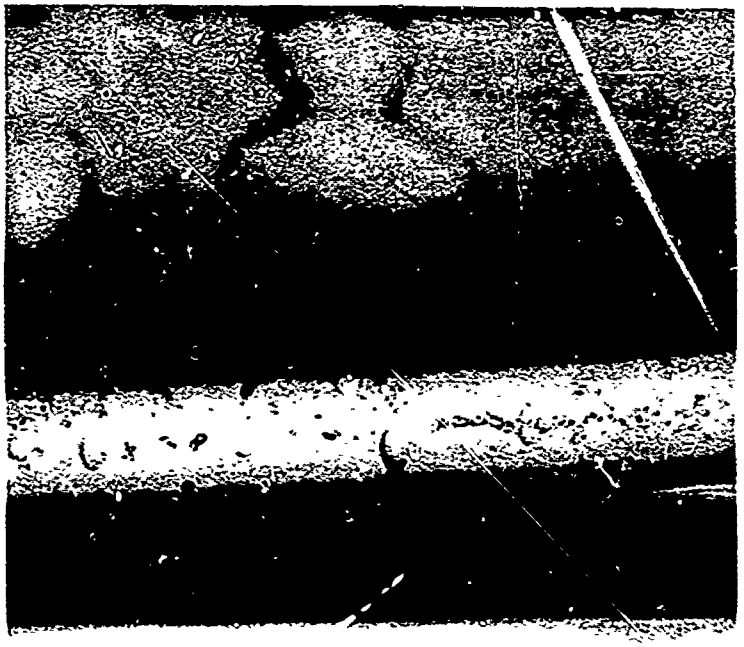

FIGURE 1B. BORON-CARBON CORE FILAMENT LONGITUDINAL VIEW (400X) OF UNEXPOSED SPECIMEN

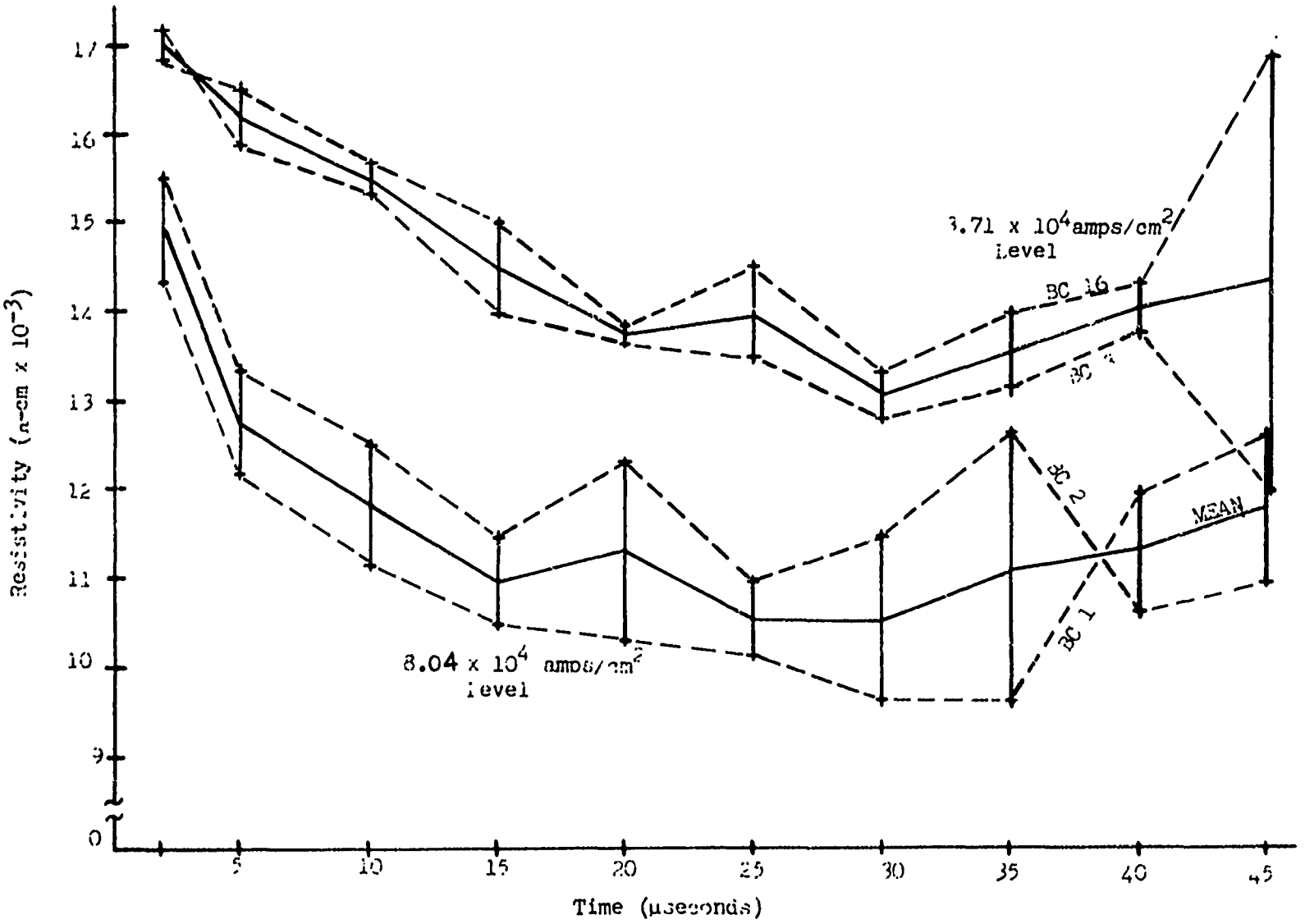

FIGURE 2. DYNAMIC RESISTIVITY - BORON-CARBON CORE FILAMENTS (BC)
3 x 24 μs INJECTED CURRENT WAVEFORM

Curves based on: Area of Specimen: $A = 80.7 \times 10^{-6}$cm^2
Area to length ratio: $A/l = 4.4 \times 10^{-6}$cm

for the boron-tungsten core filament type. This is typically illustrated in Figure 3 for Specimen BC-3 in both a longitudinal and cross-sectional view. From the SEM and visual observations, it appears that the degradation level of the boron-carbon core filaments compares to that of the boron-tungsten core filaments as reported in the previous program.[1]

With either the tungsten or the carbon core, the majority of the current is carried by the core because of the very low conductivity of the boron.[1] It appears, from results to date, that the boron filaments fail when the core is unable to dissipate the electrical energy injected. On this basis let us compare two cores of equal length.

Based on the manufacturer's data, the diameter of the carbon core (D_c) is seen to be four times larger than the diameter of the tungsten core (D_t). For example,

$$D_c = 4D_t$$

and therefore a 16:1 difference in areas is seen:

$$A_c = 16\,A_t\ .$$

For equal lengths of filament, resistance measurements give

$$\frac{R_c}{R_t} = \frac{4550}{2770} \approx 2\ .$$

Since $\rho = R\frac{A}{\ell}$, then for equal lengths:

$$\frac{\rho_c}{\rho_t} = \frac{R_c A_c}{R_t A_t} = \frac{(2R_t)(16A_t)}{R_t A_t}$$

or

$$\rho_c = 32\rho_t$$

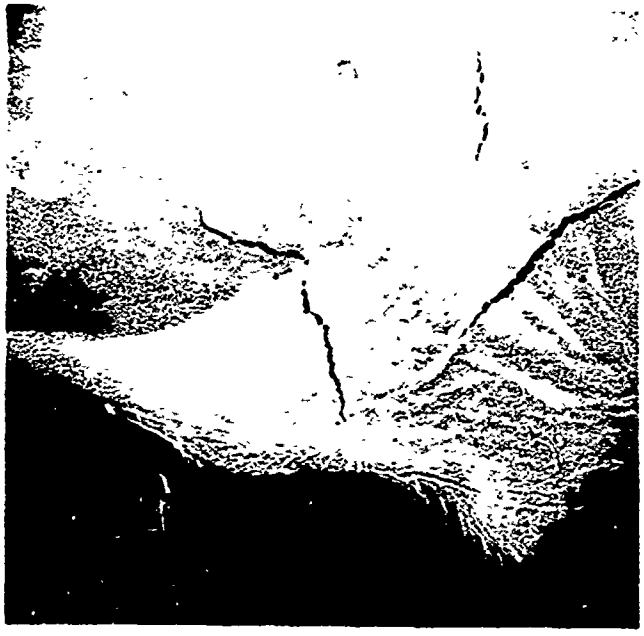

FIGURE 3A. BORON-CARBON CORE FILAMENT-SEM CROSS-SECTIONAL VIEW (600X) OF SPECIMEN BC-3 EXPOSED TO 3.7×10^4 AMPS/CM^2 INJECTION

FIGURE 3B. BORON-CARBON CORE FILAMENT-SEM LONGITUDINAL VIEW (200X) OF SPECIMEN BC-3 EXPOSED TO 3.7×10^4 AMPS/CM^2 CURRENT INJECTION

Now, looking at the energy dissipated:

$En = \int i(t)Rdt$ for both materials.

Assuming identical current waveforms are injected, one obtains after integration of both sides:

$$KI_c^2 \rho_c \frac{1}{A_c} = KI_t^2 \rho_t \frac{1}{A_t}$$

$$I_c^2 (32\rho_t) \frac{1}{16} A_t = I_t^2 \rho_t \left(\frac{1}{A_t}\right)$$

$$I_c^2 = \frac{I_t^2}{2}$$

$$I_c = 0.7 I_t$$

This result shows that one might expect the carbon core to fail at 70% of that current at which the tungsten fails (based on energy dissipation alone) and that degradation (cracking of the core) at a value of 3.7×10^4 amps/cm^2 for boron-carbon core filaments can realistically be expected. Since failure of both carbon and tungsten core filaments is apparent at approximately this current intensity level, the above calculation of $I_c = 0.7 I_t$ is apparently within the uncertainty of the calculation.

2.2 TASK II - ENERGY RELATIONSHIP STUDIES OF BORON AND GRAPHITE COMPOSITES

During the previous N00019-70-C-0073 program,[1] it was determined that degradation levels in boron epoxy composites could be correlated to the resistive energy dissipation of electric current flow in such composites. During that program, however, only a few typical waveforms of current injection were utilized. As a continuation of that effort this task was initiated to

(1) Determine if a correlation also exists between energy dissipation and degradation level for graphite epoxy composites.

(2) Determine if the correlations persist when wide variations of waveforms [front time (t_f) and tail time (t_t)] are utilized and in addition investigate the effect of low amplitude continuing currents such as occur between the peaks of multiple stroke lightning strikes.

Unidirectional tensile specimens (0.025 in. thickness x 0.10 in. width x 7 in. length) were fabricated of HMG-50 graphite with DEN 438-MNA epoxy and of 3M's SP-272 boron epoxy tape with typical alternating plies of 104 glass scrim cloth. Each end of the inidividual specimens was scarfed, vapor honed and nickel plated for electrical contact. Specimen fabrication to produce composites with 50-55% fiber volume was as in the previous program.[1]

Tensile specimens of boron epoxy and HMG-50 graphite epoxy were exposed to current crest level variables and waveform variables as listed in Appendix Tables II and III. Four variations in waveform were investigated: t_f and t_t of 1 x 10, 3 x 10, 3 x 24, and 3 x 50 microseconds. Variations in the current intensity injected based on the total cross-sectional area of the filaments in each specimen in amps/cm^2 were in the range of 5 to 60 x 10^4 for boron composites and 10 to 33 x 10^4 for the graphite composites. Tensile strengths of control undamaged specimens and of electrically exposed specimens are recorded in the aforementioned tables.

The loss in tensile strength of the exposed specimens, expressed as tensile strength degradation in % as compared to an undamaged control specimen, is presented in Appendix Table VII and includes a column of visual observations reflecting any change in the specimen after electrical exposure.

The relation of the percent tensile strength degradation for three waveforms at various current crest levels is graphically presented in Figure 4 for both the boron-epoxy and graphite-epoxy composites. It appears that one relationship holds true for both the boron and graphite composites, i.e., damage in both composites is directly related to the total energy deposition.

It became apparent during this program that the results from the prior program[1] appear somewhat lower in value. The damage threshold for boron-epoxy, under the prior program, was 3.7-5.7 x 10^4 amps/cm^2 of filament cross-sectional area for a 3 x 24 (t_f x t_t) microsecond waveform. In this program the damage threshold appears somewhat higher, as high as 8-10 x 10^4 amps/cm^2 for the 3 x 24 microsecond waveform.

A comparison of boron specimen resistivities of the present and prior programs show

$$\frac{\text{resistivities of prior program}^1}{\text{resistivities of present program}} = \frac{\rho 1^*}{\rho 2} \approx 1.7$$

*Note that in this discussion the subscript (1) refers to the prior program, while the subscript (2) refers to the present program.

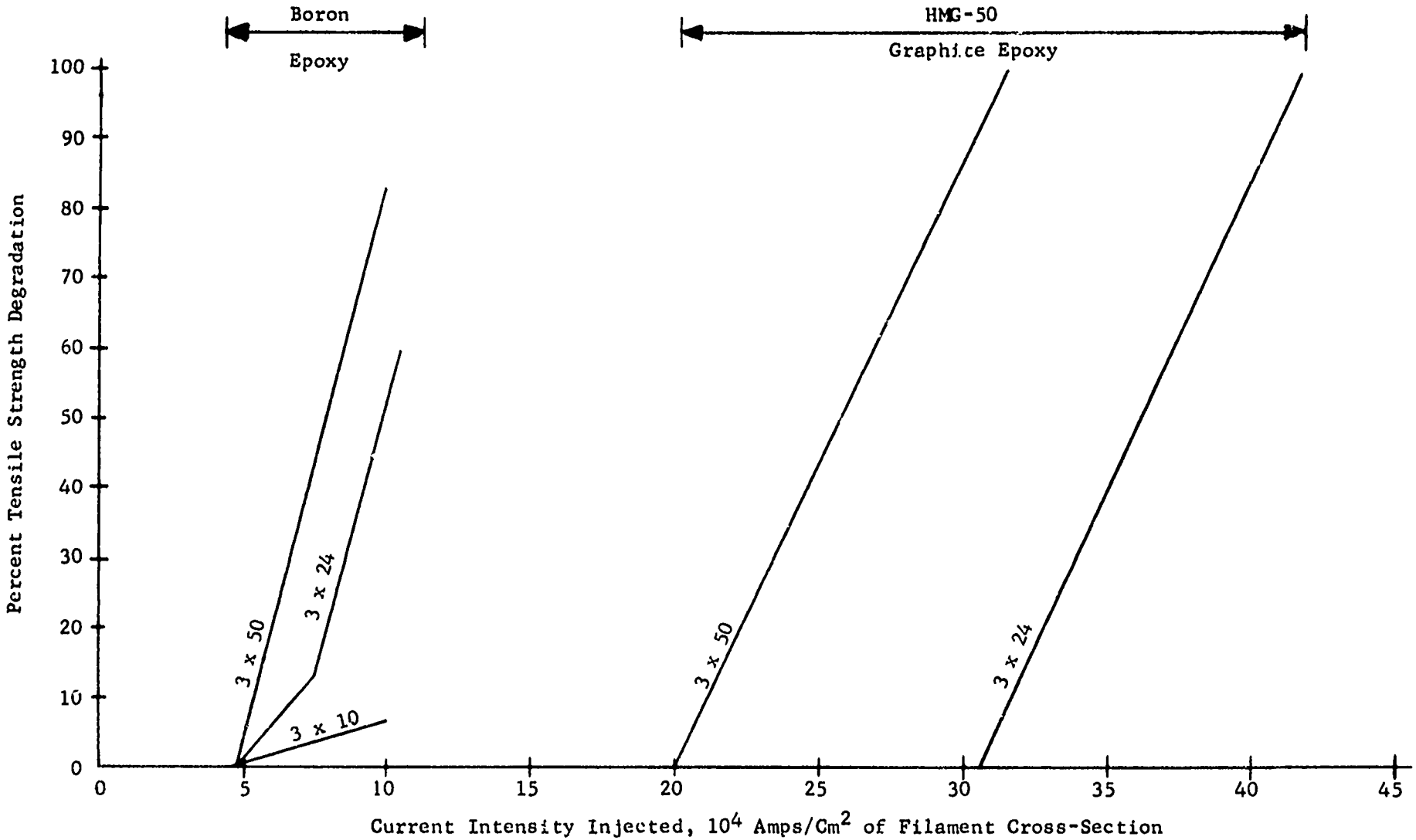

FIGURE 4. TENSILE STRENGTH DEGRADATION AT VARIOUS WAVEFORM AND CURRENT AMPLITUDES FOR BORON AND GRAPHITE EPOXY COMPOSITES

Under the energy hypothesis being considered in this task, one would expect the damage threshold in any sample type to occur when equal energies had been dissipated.

That is, when

$$(\text{Total energy})_1 = (\text{Total energy})_2$$

for similar samples.

This may be rewritten as

$$\int_o^\infty i^2(t)_1 \cdot R_1 \cdot dt = \int_o^\infty i^2(t)_2 \cdot R_2 \cdot dt$$

which for the same 3 x 24μs wave, and same sample geometry becomes

$$KI_1^2 \rho_1 \frac{1}{A} = KI_2^2 \rho_2 \frac{1}{A}$$

Considering the difference in resistivities stated above,

$$I_2 = I_1 \sqrt{\frac{\rho 1}{\rho 2}} = 1.3\ I_1$$

That is to say, the expected damage threshold under the present program should be expected to occur at approximately 1.3 I_1 (7.48×10^4 amps/cm^2 of filament cross section) due to the difference in resistivities of samples between the two programs. The correlation between the two programs can be seen in Figure 5. The dashed lines in Figure 5 are the boundaries of the results of the pri r program.

As previously mentioned, a comparison of Appendix Table II of this report with Table A6 of the program final report[1] shows that the resistance values for boron epoxy unidirectional laminates are considerably lower in the present program (1:1.7). Because of this difference between the two program results, a review of the testing procedure was made. A review of these measurements and the oscillograms which were taken indicates that both sets of data are correct. Figure 6 is a plot of the dynamic resistivity for the boron epoxy composites which were evaluated in the previous program effort. Figure 7 is a similar plot for the boron epoxy composites evaluated in the current program. Both plots are for a 3 x 24 microsecond injected current waveform. In both cases the dynamic resistivity at times near 0+ agree with initial static resistivity measurement of resistivity, which indicates that both observed values are correct. The lower resistivity of the boron filaments in the current program must then be attributed to more recently manufactured filaments and process changes inherent thereto.

Figures 8 and 9 show typical changes in resistivity for boron epoxy and graphite epoxy specimens when exposed to a continuous d-c constant voltage.

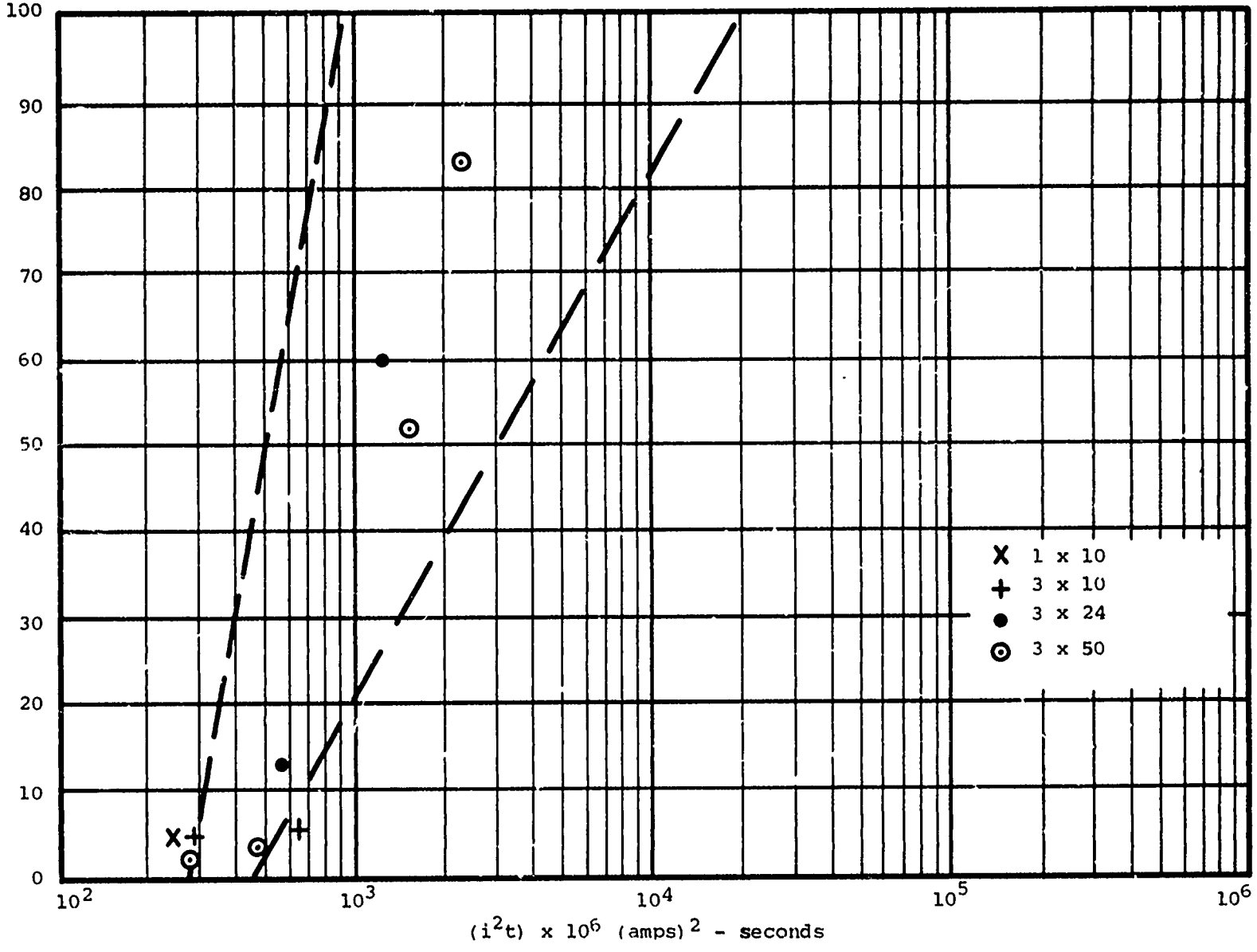

FIGURE 5. DEGRADATION VS. ENERGY PER UNIT RESISTANCE (BORON UNIDIRECTIONAL LAMINATES - ON A PER FILAMENT BASIS)

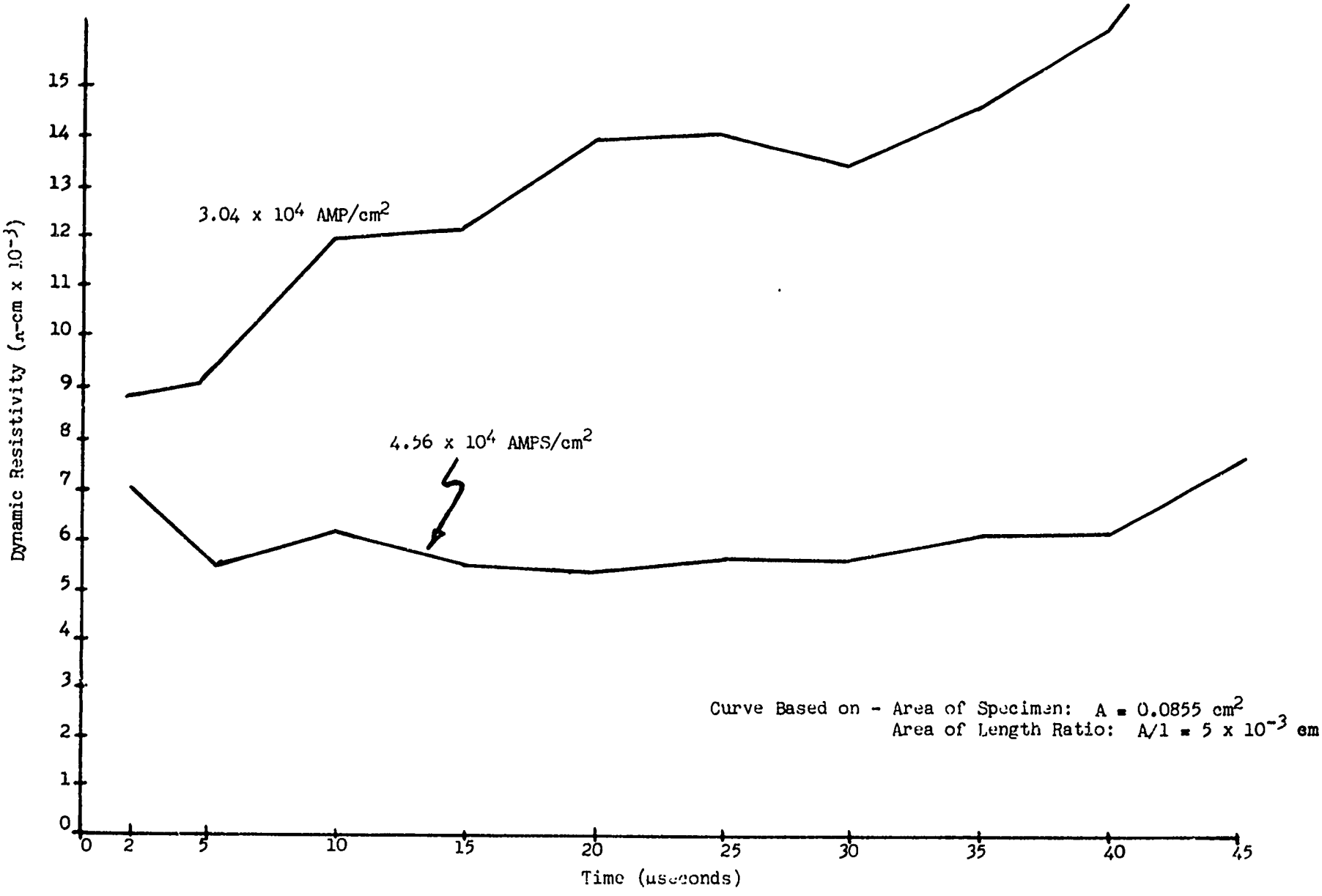

FIGURE 6. DYNAMIC RESISTIVITY OF BORON UNIDIRECTIONAL LAMINATES (BU) - 3 x 24 μs INJECTED CURRENT WAVEFORM (FROM PREVIOUS PROGRAM[1])

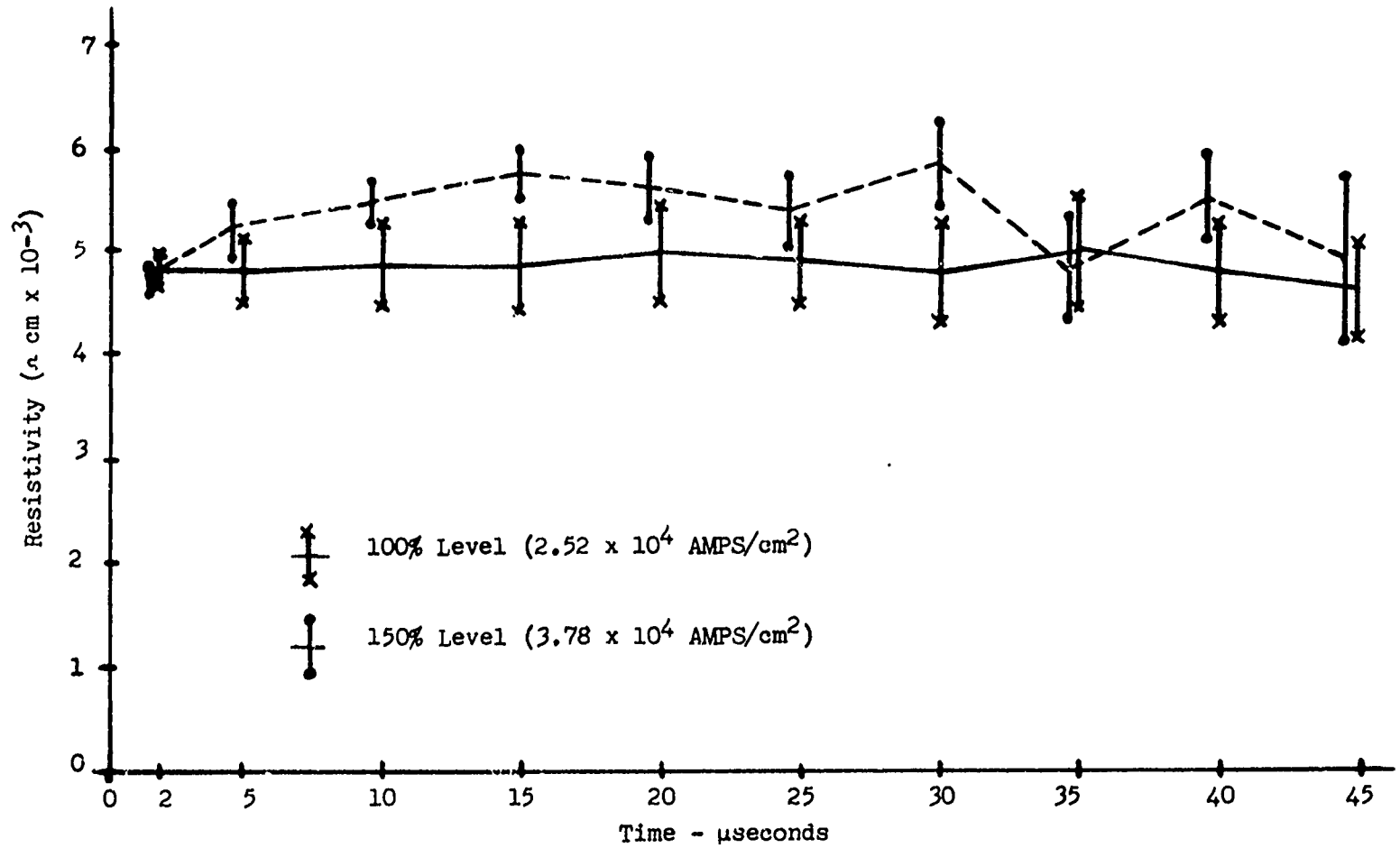

FIGURE 7. DYNAMIC RESISTIVITY (TASK II) - BORON/EPOXY LAMINATES (BT)
3 x 24 μs INJECTED CURRENT WAVEFORM

Curve Based on - Area of Specimen: $A = 0.0141\ cm^2$
Area to length ratio: $A/l = 7.94 \times 10^{-4}$ cm

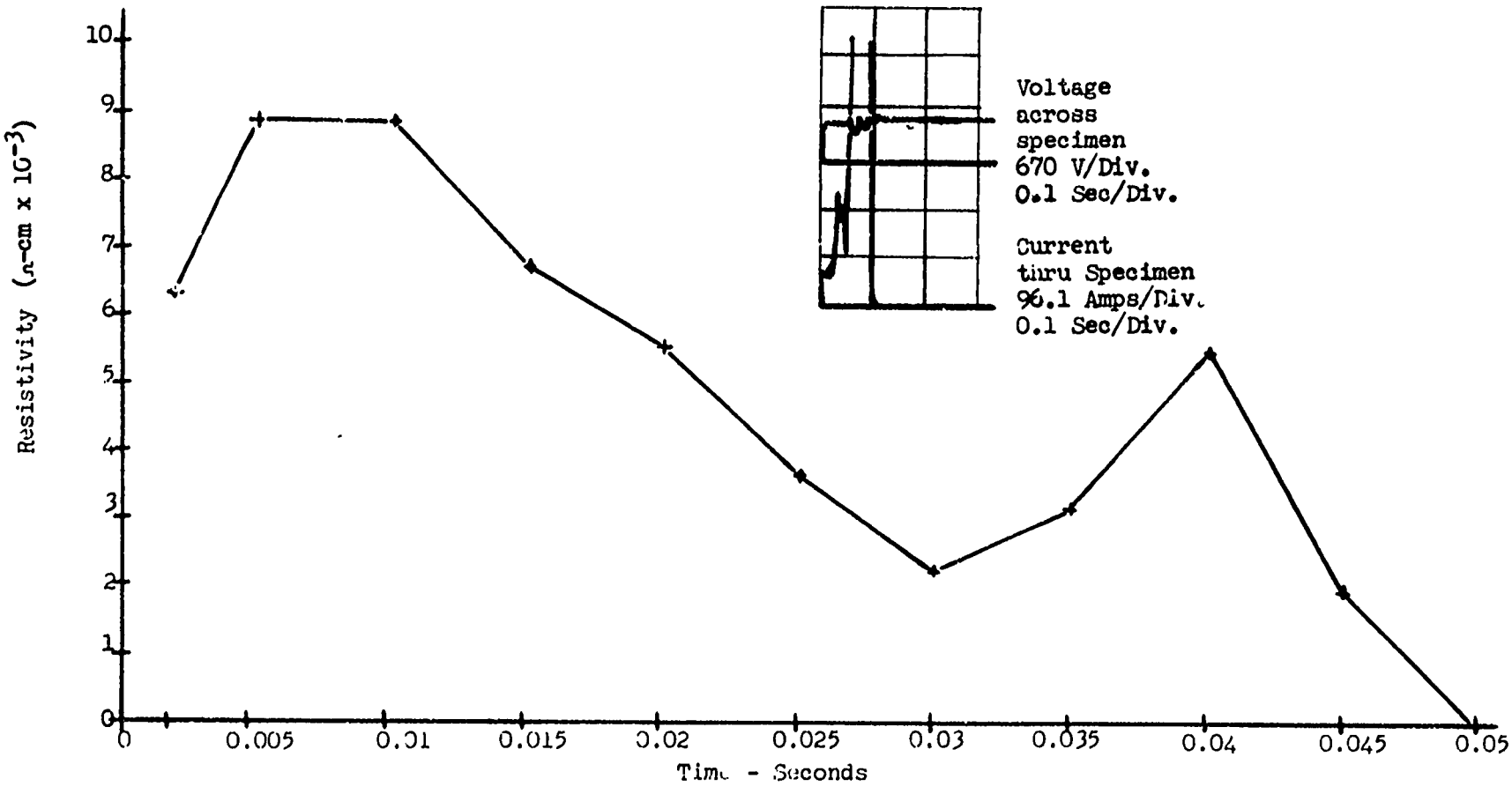

FIGURE 8. DYNAMIC RESISTIVITY - BORON/EPOXY LAMINATE BT58
~500 vdc APPLIED FOR 0.5 SEC.

Curve Based on - Area of Specimen: $A = 0.0141\ cm^2$
Area to Length Ratio: $A/l = 7.94 \times 10^{-4}$ cm

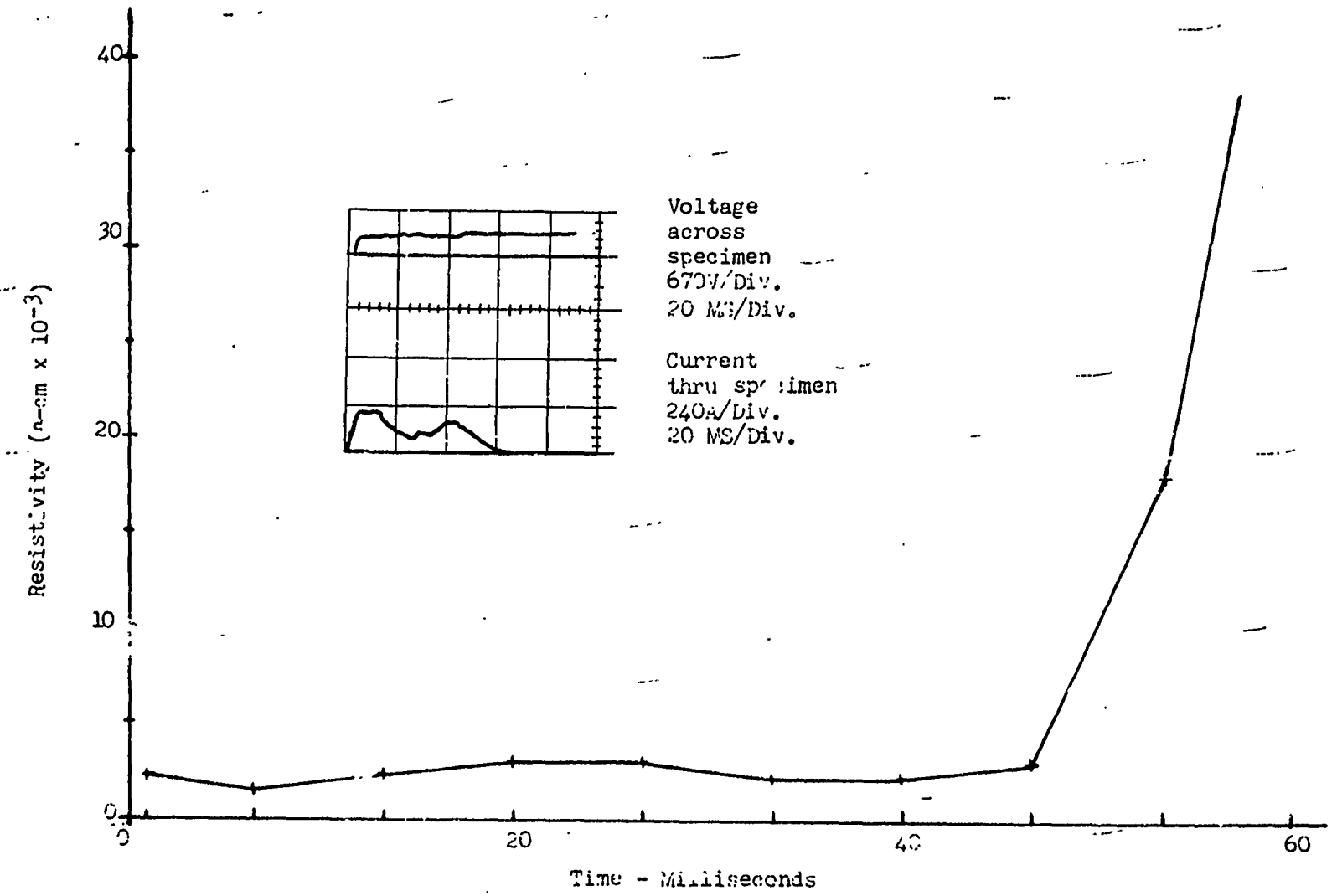

FIGURE 9. DYNAMIC RESISTIVITY - GRAPHITE/EPOXY LAMINATE (HMG-50T-30)
~330 vdc APPLIED FOR 0.5 SECOND

Curve based on - Area of Specimen: $A = 0.0141$ cm^2
Area to Length Ratio: $A/l = 7.94 \times 10^{-4}$ cm

It should be noted that since the resistivities of the specimens do not remain constant the currents also vary and are inversely proportional to the resistance. The d-c continuing current tests were conducted in the same manner as previous tests except with the impulse generator being replaced by two 500 vdc generators in series. The desired voltage level corresponding to the lowest current level (178 amps for boron/epoxy) was set using a fixed resistor. The duration of the voltage (0.5 sec.) was controlled by timers which automatically opened the circuit breakers. The first sample (BT-21) was placed in the test fixture and voltage applied. The specimen exploded. The oscillogram taken was poor but showed the current to rise to approximately 100 amps in about 0.01 second. It then increased in the next 0.01 second and returned to zero at 0.06 second as the specimen burned open. The applied voltage was then lowered to 500 vdc and Specimen BG-58 was tested. No explosion occurred this time, but the specimen was still destroyed (refer to Figure 10). Three additional boron filament epoxy specimens were electrically exposed in order to obtain an oscillogram on a faster sweep but the oscilloscope did not trigger properly.

The HMG-50 graphite filament epoxy specimens at continuing current 500 vdc produced a burning damage response almost identical to that produced with waveform injection; however, with the voltage lowered to 300 vdc the current remained finite as shown in Figure 9. As reported in the prior program, the graphite filament epoxy composites are damaged at the point where the filaments are hot enough to initiate resin pyrolysis. The gases so produced cause the composite to explode. Then, when air comes in contact with the gasses and hot filaments, burning is initiated.

A plot of percent degradation versus energy deposition for the HMG-50 graphite filament unidirectional composites is shown in Figure 11. It will be noted that these specimens seem to degrade totally at the instant where the graphite filaments become hot enough to initiate resin pyrolysis, as discussed in the previous program. As a result, the graphite/epoxy composite specimens were either not degraded or totally degraded. This use of resin pyrolization as indicating the 100% degradation point seems quite valid since all structural integrity is lost.

The more complete results obtained throughout this program verify the "energy" hypothesis put forth in the prior program.[1] All analytical work to date has involved expressing the injected current waveforms as the difference of two equipotentials:

$$\text{Injected current waveform} = I(\epsilon^{-a_t} - \epsilon^{-b_t})$$

in which E, a, and b arbitrary constants. This approach is quite useful, but considerable time may be spent in the "curve fitting."

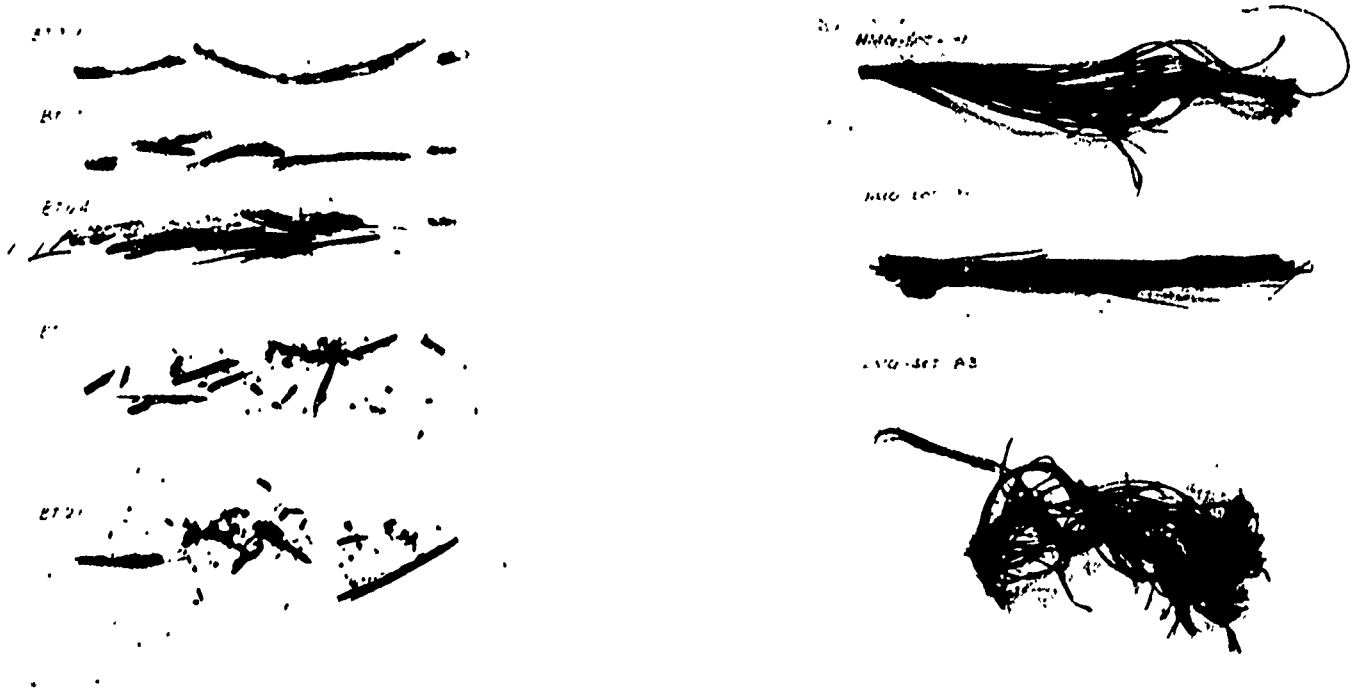

FIGURE 10. RESULTANT DAMAGE TO SPECIMENS EXPOSED TO D-C VOLTAGES TO SIMULATE CONTINUING CURRENTS (Left: Boron Filament Epoxy - Right: Graphite Filament Epoxy)

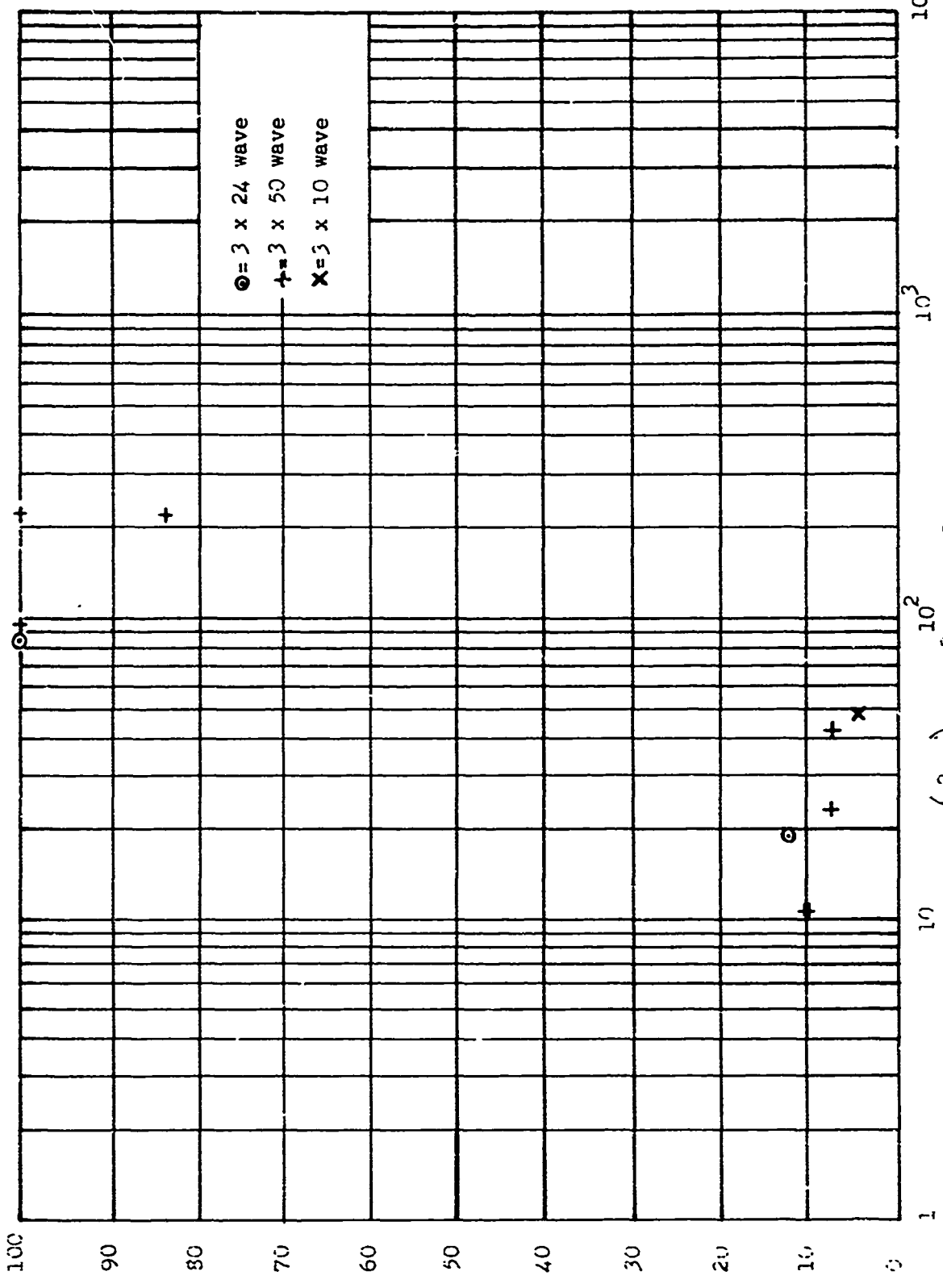

FIGURE 11. DEGRADATION VS. ENERGY PER UNIT RESISTANCE
(HMG-50 Graphite Filament DEN 438 Epoxy
Unidirectional Composites)

For those times when only a quick estimate is desired, a straight line approximation may prove valuable.

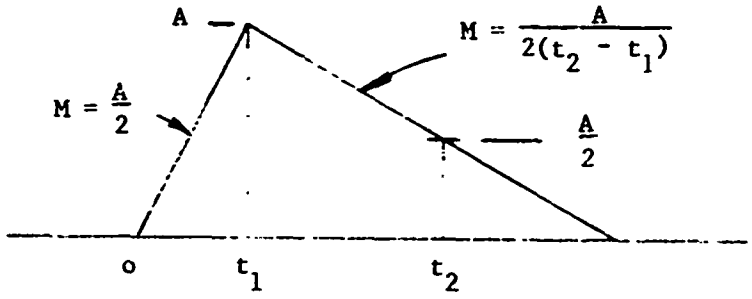

The total energy given by this approximation is:

$$En = \frac{A^2}{3}\left[t_1 + 2(t_2 - t_1) - \frac{1}{4}\left(\frac{t_1^3}{t_2 - t_1}\right)^2\right]$$

With this approximation one can readily see what effects a change in the t_1 and/or t_2 might have. In general the results from this straight line approach are within 5% of those obtained by more sophisticated techniques (at least for waveshapes used to date).

As an aid in assessing composite degradation, a group of aluminum strips were subjected to injected current intensities at levels causing severe composite damage. These levels were 11.6, 13.8, 18.1, and 25.6 x 10^4 amps/cm^2. There was no apparent change in the aluminum, which is substantiated by an elementary comparison of the resistivities of the highly conductive aluminum and the poorly conductive composites. At given energy levels much less energy is deposited within the low resistivity aluminum as compared to the composites.

2.3 TASK III - VISUAL OBSERVATIONS OF DAMAGE MECHANISMS

During the previous N00019-70-C-0073 program,[1] mechanisms of damage resulting from electric current flow for boron and graphite filament composites were postulated and verified analytically through mathematical modeling. The degradation threshold for graphite filament composites was determined to be resin dependent and occurred at the point where the thermal energy buildup in the filaments due to resistive energy dissipation exceeded the point at which epoxy resin pyrolysis initiated. The gaseous decomposition products from the resin pyrolysis then causes an increase in internal pressure that ruptures the composite. Then, as air comes in contact with the hot graphite filaments and gaseous products, burning is initiated. In boron filament epoxy composites, the degradation threshold appears to be filament limited. Because of the highly resistive nature of the boron filament outer shell, electric current is carried predominantly by the inner 0.0005 in. diameter core that was converted to tungsten boride, from tungsten, during the chemical vapor deposition of the boron. The electric energy is then converted to thermal energy within the core due to the resistivity of the core. It is over a very short period of time that the increase in thermal energy occurs and essentially is confined to the core which thermally expands. The expansion of the core puts the surrounding boron in a state of stress and at the degradation threshold results in the fracture of boron. The concept that the boron filament degradation is caused by thermal energy buildup is further indicated by the observation that the fracturing does not occur until after the current waveform has passed through the filaments.

The boron filament composite specimen degradation is filament limited and occurs at the threshold where the filaments crack. As previously reported[1] there is no visual evidence of this, and, in fact, completely degraded boron/epoxy composites show no visual evidence of degradation unless microscopically inspected for cracks in the filaments. The graphite filament epoxy composites, however, degrade visually and the sequence predicted analytically[1] was:

(1) Composite exfoliating or exploding apart due to pyrolytic gases resulting from epoxy resin pyrolysis as caused by the hot filaments.

(2) Initiation of burning as air comes into contact with the exposed hot filaments and pyrolytic gases.

This visual degradation sequence was not obvious from mere visual observations because of the extremely short time sequence involved; therefore, it was decided to take high speed motion pictures to verify the degradation sequence that had been analytically predicted.

For the high speed motion pictures 50 x 10^6 psi elastic modulus graphite filaments (Hitco HMG-50) were used to fabricate unidirectional epoxy matrix composites with the Dow DEN 438/MNA resin, in exactly the same manner as reported in the previous program.[1] These specimens were electrically exposed and filmed at 6,000 frames per second in an attempt to capture the degradation sequence at a film speed which would at least provide several frames that recorded the sequence. The specimens were 0.5 in. width, 7 in. length, and 0.025 in. thickness and nickel plated on the ends for electrical contact. A waveform of 3 x 24 microseconds was used, and three levels of electrical current intensity were injected: 18 x 10^4, 25 x 10^4, and 29 x 10^4 amps per cm^2 of filament cross-section. These electric current intensity values correspond to 8,420 amps, 11,700 amps, and 13,800 amps as based on the actual amperage applied to the specimen. Figure 12 shows the appearance of these specimens after current injection. A control specimen was included for visual comparative purposes, and the light source for the photograph was adjusted in order to emphasize the difference in resin gloss between the control and exposed specimens. Figure 12 is an excellent illustration of the typical electrical current damage sequence that is exhibited by graphite filament epoxy composites. Specimen GY 42 (8,420 amps) is just on the degradation borderline. The movie film of this specimen shows an electrical flash, a small amount of smoke, and no visible change in the specimen. As can be seen in Figure 12, a very slight amount of resin pyrolysis has occurred as evidenced by the black discoloration on the specimen. Note that the specimen is intact. This is due to the fact that the energy level was just past the damage threshold and resin pyrolysis was barely initiated. As a result, there was not sufficient gaseous products generated to cause rupturing or exploding of the specimens.

Specimen GY-30 (11,700 amps) has definitely exceeded the degradation threshold. The film of this specimen shows the electrical flash, flames, and smoke from the resin pyrolysis, but note the specimen is still intact in Figure 12, indicating that the pyrolysis gases still were not generated to a degree that rupturing occurred.

GY-3 (13,800 amps) shows the catastrophic failure (resin pyrolysis and rupture of the graphite reinforcement) that accompanies this current injection level. In examination of the motion pictures the burning (flames) did not appear until after specimen rupture.

It appears then that the 18-25 x 10^4 amps/cm^2 current intensity levels were just at the threshold where the epoxy resin began to pyrolyze but the 29 x 10^4 amps/cm^2 level was sufficient to produce rapid pyrolysis and sufficient gases to produce specimen rupture.

FIGURE 12. HMG-50 GRAPHITE FILAMENT DEN 438 EPOXY SPECIMENS AFTER EXPOSURE TO HIGH INTENSITY ELECTRIC CURRENT INJECTION

2.4 TASK IV - INVESTIGATIONS INTO VARIATIONS IN BORON FILAMENT ELECTRICAL CONDUCTIVITY

During the previous investigation[1] of current flow within and degradation of boron filaments and boron filament epoxy composites, the following observations were made:

(1) Boron filaments vary in resistivity.

(2) Within a composite exposed to current injection, boron filament degradation is random, indicating variations in electrical conductivity and/or resistance of the boron filaments.

As a result of these observations, it has been speculated that boron filament lengths may vary in electrical properties because of variations in their chemistry. Two such variations were thought possible:

(1) Types and levels of impurities within the filaments.

(2) Variations in the diffusion zone of boron into the substrate core. As discovered in the previous program,[1] boron diffuses into the tungsten substrate during the chemical vapor deposition process and converts the core to W_2B_5 at its center, WB_{12} in an intermediate zone, and WB_{12} + B in the zone next to the boron shell.

To investigate such possible variations, 160 standard 10 in. long boron filament mounts prepared as in the previous program[1] were selected (10 each from 16 different rolls) and identified. Each end of the specimen was identified (such as "A" and "B"). A two in. (2 in.) section between each filament used for a specimen mount was also identified and retained.

The following subsections describe the efforts that were made to identify the cause for the apparent variation in boron filament conductivity.

2.4.1 EVALUATION OF SPECTROGRAPHIC ANALYSIS FOR FILAMENTS

A dc arc spectrographic analysis of filament pieces of four different lots of boron filaments was performed by Pacific Spectrochemical Laboratory. The specimens submitted were selected from four of the sixteen different lots of boron filaments and consisted of the following six specimens:

Lot #H57-715*	1.	Fifteen linear inches (approx. 15 milligrams).
Lot #H57-715	2.	Two linear inches (approx. 2 milligrams).
Lot #H56687	3.	Fifteen linear inches (approx. 15 milligrams).
Lot #H56687	4.	Two linear inches (approx. 2 milligrams).
Lot #H52-956	5.	Fifteen linear inches (approx. 15 milligrams).
Lot #H56549	6.	Fifteen linear inches (approx. 15 milligrams).

*United Aircraft Co. lot numbers.

Note that samples 2 and 4 are identical to 1 and 3. Identical lot samples were analyzed in order to obtain an indication of accuracy of the method as a function of sample size.

The results of the analysis are recorded in Table I. In those instances where the symbol < appears with the reported element concentration, it signifies that the element was not present or that the reported concentration is the lower limit which can be detected. Note that the concentration of tungsten is not reproducible in the same lot of material (large sample versus small sample) and the detection of tungsten in the small sample more closely approaches the theoretical tungsten concentration (11.5%). It was assumed that an unacceptable error exists with the larger sample due to incomplete ignition of the tungsten.

Silicon was detected in all but one of the samples. Magnesium was detected in all samples. Bismuth and calcium were detected in two samples.

With regard to interpretation of the method of analysis, Pacific Spectrochemical explained that because tungsten is highly refractory, burnoff of the smaller sample resulted in more burnoff of the element than could be obtained with the larger sample. Therefore, the dc arc spectrographic method is not a quantitative method for the detection of tungsten.

Because of the inability to obtain a complete analysis of the boron filaments by the above method, it was decided to analyze the filaments by a mass spectrographic technique. The facility selected for this was the Electronics Materials Division of Bell and Howell because of their prior experience in boron filament analysis.

Two boron filament specimens were selected from two different manufacturing lots of boron filaments which had been selected by General Electric High Voltage Laboratory as typical boron specimens with different electrical resistivity (1,000 ohms to 10,000 ohms). Two of these filaments were evaluated by microprobe analysis (discussed later), and the remaining two

TABLE I

SPECTROGRAPHIC ANALYSIS OF BORON FILAMENT

Element		Boron Lot Number HS-7 715, (1 Part)	HS-7 715, (10 Parts)	HS-6687 (1 Part)	HS-6687 (10 Parts)	HS-2 956 (10 Parts)	HS-6549 (10 Parts)
B		(1)	(1)	(1)	(1)	(1)	(1)
W		8.1%	0.72%	11.0%	0.45%	0.72%	0.57%
Si		0.057	0.036	0.057	0.003	0.036	<0.003
Mg	Trace	<0.002	0.003	0.0044	0.0025	0.0030	0.00087
As		<0.05	<0.09	<0.05	<0.09	<0.09	<0.09
Bi		<0.01	<0.42	<0.01	<0.003	0.42	<0.003
Ca		<0.001	<0.00092	<0.001	<0.0003	0.00092	<0.0003
Hg		<0.05	<0.03	<0.05	<0.03	<0.03	<0.03
Other		nil	nil	hil	nil	nil	nil

(1) Not determined, reported by difference.

were used for the mass spectrographic analysis. These specimens were 2BW7 and 15BW8 with 905 ohms resistance and 9,500 ohms resistance, respectively.

The impurity concentrations which were found in these specimens are given in Table II. As the individual filaments could not withstand the force of the spark used in the mass spectrometer, it was necessary to break each filament into several pieces. These pieces were bundled together, wrapped in gold foil for support, and then sparked against high purity gold counterelectrodes. The maximum exposure obtained for sample 15BW8 was 3×10^{-7} coulomb total charge. The maximum exposure obtained for sample 2BW7 was 3×10^{-8} coulomb total charge. Because of these total charge differences between specimens, it was impossible to obtain the same sensitivity for sample 2BW7 as was obtained for 15BW8; and, consequently, for some elements the detection limits are indicated rather than the actual elemental concentration.

The impurity element differences between the two specimens were not of a significant magnitude. Hydrogen and fluorine were the only elements which appeared to have significant differences, but there were no apparent differences between any elements which could account for the differences in the two filaments' electrical resistance.

2.4.2 MICROPROBE ANALYSES OF BORON FILAMENTS

There were two principal objectives of this analysis. The first is to define and delineate the relative amounts of the principal phases in the cross section of electrically characterized boron filaments. With this information, it was hoped that a correlation could be established between the crystal chemical nature of boron filament and their electrical conductivity. The solution to this problem required precision measurements of the thickness and composition of the diffusion zone between the tungsten core and boron shell of the filament. The second objective was a spectral analysis of the filament for impurities. Limits of detectability of the electron microprobe in the spectrographic scanning mode are characteristically 0.5% or greater, depending on the degree of heterogeneity of the respective elements. Here also, a measureable impurity level would be factored into the electrical-chemical behavior of the boron filament.

a. Equipment and Procedure

The electron microprobe is used for performing non-destructive, qualitative, and quantitative elemental analysis of minute volumes at the surface of solid specimens. A finely focused beam of electrons is directed at the specimen surface exactly on the spot to be analyzed. The electron bombardment causes characteristic X-rays to be emitted by the atoms affected by the electron excitation. Crystals of appropriate material are employed to diffract the X-rays into their component wavelengths which in turn are focused on X-ray detectors. There the X-ray photons are converted to pulses

TABLE II

IMPURITY CONCENTRATIONS IN TWO BORON FILAMENTS
WHICH DIFFER IN ELECTRICAL RESISTIVITY
(In Parts Per Million Atomic)

Element*	15BW8	2BW7
H	41	270
Li	0.059	<0.07
C	54	52
N	8.0	6.3
O	280	340
F	4.7	0.3
Na	2.9	2.8
Mg	6.8	3.6
Al	2.5	5.0
Si	30	52
P	2.6	1.9
S	17	4.9
Cl	9.8	8.9
K	23	19
Ca	3.5	2.5
Ti	1.5	1
Cr	0.17	<0.5
Mn	0.087	<0.5
Fe	11	14
Ni	0.25	<0.5
Cu	2.7	1
Zn	0.1	<0.7
Ga	0.67	<0.5
As	4.1	1.6
Rb	0.034	<0.1
Ag	0.51	<0.5

*Analysis for tungsten is not included, since the samples were deposited on tungsten cores. Analysis for gold is not given since the samples were sparked against high purity gold counterelectrodes. Other impurities not listed were not detected and have concentrations less than 0.2 ppma in 15BW8 and 2 ppma in 2BW7.

of electrical energy. The number of pulses is directly proportioned to the intensity of the X-radiation, which in turn bears a relationship to the mass concentration of the element producing the X-rays. The pulses of energy from the detectors can be utilized in a number of read-out systems.

The Applied Research Laboratory microprobe, Model EMX, at Aeronutronic is equipped with a light element detector modification permitting analysis of elements of atomic numbers 5 (boron) through 92, uranium. The electron probe spot size ranges from 0.3μ to 300μ; and the spatial resolution is approximately 1 micron. The unit is equipped with a light optical system which has a magnification of 280, thus allowing the operator to visually locate and observe the sample surface during analysis. Specimens 1 in. in diameter are supported in a stage containing eight stations. Generally, 3 to 5 of these stations are reserved for standards and the remainder for analyses. Samples can be displaced manually or automatically, horizontally, vertically, or rotated 360° in their own plane. Automatic step scans can be simultaneously performed for these elements at each step. For this program, step traverses across the cross section of boron filaments were made in intervals of 2 microns with a simultaneous analysis of the concentration of tungsten and boron at each step. The data were automatically recorded by a strip chart recorder and a digital typewriter print out of the respective X-ray pulses. Spectral qualitative analysis was performed by focusing the electron beam on the area of interest and automatically scanning through the X-ray monochrometers and recording the X-ray emission of the sample throughout the range of detection (0.36Å to 94.10Å). The presence of a specific element is thus denoted by a peak on the output chart occurring at its particular wavelength.

It was previously reported[1] that due to the chemical vapor deposition boron is diffused into the substrate core resulting in a variation in the boron/tungsten ratio with the higher boron diffusion near the core/shell interface. The purpose of this investigation was to ascertain if a variation in the diffusion zone from one filament to another could be identified. Also an attempt was to be made to determine if the diffusion zone in the core changes as the result of exposure to high current pulses short of those required for melting. The significance of this finding would hopefully offer some insight into why the resistivities of boron filaments vary and why some filaments within a composite suffer damage and others do not.

The diffusion zone was analyzed by electron microprobe traverses across the interfaces between the tungsten boride core and the outer boron structure.

b. Experimental Procedure

Nine pairs (exposed and retained unexposed sections of the same filaments) of boron filaments were mounted in a 1 in. diameter "Lucite" metallurgical mount filled with copper powder. The unexposed pieces were broken from the ends of each filament specimen prior to its current injection exposure.

Each filament sample was broken into six to eight 1/4 in. long sections and dropped into a 0.030 in. diameter hole drilled in the prepressed mount. After filling a matrix of holes, the mount was repressed and the filaments were submitted for polishing. Polishing was performed with a minimum of time on the laps to preclude excessive removal of the boron around the tungsten boride core. This prevents a high core protrusion above the boron filaments and retains a relatively smooth cross section desired for electron beam traverses. Polishing was performed from an initial cut on 600 grit SiC paper through 6 micron to 1 micron diamond and kerosene on nylon cloth laps. The polished mount is shown in Figure 13.

The microprobe analysis was performed with an Applied Research Laboratory, microprobe Model EMX. Operating conditions were 15KV at 50 na nominal. In practice, the sample current was set at 56 na on boron which resulted in a sample current of 36 na on the tungsten rich core. Boron Kα radiation was detected with a lead stearate crystal and tungsten mα radiation with an ADP crystal. Calibration was obtained with pure standards of boron and tungsten, both cleaned and simultaneously vacuum carbon coated with the filaments prior to analysis. This eliminated the need for having to account for attenuating effects of the carbon coating if only the filaments had been coated. The carbon coating is required to facilitate charge removal from the filaments to enhance the stability of the electron beam. Beam diameter was 1 micron or less and at 15KV penetrated the boron and core 2.9 and 0.3 microns, respectively. The output of the tungsten detector was fed into a 400 channel pulse height analyzer and memory unit operating in a multi-scaler mode. In this mode the input section of the multi-channel PHA was set up as a single channel analyzer to accept a narrow band of pulse amplitudes corresponding to the energy of the element (tungsten) of interest. The 400 channels were then used to count and store pulses as a scaler for a preset time interval. This event occurred at 1 micron intervals as the electron beam automatically step traversed across the interface and core of a boron filament. The integration time at each step for each element (boron and tungsten) was 15 seconds. Since the greatest sensitivity could be attained with tungsten, its output was read through the multi-channel analyzer. Following the traverse of the region of interest, the multi-channel PHA memory was interrogated and the tungsten counts at each step were automatically printed out by an electric typewriter. This was in addition to a conventional strip chart read out of the relative intensities of boron and tungsten at each step interval. The digital data from the multi-channel PHA was then plotted versus distance for comparison of the diffusion profiles and widths of the respective tungsten-boron diffusion zones. Boron concentrations were calculated as the difference between the tungsten concentration and its 100% pure standard. This was also confirmed by the relative intensity of the strip chart boron data.

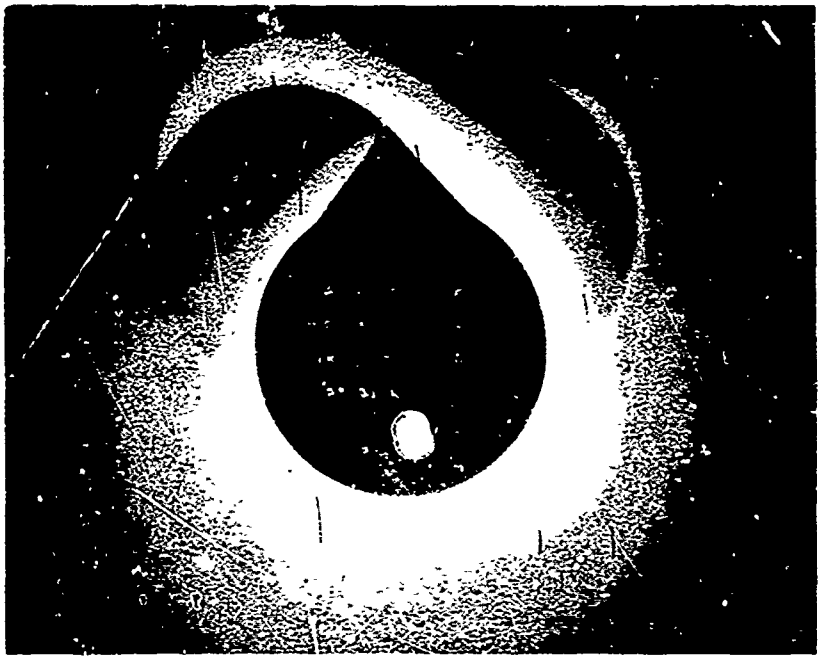

FIGURE 13. COPPER FILLED "LUCITE" MOUNT CONTAINING 9 PAIRS OF BORON FILAMENTS NUMBERED A THROUGH R

c. Discussion of Experimental Results

Approximately 20 step traverses were recorded across the cores of control and electrically exposed filaments. Initially some difficulty was experienced in maintaining the stability of the electron microprobe beam as it traversed from the boron zone to the tungsten boride core. This was greatly reduced by decreasing the microprobe voltage to 15KV and maintaining a low beam current of 50 na. In addition a 1000Å carbon coating was vapor deposited on the surfaces of the filaments to facilitate charge removal.

Table III summarizes the results of the microprobe traverses performed during this investigation. Shown here are the mount numbers (see Figure 13) and the specimen identification codes. The widths of each core were based on the number of 1 micron steps required for the electron beam to travel across the core. These dimensions varied from 14 to 17 microns. An examination of photomicrographs of the traversed filaments revealed that the variation in core widths was caused by the beam being off-center. Examples of this are shown in Figures 14 and 15. In the event that additional diffusion had taken place between the boron and the tungsten boride core, it is conceivable that a total increase in diameter could be resolved. An increase in core diameter was not detectable by the microprobe traverses. The randomness of the widths of the filament cores between control and exposed specimens is evident in Table III. Also shown in Table III are the average thicknesses of the tungsten boride interface zone. If orderly changes in the thickness of composition of this zone in exposed filaments compared to control filaments were detected, one could conclude a diffusional change to have occurred. The relative uniformity of the thickness of the tungsten boride-boron interface zone, 5.0 to 5.5 microns, indicates that no detectable change has occurred.

In Figure 16 the relative concentrations, slopes, and widths of the core zones of two typical sets of filaments are presented. The narrower exposed core depicted in Figure 16 (specimen 1BW8) is the result of an off-center traverse of the electron beam shown in Figure 14A. In Figure 16B (specimen 8BW1) a slight shift in the two curves reflects variation in arbitrarily selecting the center point of the traverse. Photomicrographs of the respective cores are shown in Figures 15A and 15B. Neither of the plots in Figure 16 indicate any significant variation in the composition of slope of the tungsten boride-boron interface zones.

The composition of the tungsten boride core closely matches W_2B_5 which contains 87%W and 13%B. The interface zone probably contains a heterogeneous mixture of WB_{12} and B after the phase diagram of Rudy and Windesch.[2] Panel 26, a composite previously reported, was also analyzed using the techniques developed for the above filaments. Analysis of a filament showing no visible interface melting was similar in every respect to those reported above. The relative width and thickness of the interface zone are reported at the bottom of Table III.

TABLE III

SUMMARY OF MICROPROBE ANALYSIS OF DIFFUSION ZONES
OF BORON FILAMENTS

Mount No.	Specimen No.	Total Width Core Diffusion Zone, Microns	Av. Thick. W/B Interface Zone, Microns	Δ W/μ At Interface	Alignment of Beam Through Center of Core
A	1BW8 C	16	5.5	15.7	Good
B	1BW8 E	15	5.0	17.4	Fair
C	2BW2 C	15	5.5	15.7	Good
D	2BW2 E	16	5.0	17.4	Fair
E	5BW4 C	15	5.0	17.4	Poor
F	5BW4 E	16	5.5	15.7	Poor
G	9BW6 C	16	5.5	15.7	Good
H	9BW6 E	15	5.0	17.4	Poor
I	10BW8 C	16	5.5	15.7	Fair
J	10BW8 E	14	5.0	17.4	Fair
K	3BW3 C	16	5.0	17.4	Fair
L	3BW3 E	17	5.0	17.4	Good (Cracked)
M	8BW1 C	16	5.0	17.4	Good
N	8BW1 E	16	5.0	17.4	Good
O	7BW1 C	17	5.0	17.4	Good
P	7BW1 E	17	5.5	15.7	Good
Q	14BW1 C	16	5.0	17.4	Good
R	14BW1 E	16	5.5	15.7	Good
Panel No.	26	16	5.5	15.7	

C = Control

E = Exposed

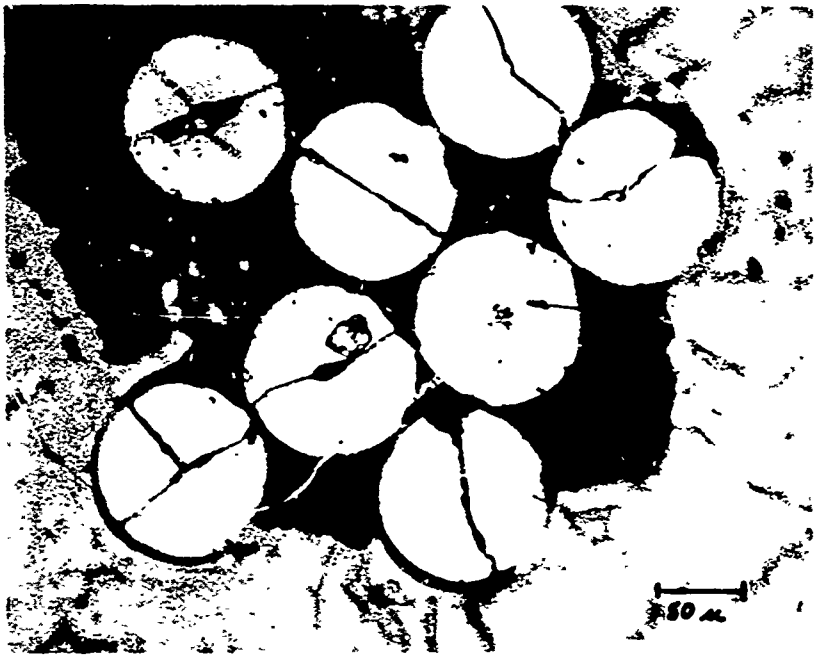

A. 1BW8 EXPOSED

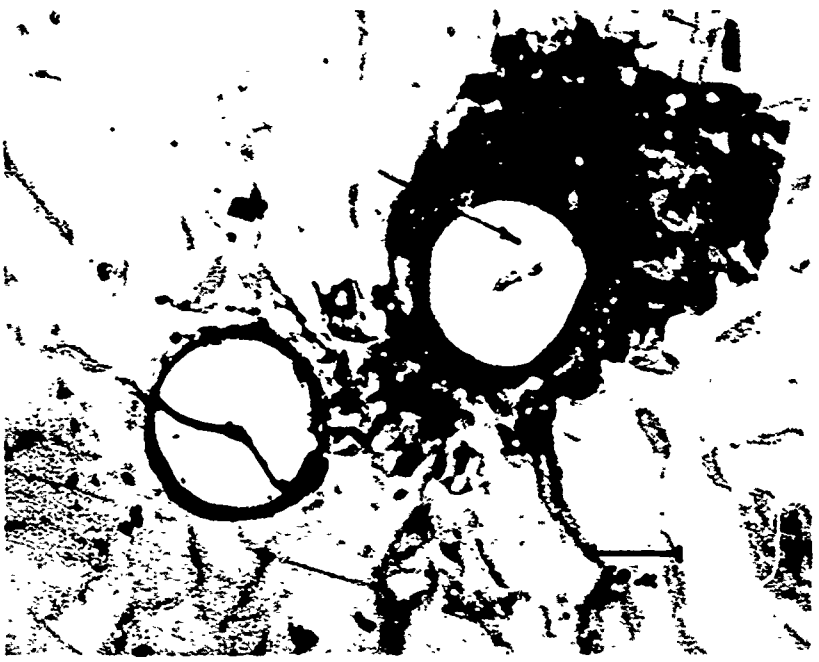

B. 1BW8 CONTROL

FIGURE 14. MICROPHOTOGRAPHS OF MICROPROBE TRAVERSE PATHS ON 1BW8 BORON FILAMENTS

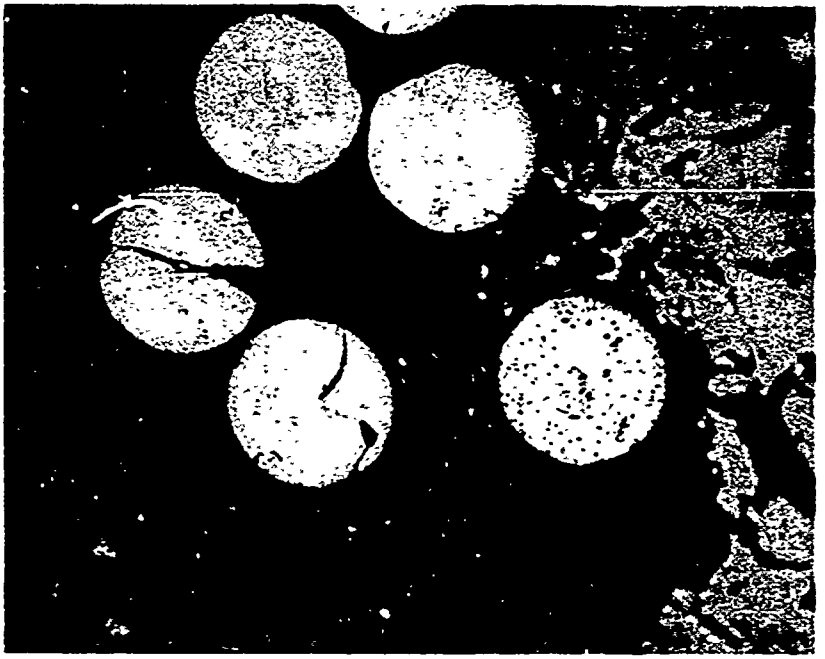

A. 8BW1 EXPOSED

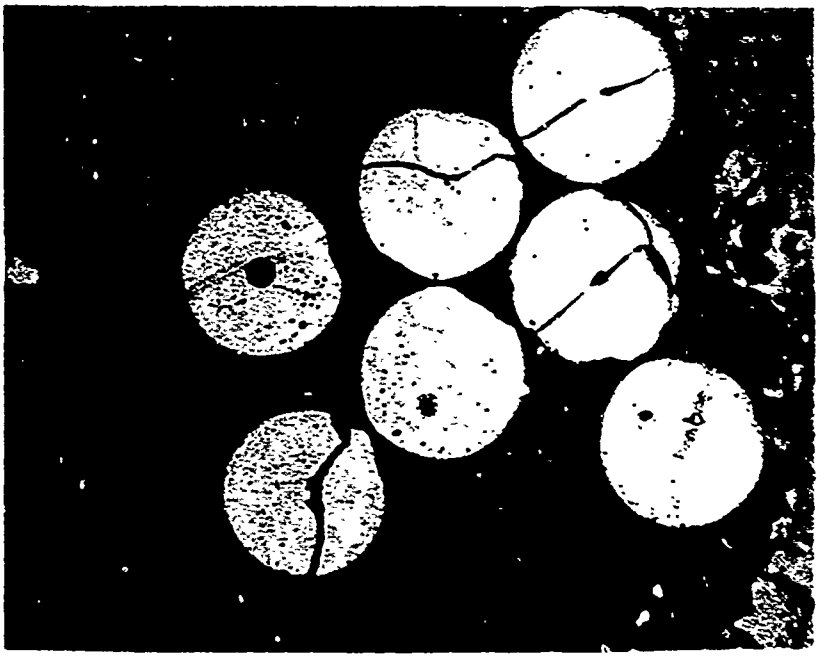

B. 8BW1 CONTROL

FIGURE 15. MICROPHOTOGRAPHS OF MICROPROBE TRAVERSE PATHS ON 8BW1 BORON FILAMENTS

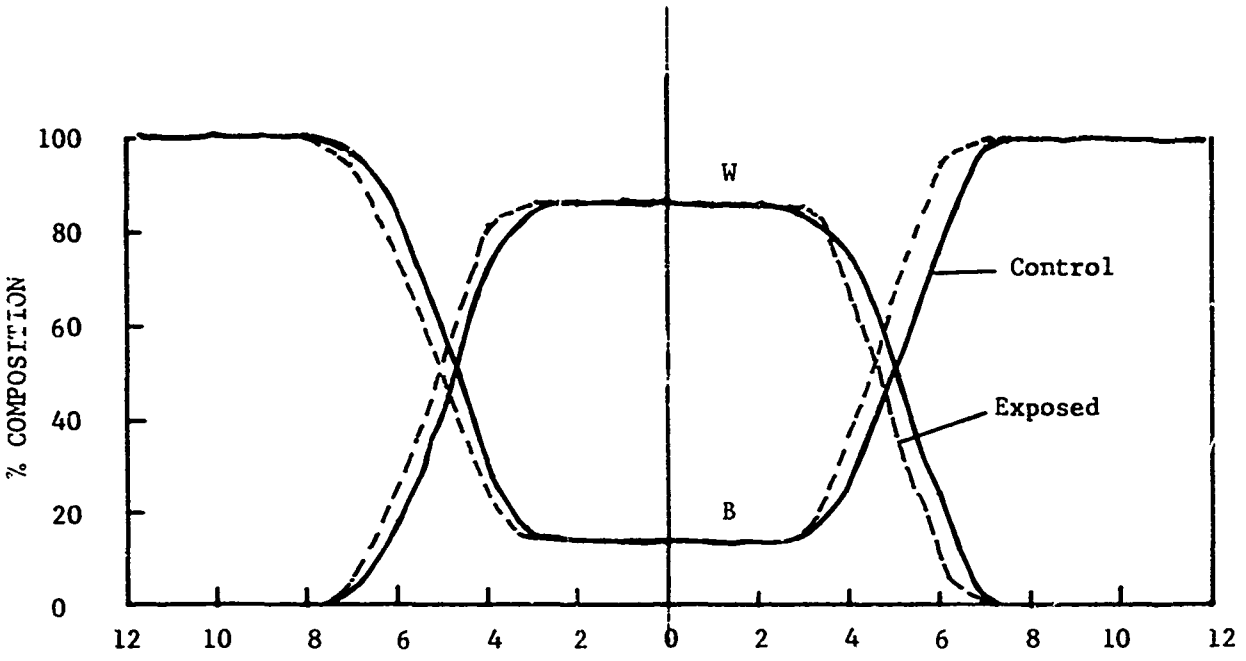

MICRONS FROM CENTER OF CORE
B. Specimen 8BW1

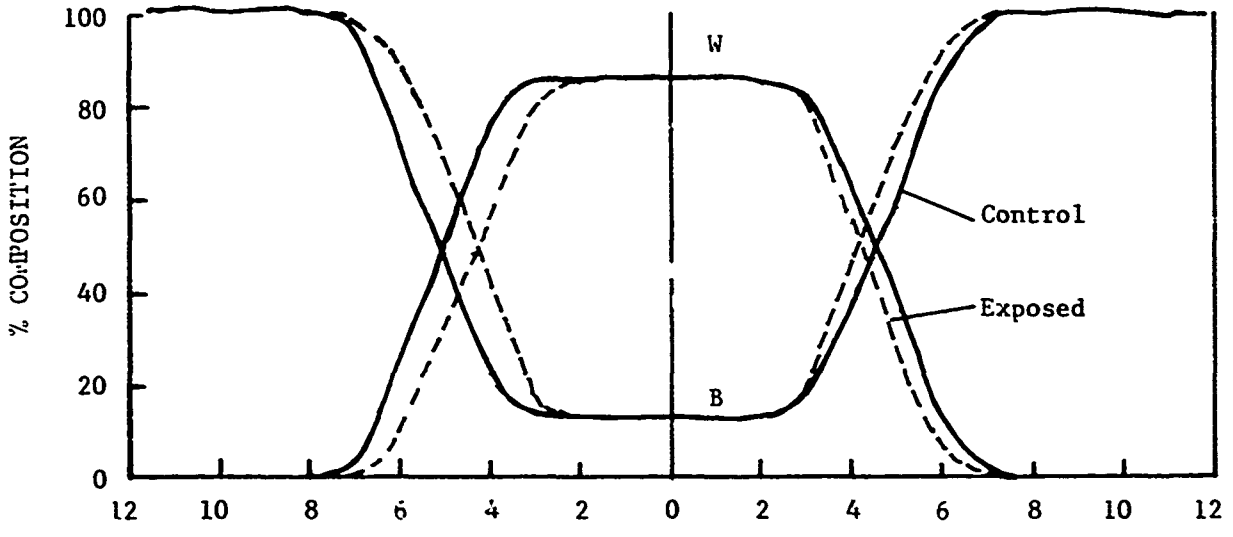

MICRONS FROM CENTER OF CORE
A. Specimen 1BW8

FIGURE 16. MICROPROBE ANALYSIS OF BORON FILAMENT CORES

d. Microprobe Analysis of Boron Filaments Differing in Electrical Resistance

Two filaments designated 13BW7 and 13BW1 were reported by General Electric to have resistance of 998 ohms and 6030 ohms, respectively, for equivalent 14 in. lengths. Microprobe and metallographic analyses were performed on these filaments to determine the presence of chemical or physical differences which might be associated with the 6 to 1 difference in resistance.

Sample preparation was comprised of loading a cluster of five to nine 1/4 in. lengths of each filament in a 1/64th in. diameter hole drilled in a pre-pressed copper filled lucite metallurgical mount. By pressing a second time, the filaments were then bonded into the mount and suitable for polishing. Rough grinding was done with SiC and intermediate polishing with 6 micron diamond followed with 1 micron diamond for the final finishes.

To facilitate charge removal during electron impingement in the microprobe, conducting films (500Å) of carbon or aluminum were vapor deposited on the surface of the samples and standards. Carbon was first used and later abandoned in favor of aluminum. Carbon appeared to be displaced by the beam and did not efficiently remove the charge to ground, resulting in beam wander and poor focus. This problem was measurably reduced by the use of the aluminum coating.

Analysis was performed with an Applied Research Laboratory microprobe, Model EMX. Data were recorded with a multi-channel pulse height analyzer operating as a multi-scaler in which tungsten radiation counting was stored and printed out by typewriter. Operation of the microprobe was set up for step traverses across the tungsten boride cores of the filaments. Steps were in 1 micron intervals with an integration time of 15 seconds at each step. During counting at each step the pulses were stored in the pulse height analyzer and printed out at the conclusion of the traverse. Calibration was performed with tungsten and boron standards, both coated in the vacuum coater with the filament samples to avoid surface absorption anomalies between the standards and the filaments. Quantitative accuracy of the analysis was improved by using the tungsten concentration to determine the composition gradient across the core. Detectability and counting are directly related to the relative masses of the constituents involved, thus the large relative difference between the masses of tungsten and boron (183.86 and 10.82, respectively) strongly favors the tungsten. Although the relative concentrations of tungsten and boron were simultaneously recorded on a step chart, counting and print out with the pulse height analyzer was limited to one element, in this case tungsten. Microprobe operating conditions were 15KV and 50 na with a beam diameter of 3 to 4 microns. Actual spot size of the beam was focused to resolve 1 to 2 micron particles, but during integration sufficient oscillation occurred to give an effective beam diameter 2 to 3 times larger. The results of

typical traverses of the cross section of filaments 13BW7 and 13BW1 are plotted in Figures 17 and 18. Each count at the respective one micron step interval is shown. Repeated traverses across different cross-sections in each filament group failed to reveal a detectable difference in the slopes of the diffusion zones adjacent to the tungsten-boron interface.

Calibration of the tungsten standard both before and after the specimen traverses showed averages of 4450 and 4468 counts per integration interval. Comparing the average of these values with the average counts at the center of the cores of samples 13BW1 and 13BW7, i.e., 3367 and 3715 counts, respectively, gives an uncorrected tungsten concentration of 82 to 83% in each core. This compares favorably with the theoretical value of 87% tungsten in W_2B_5. The interface zone between the boron and W_2B_5 is very steep and allowing for beam diameter is probably 1 to 2 microns thick. Photomicrographs of microprobe traverse paths on filaments 13BW7 and 13BW1 are shown in Figures 19A and 19B. Measurements of the diameters of the cores indicate them to be 17 microns.

Following the microprobe analysis the aluminum coating was removed and photomicrographs were made to ascertain any visual differences between the cores. Figure 20A, filament 13BW7, shows a notch or crack in the core and a slightly thicker interface diffusion zone than filament 13BW1. All nine (9) of the 13BW7 filaments in the mount displayed this characteristic notch. Although optical aberrations occur between the filament core and the boron, the specimens shown in Figure 20 were in the same mount and thus exposed to the same preparation and polishing techniques. This suggests that there may be a real difference in the thickness of the interface diffusion zone and that a scanning electron microscope examination of this zone might pinpoint a plausible reason for the 6 to 1 difference in resistance of 13BW7 and 13BW1 filaments.

e. Conclusion and Recommendations

Changes in the diffusion zone composition and overall width of the tungsten-boride core of boron filaments (boron filaments from different lots and boron filaments exposed to nonmelting high current pulses) were not detectable by microprobe analysis. The relative widths and characteristics of the tungsten boride boron diffusion zones were identified. Core composition appears to be comprised of a 6-7 micron center of W_2B_5 surrounded by a 5 micron diffusion zone of WB_{12} and B. The W/B profile plot (Figure 16) followed the same curve as previously reported[1] and was further verified by analyzing a specimen from the previous effort (Panel 26). The results and characteristics of the filaments examined in this work may be useful for future identification of variation between lots of boron filaments.

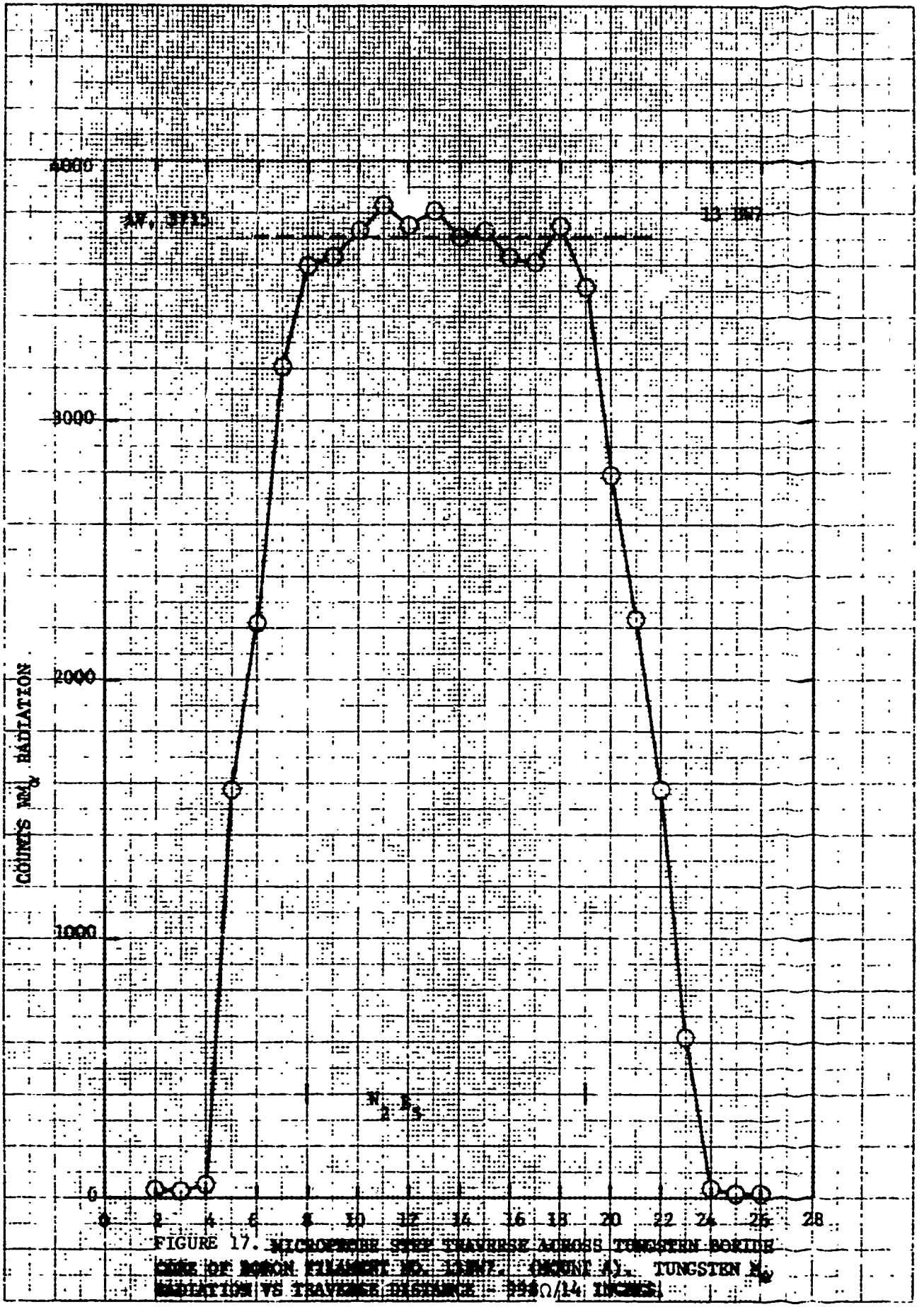

FIGURE 17. MICROPROBE STEP TRAVERSE ACROSS TUNGSTEN BORIDE CORE OF BORON FILAMENT NO. 11BM2, (MOUNT A). TUNGSTEN M_β RADIATION VS TRAVERSE DISTANCE - 996Ω/14 INCHES.

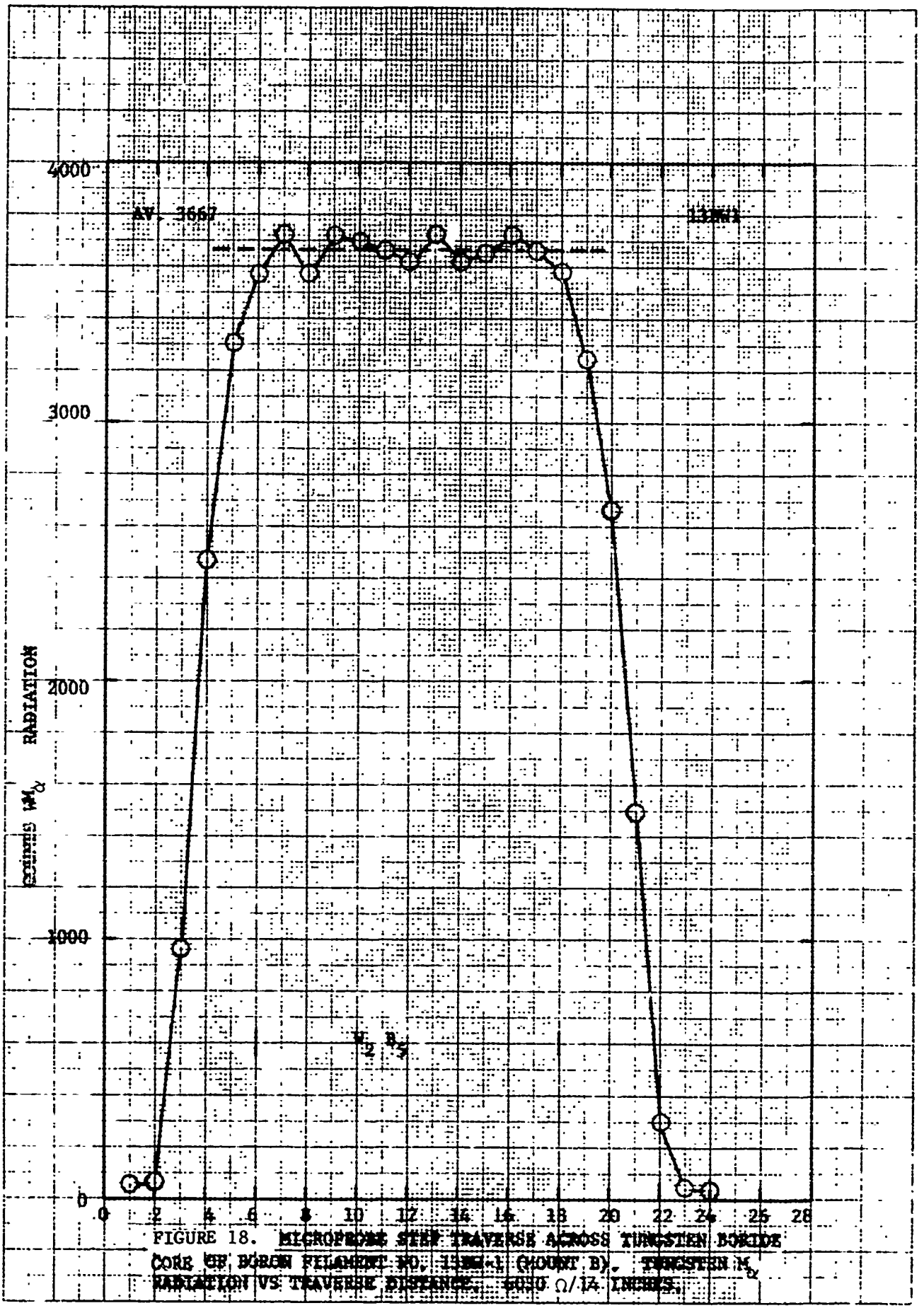

FIGURE 18. MICROPROBE STEP TRAVERSE ACROSS TUNGSTEN BORIDE CORE OF BORON FILAMENT NO. 1336-1 (MOUNT B). TUNGSTEN M_α RADIATION VS TRAVERSE DISTANCE. 4030 Ω/14 INCHES.

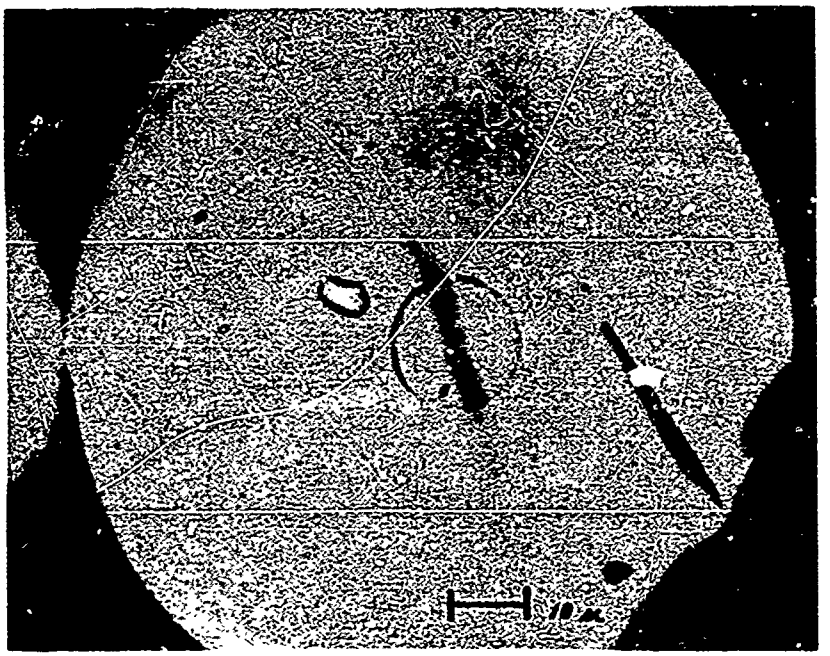

A. BORON FILAMENT 13BW7

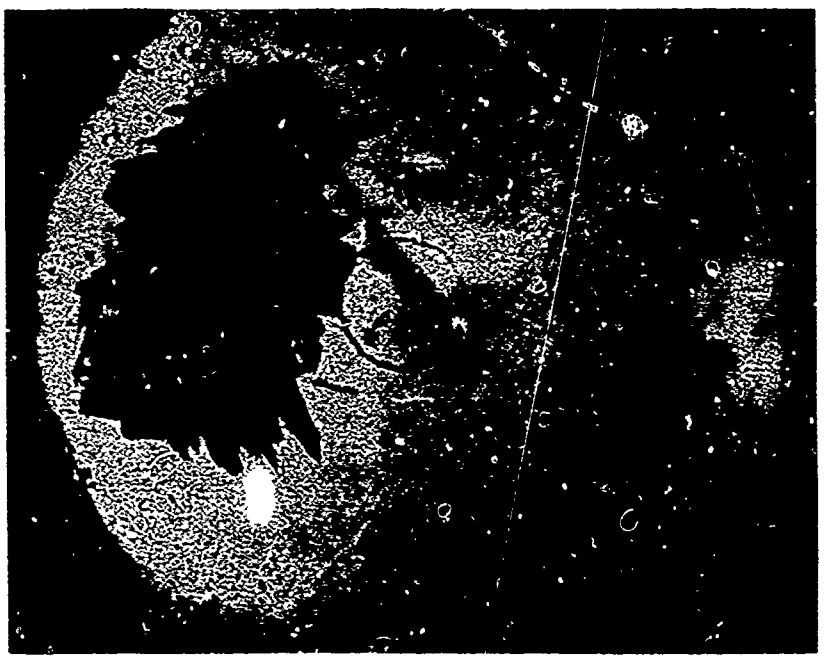

B. BORON FILAMENT 13BW1

FIGURE 19. MICROPROBE TRACKS ON TUNGSTEN BORIDE CORES OF BORON FILAMENTS 13BW1 AND 13BW7. AVERAGE DIAMETERS OF CORES ARE 17 MICRONS - BEAM WIDTH, 3-4 MICRONS. VAPOR COATED WITH 500Å ALUMINUM.

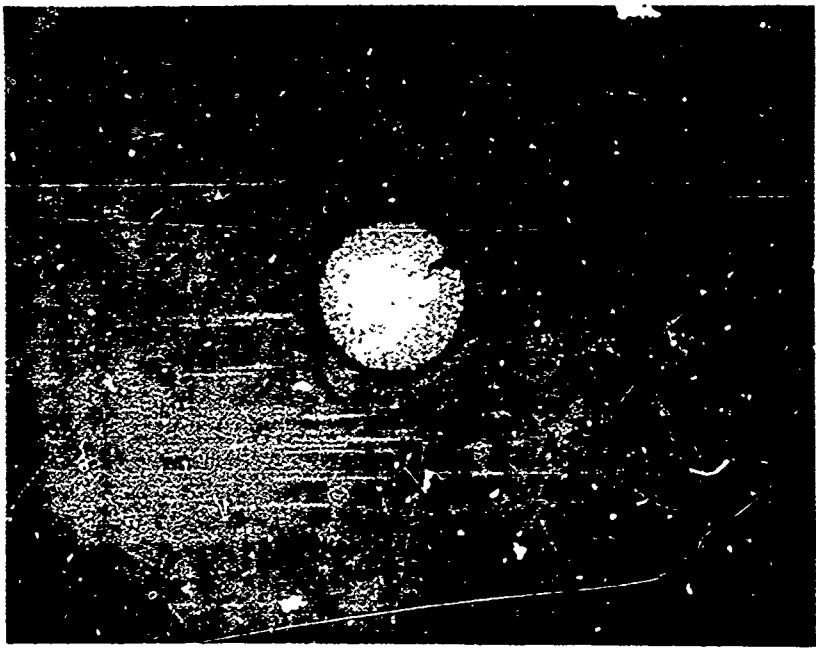

A. BORON FILAMENT 13BW7

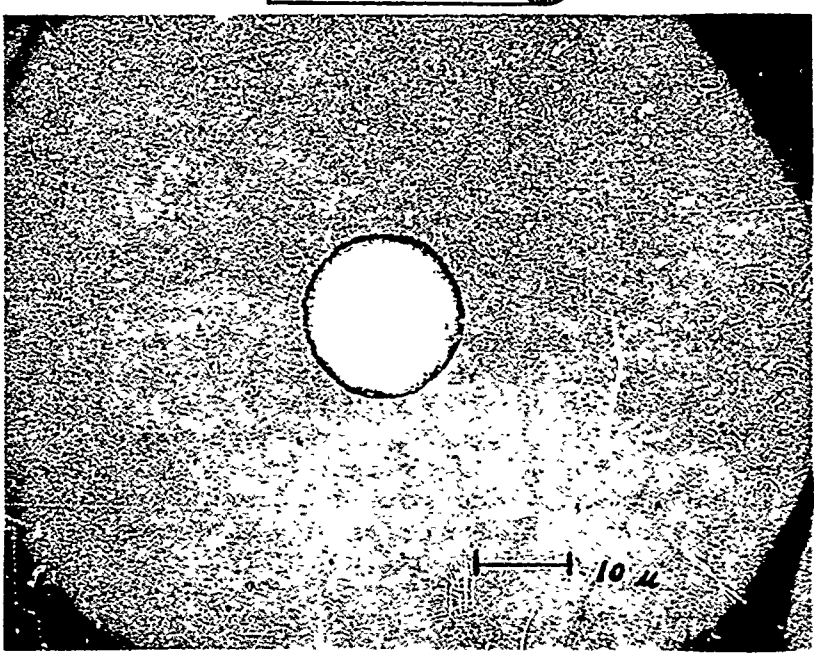

B. BORON FILAMENT 13BW1

FIGURE 20. TUNGSTEN BORIDE CORES OF BORON FILAMENTS 13BW7 AND 13BW1. ETCHED 1 TO 2 SECONDS WITH DILUTE MURIKAMI ETCHANT (5 gm $K_3Fe(CN)_6$, 5 gm KOH, 100 ml H_2O).

2.4.3 PHYSICAL FACTORS REGARDING BORON FILAMENT ELECTRICAL CONDUCTION

It has long been observed that boron filaments, due to their very high stiffness and brittle behavior, are highly susceptible to breaking. When boron filament reinforced plastic composites are trimmed or machined to size, the filaments that intersect the cut surface are not cut in a smooth plane. Instesd, the mechanism whereby the filaments are parted move by a chipping mode. This was quite evident in the initial investigations in the prior program[1] wherein special care was required to prepare photomicrographic mounts of boron filaments. To eliminate the ragged, broken ends of boron filaments that result from machining the boron filament composites, it was necessary to proceed through several series of different grit sizes in polishing the photomicrographic mounts.

Because of the above observations it was suspected that the condition of the boron filament ends on the cut or machined edges of boron filament composites could materially affect the ability of electric current to enter the filaments. In other words, if the conditions of the filament ends vary significantly, the electric current may more readily enter the core of some filaments than of others. Note: In boron filaments only the tungsten boride core conducts the electricity.[1] To investigate this hypothesis a conventionally edge machined boron filament epoxy composite was inspected using a scanning electron microscope (SEM). To better observe the condition of the filament ends on the machined edge, the epoxy resin was carefully vapor honed away to expose the filament ends for improved visibility. A representative SEM picture is shown in Figure 21. As can be seen, the various filament ends are ragged and chipped. Also, the cores of some filaments, like the one in the center of the picture, are much more exposed.

The filament end conditions observed in Figure 21 would in fact permit electric current to enter the filament ends with exposed center cores more readily. In some cases it was also observed the filament cores not only are not exposed but are broken off back inside the boron shell, thereby presenting difficulty for electric current entry. In this program all boron filament composite ends were coated with nickel to try to insure improved electric current coupling to the filament ends, but it is likely that this was not completely effective in equalizing the resistive gap to filament ends. It is therefore concluded that perhaps the major cause of apparent variations in boron filament conductivity or resistivity is due to the conditions of filament ends, which results in wide variations in resistive gaps when electric coupling is attempted.

2.4.4 DAMAGE INSPECTION OF ELECTRICALLY EXPOSED BORON FILAMENTS

In the prior program[1] and as previously mentioned in the introduction to Section 2.4, it has been observed that boron filament epoxy composites that have been degraded by electric current contain some filaments that are

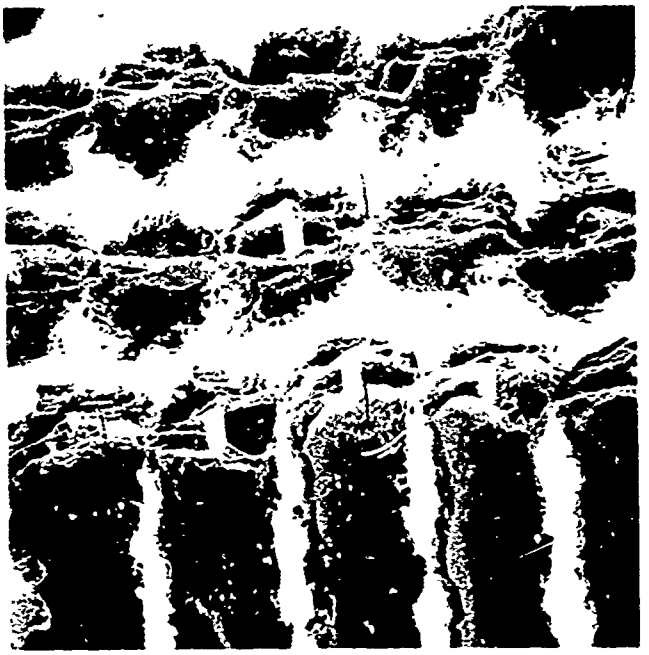

FIGURE 21. SCANNING ELECTRON MICROSCOPE VIEW OF THE CONDITION OF BORON FILAMENT ENDS ON MACHINED EDGE OF A BORON FILAMENT EPOXY COMPOSITE. (20CX)

cracked and some that are not. The photomicrographic studies illustrated that the proportion of the number of filaments with radial cracks was higher in more severely degraded composites. These observations contributed to the suspicion that that is considerable variation in the conductivity of boron filaments within the composites, with the higher conductivity filaments carrying current and being damaged. This would be true only if the cracks in filaments are not local. In other words, is a filament that is observed to be cracked at one point in the composite also cracked at other points along its length, or are all filaments cracked locally at different points along their length? Attempts to trace single filaments in the prior program[1] micrographically along their lengths in a composite were not successful. Also, such observations were not possible in single boron filament electrical exposures. At a point where any cracking occurred in the absence of a confining plastic matrix the filaments would fall apart into a multitude of fine pieces. Therefore, in order to prevent this filament disarray, it was decided to encapsulate individual boron filaments within a resinous sheath. The embedment of the filament in a resin casting was to prevent any displacement of individual pieces caused by electrical degradation and to allow photomicrographs to be made along the length in order to determine if the damage is of a continuous or a local nature. Twenty-two boron filaments from two manufacturing lots of filaments were

encased within a plastic casting by centering each filament within a thermoplastic soda straw. After closing one end, the straw was filled with a mixture of epoxy and polyamide resins (50-50 mixture of Epon 828 and Versamid 140), cured at room temperature and removed from the straw. The embedded filament specimen configuration was 7 in. in length, 0.20 in. diameter with a free end of the filament 3/4 in. in length protruding from each end of the casting. Specimens EB1 through EB9 were taken from lot No. HS3-658, and EB10 through EB22 were from lot No. HS6-688. The specimens were exposed to 5, 8, and 10 x 10^4 amps/cm^2 (3 x 24μsec. waveform) based on the cross-sectional area as given in Appendix Table IX. Specimens from each series were mounted, polished, and photomicrographed at three positions along the length of the fiber (1/4 in., 2 in., and 4 in. from one end) in order to ascertain the severity and location of the degraded areas in the filament. Representative photomicrographs from each group are shown in Figures 22, 23, and 24. The specimen in Figure 22 which was exposed to 5.0 x 10^4 amps/cm^2 of filament cross-sectional area had axial cracking present at the 2 in. and 4 in. position but not at the 1/4 in. position. The specimen in Figure 23 which was exposed to 8.0 x 10^4 amps/cm^2 of filament cross-sectional area was cracked at all three locations (1/4 in., 2 in., and 4 in.) and the degradation (axial cracks) were more severe than was seen in the specimen in Figure 22 which was exposed to a lower current test. The specimen in Figure 24 which was exposed to 10.0 x 10^4 amps/cm^2 of filament cross-sectional area was cracked at all three locations and was the most severely degraded of all three specimens. The photomicrographs clearly indicate the following:

(1) The degradation is directly related to the injection current level.

(2) The boron filament (degraded by the passage of electrical current) is characterized by circumferential and axial cracking of the tungsten core and the boron shell.

(3) The degradation appears to be of a local nature (Figure 22) at lower levels of damaging current flow and may appear at weak locations of the specimens.

(4) The degradation appears to be continuous along the filament length (Figures 23 and 24) for those specimens which have been exposed to higher current injection levels.

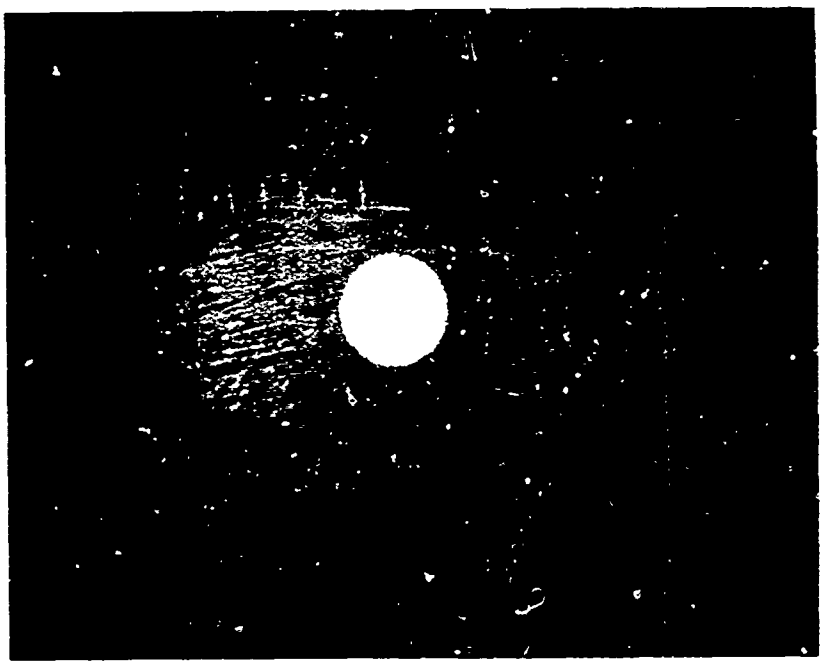

A. (800X)

B. (800X)

FIGURE 22. SPECIMEN NO. 22 - BORON FILAMENT AFTER EXPOSURE TO 5.0×10^4 AMPS/CM^2 ELECTRIC CURRENT INTENSITY (A = cross-sectional view 1/4 inch from filament end; B = cross-sectional view of 2 inches from filament end) (Continued on page 2-46)

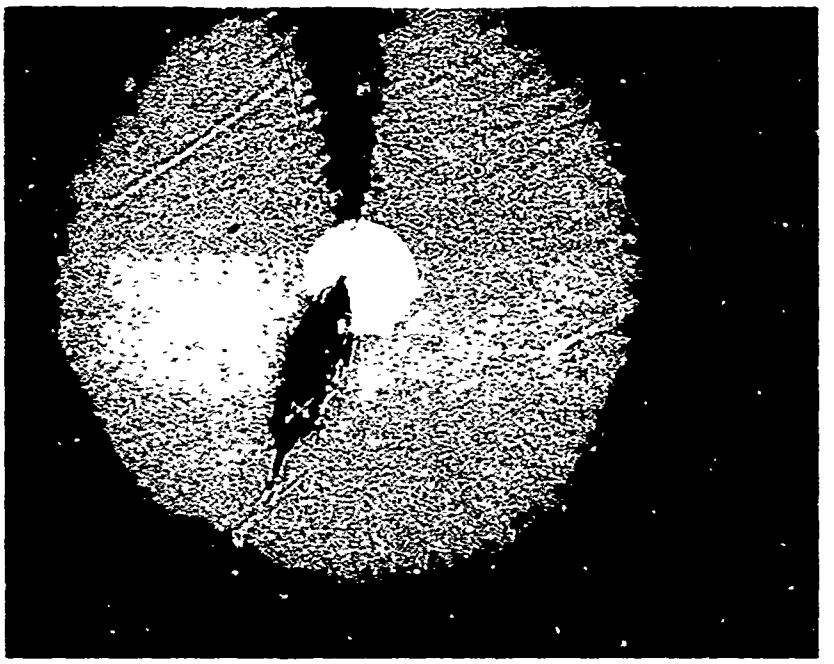

C. (800X)

FIGURE 22. SPECIMEN NO. 22 - BORON FILAMENT AFTER EXPOSURE TO 5.0×10^4 AMPS/CM^2 ELECTRIC CURRENT INTENSITY (C = cross-sectional view 4 inches from filament end)

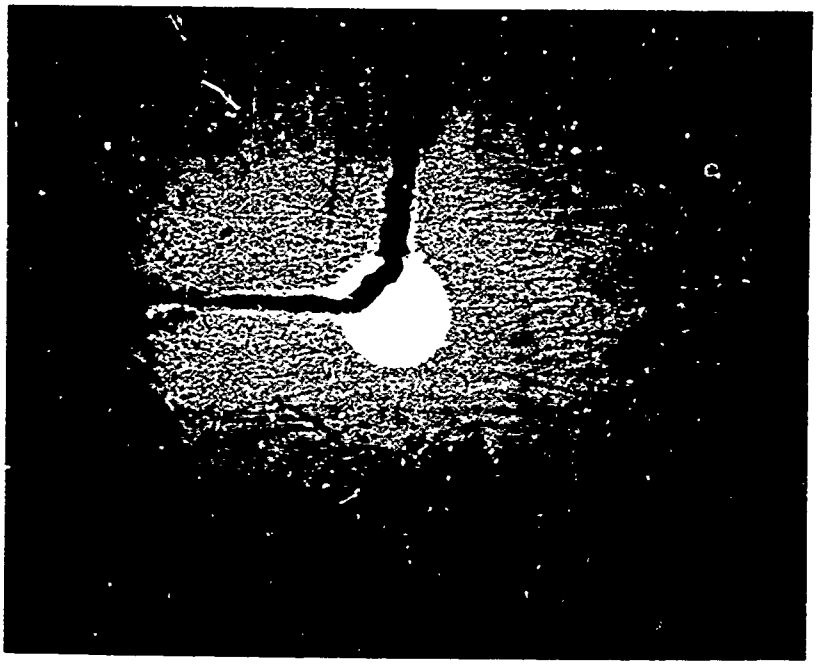

A. (800X)

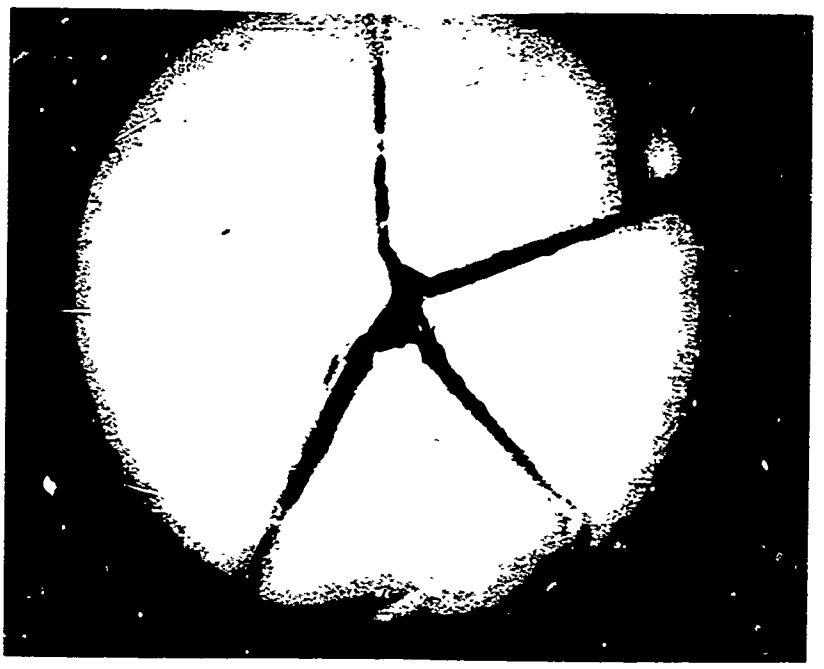

B. (800X)

FIGURE 23. SPECIMEN NO. 23 - BORON FILAMENT AFTER EXPOSURE TO 8.0×10^4 AMPS/CM^2 ELECTRIC CURRENT INTENSITY (A = cross-sectional view 1/4 inch from filament end; B = cross-sectional view 2 inches from filament end) (Continued on page 2-48)

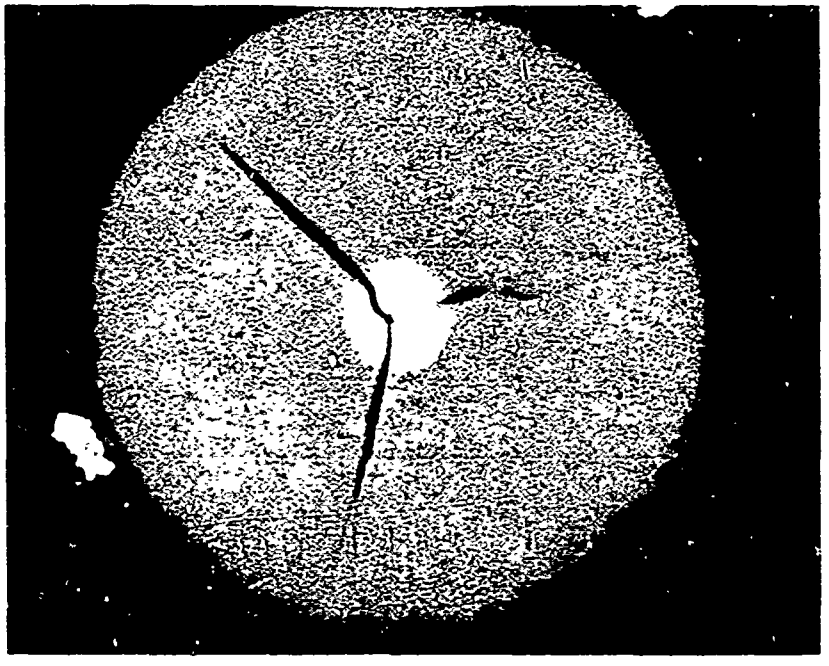

C. (800X)

FIGURE 23. SPECIMEN NO. 23 - BORON FILAMENT AFTER EXPOSURE TO 8.0×10^4 AMPS/CM^2 ELECTRIC CURRENT INTENSITY (C = cross-sectional view 4 inches from filament end)

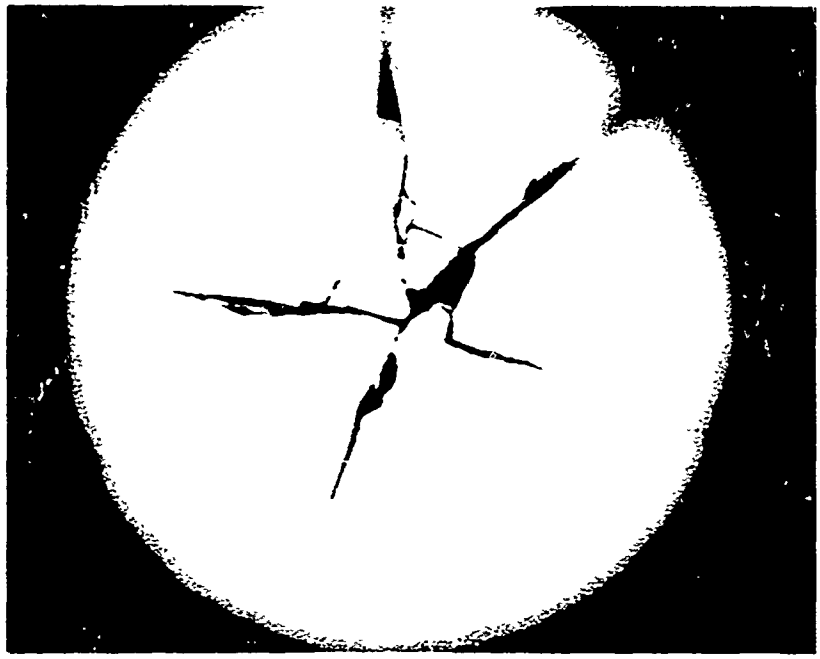

A. (800X)

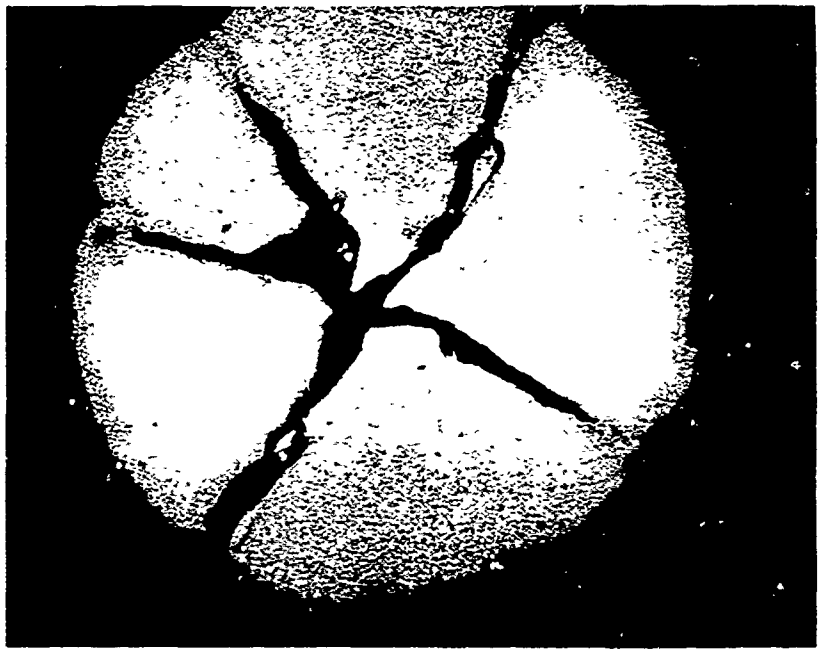

B. (800X)

FIGURE 24. BORON FILAMENT AFTER EXPOSURE TO 10.0 x 10^4 AMPS/CM^2 ELECTRIC CURRENT INTENSITIES (A = cross-sectional view 1/4 inch from filament end; B = cross-sectional view 2 inches from filament end) (Continued on page 2-50)

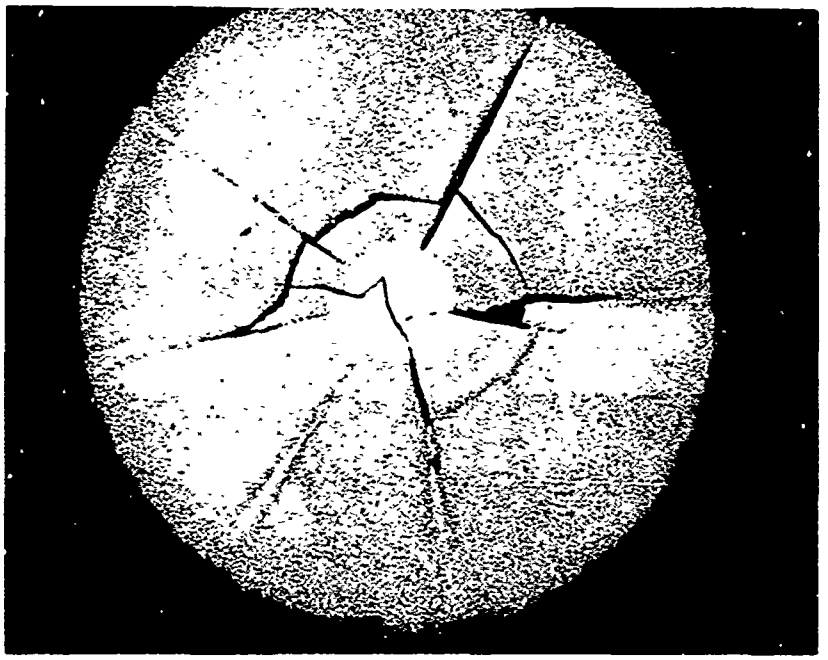

C. (800X)

FIGURE 24. BORON FILAMENT AFTER EXPOSURE TO 10.0×10^4 AMPS/CM^2 ELECTRIC CURRENT INTENSITIES (C = cross-sectional view 4 inches from filament end)

2.5 TASK V - VARIATIONS IN GRAPHITE FILAMENT CHEMISTRY AND CRYSTALLITE STRUCTURE AS RELATED TO ELECTRICAL CONDUCTIVITY

In the previous N00019-70-C-0073 program,[1] it was noted that the resistivity of graphite filaments varied from one type to another. Specifically, the polyacrylonitrile precursor Courtaulds HM-S filaments had a lower resistivity than did the rayon precursor HITCO HMG-50 filaments. Because of its lower resistivity and resulting lower resistive energy dissipations, it was experimentally demonstrated that the HM-S filaments resulted in epoxy matrix composites with slightly higher electric current degradation thresholds than composites made of HMG-50 filaments. It was theorized that the resistivity is reduced by a higher order of graphite filament orientations parallel to the filament axis. Such high order of orientation is known also to produce a higher elastic modulus in the filaments. It has also been shown that the Courtaulds HM-S has a slightly higher elastic modulus (55-60 x 10^6 psi) than the HITCO HMG-50 (50 x 10^6 psi) which in itself is an indication that it does in fact have a higher order of orientation and would, as will be shown, also possess a lower resistivity.

Processing conditions such as temperature of processing control the degree of order of graphite filaments. To experimentally determine the effect of degree of order on electrical properties, polyacrylonitrile precursor graphite filaments were obtained from Whittaker-Morgan Inc. with the ranges of temperature of processing indicated in Table IV.

TABLE IV

PROCESSING TEMPERATURE OF PRECURSOR FILAMENTS

Temperature, °C	Identification Numbered Section	Weight (gms) per Linear Yard
1,000° - 1,400°	21	0.8894
1,500° ± 100°	22	0.8669
1,700° ± 75°	23	0.8788
1,900° ± 20°	24	0.8524

A 3 foot section was taken from the beginning of each numbered section. Fiber weight per linear yard was determined, and two 15 in. specimens from each section were sent to General Electric. Eight specimens of the heat treated graphite were subjected to single current pulse injections in the range of 12.5 amps/cm^2 of filament cross-section as recorded in Appendix Table I. Resistivity, measured before and after current injection, showed no change in value.

The remaining 6 in. piece of each section was retained at Philco-Ford and the diffraction pattern of each group studied by X-ray diffraction analysis to determine any variations in crystallinity and its influence on the electrical properties. For purposes of comparison, X-ray diffraction studies were also made of graphite filaments with a reported high order of crystallite orientation (Thornel 75S), a sample of natural graphite, and a purified spectral grade of graphite (Union Carbide SP-2). The purpose of the X-ray diffraction study was to determine differences that could occur in each of the processing temperature ranges with respect to modifications of the graphitic structure of the filaments. Filament specimens were prepared by first cutting sections approximately 0.10 in. long from tow bundles. They were then ground with an alumina mortar and pestle. The powders were placed on glass slides and flattened down next to a shim to produce thin smoothly packaged sample surfaces whose depths measured 127 microns, or 5 mils. Keeping samples to this thickness lessened the effects of absorption and scattering which produce X-ray line broadening. Noticeable during sample preparation was the absence of any graphitic "grease" and sheen characteristics inherent in graphite when it is powdered in this manner.

Samplings were run on a Norelco X-ray diffractometer-goniometer unit set at 1° 2θ scanning speed using copper Kα radiation with 1° scatter and receiving slits. Each specimen was scanned from 16° to 33° 2θ and the (002) lines were corrected for scatter and background to determine diffraction line maximums which indicate the "d" spacings of each.

The first three samples, Natural Graphite, Union Carbide SP-2 Graphite, and Thornel 75S produced reflections for (002), (100), (101), and (004) planes, whereas the filaments with different ranges of processing temperatures produced (002) basal reflections only, which were broad and diffused.

Klug and Alexander[3] state, "In the event of truly random orientations of two dimensional layers, no (001) reflections would be produced, but in the great majority of cases the layers tend to stack together into parallel-layer groups. These pseudo-crystallites possess no interlayer order other than the parallelism and degree of separation into layers. Such groups give rise to more or less diffuse (001) reflections because of the limited number of layers and also, in some cases, because of a lack of constancy of the interlayer spacing. The mean dimension of a parallel-layer group perpendicular to the layers can be calculated from the breadth of the (001) reflection by employing Scherrer's equation

$$D_{hkl} = \frac{0.9\lambda}{\beta_{\frac{1}{2}} \cos \theta} \text{ ".}$$

The calculations showing crystallite dimensions are contained in the last column of Table V. Steward and Davidson[4] state, "In graphitic carbons, it appears to be well established (from independent works by Bacon, Franklin and Housha) that the observed interlayer spacing is a mean between the value of 3.354Å for pairs of planes with the graphite relation, and 3.44Å corresponding to pairs with random orientation. In the materials which show no development of three-dimensional ordering, interlayer spacings greater than 3.44Å exist." Also, "there is some correlation for the carbon blacks between particle size and maximum observed crystal dimensions." The relationships can be seen in Table V between the HT6-3 through 6-12 filaments by comparing their processing temperatures, "d" spacing values (or unit cell c_o values), and crystallite diameters. As temperatures increase, "d" spacings decrease and crystallites become larger.

Degrees of order in graphitization of each specimen were established from a graphic solution established from work done by Mering and Maire,[5] and Franklin[6] in which models were proposed by each of the authors and curves established to determine degrees of order-disorder in graphitized carbon.

Slight modifications of structural factors have been shown, and tendencies toward graphitization resulted from the different temperature runs of graphite filaments. All four of the processing temperature controlled filament samples are non-ordered carbon with a pseudo-layer structure only. Even though there was no ordering evident in the process temperature controlled specimens, the electrical conductivity of the higher temperature processed fiber was greatest. For instance, as seen in the Appendix Table I specimen 24 which had been processed to 1900°C had a resistivity of 1.1×10^{-3} ohm-cm as compared to 1.4×10^{-3} ohm-cm for specimen 21 which had been processed to only 1000-1400°C. This indicates that even though there was no ordering, there must have been more connected carbon in the higher temperature processed filaments. The Thornel 75 reference fiber, as shown in Table V, had 19% ordering of the carbon structure. Also, as seen in the Appendix Table I it had, as would be expected, a resistivity of 0.9×10^{-3} ohm-cm, which was lower than the filament specimens with no ordered structure.

2.6 TASK VI - DAMAGE THRESHOLDS OF ADDITIONAL TYPES OF GRAPHITE FILAMENT COMPOSITES

Since the initiation of the previous program, two additional graphite filament types are being utilized extensively in aircraft structural composite applications. These two filament types, Modmor II and Thornel 75S, are expected to possess electrical characteristics different than those of the HMG-50 and HM-S filaments previously investigated and, therefore, were investigated as to electric characteristics and composite degradation due to high intensity electric current flow.

TABLE V

X-RAY DIFFRACTION ANALYSIS RESULTS

Sample	Heat Treat Temp., °C	"d" Spacing (0002) - Å	Unit Cell C_o - Å	Degree of Order - %	(0002) Half-Height-Breadth Degrees 2 θ	Crystallite Size - Å ⊥ (001)
Natural Graphite		3.358	6.716	90	0.25	1,000+
UCC SP-2 Lot T-6 Spectrographic Grade		3.370	6.740	66	0.40	470
Thornel 75		3.411	6.822	19	1.45	60
21	1,000-1,400	3.524	7.048	0	5.50	15
22	1,500 ± 100	3.510	7.020	0	5.10	17
23	1,700 ± 75	3.490	6.980	0	4.65	18
24	1,900 ± 20	3.490	6.980	0	3.85	22

The Modmor II filaments are of the same polyacrylonitrile precursor as the Courtaulds HM-S; however, the thermal processing conditions are different so as to produce a higher strength and lower modulus filament (350,000 psi and 40 x 10^6 psi) than the Courtaulds HM-S (285,000 psi and 55 x 10^6 psi). This then would represent a lower order of graphite crystallite orientation which also should correspond to a higher resistivity.

Thornel 75S represents a new graphite filament type that is both higher strength and higher stiffness than the HMG-50 and HM-S filaments tested in the previous program. As indicated by its higher modulus, it has a higher order of crystallite orientation along the filament axis. Therefore, it would be expected that its resistivity would be lower and the damage threshold of composites higher.

Filament tow and yarn mounts were prepared of Modmor II and Thornel 75S as was done in the prior program. The data obtained for the Thornel 75S and Modmor II filament current injection tests are presented in Appendix Table I. The lower resistivity value for Thornel 75S yarn indicates that this filament does possess a higher order of graphitic crystallite orientation. This higher order of orientation was also confirmed by X-ray diffraction analysis as discussed in Section 2.5. The resistivity values measured from "before-after" exposed specimens were not changed by the influence of electrical current passage through either of the two graphitic filaments. The tensile strengths of filament specimens (within one set of test specimens) were too erratic in value to establish a precise degradation value due to electrical exposure.

Fifty each Thornel 75S DEN 438 MNA epoxy and Modmor II 1004 epoxy matrix composite tensile specimens of 0.020 to 0.025 in. thickness (5 ply) x 0.10 in. in width x 7 in. in length were prepared with ends scarfed, vapor honed, and nickel plated for electrical contact. The filament volume was 50-55%. The fabrication procedure was conventional, as used previously.[1]

The data obtained in the current injection tests for Thornel 75S and Modmor II graphite filament composites are tabulated in Appendix Table IV and V. The tensile strength results for Thornel 75S (Appendix Table VII) show that composite degradation is evident at current injection levels of 43 x 10^4 amps/cm^2 of filament cross-section, where burning was initiated. Visual evidence of this degradation is presented in Figure 25 for Thornel 75S/epoxy tensile specimens which were exposed to three levels of current injection (43, 63, and 100 x 10^4 amps/cm^2 of filament cross-section area with a 3 x 26 μsec. waveform). All three of the current injection levels produced extensive damage to the specimens and tensile strength degradation (Appendix Table IV); however, for all practical purposes, all structural integrity is lost at the 43 x 10^4 amps/cm^2 level where burning is first initiated.

FIGURE 25. EFFECT OF HIGH INTENSITY ELECTRIC CURRENT FLOW ON THORNEL 75S/EPOXY COMPOSITES (3 X 26 μSEC. WAVEFORM)

T-75-T-36 and -37 exposed to 43 x 10^4 amps/cm^2 of filament cross-sectional area
T-75-T-33 exposed to 63 amps/cm^2 of filament cross-sectional area
T-75-T-49 and -46 exposed to 100 amps/cm^2 of filament cross-sectional area

It should be noted that the tensile values which are reported in Appendix Table IV for those specimens in which the injected current level has produced resin pyrolysis actually represent only the strength of the fiber and the partially pyrolyzed matrix at the most degraded cross-sectional area. This reduction in strength is more accurately reflected in Appendix Table VII in which these specimens are reported as 100% degraded.

The data for the Modmor II/1004 tensile specimens is recorded in Appendix Table V. Injection testing produced similar damage as that obtained with the Thornel 75S tensile specimen (resin pyrolysis and catastrophic delamination at degradation current levels). As noted in Appendix Table VII, burning was initiated at an injected current level of 46×10^4 amps/cm^2 of filament cross-section (3 x 26μsec. waveform).

Photographs of the exposed Modmor II/1004 specimens are presented in Figure 26, tensile strength in Appendix Table V, and percent tensile strength degradation in Appendix Table VII. As was the case with the Thornel 75S specimens, the tensile strength values reported in Appendix Table V for the Modmor II/1004 specimens where burned (as noted in Appendix Table VII) would more accurately be referred to as 100% degradation since the tensile strengths reported in Appendix Table V for burned specimens are actually only due to the fibers. Once the resin begins to pyrolyze, all structural integrity is lost.

2.7 TASK VII - ACOUSTIC EMISSION AS AN INDICATOR OF ELECTRICAL CURRENT PRODUCED DEGRADATION

Acoustic emission has been shown to be directly relatable to the mechanical properties of some materials and can, therefore, be used to detect micromechanical or microstructural changes with high sensitivity. Subjecting a material to a state of stress produces deformation and fracture processes which generate the stress waves that have been termed acoustic emission. Detectable emissions occur even at low stress levels. These internal processes include (for fiber reinforced composites) fiber fracture, matrix fracture, fiber debonding, and delamination. These processes are irreversible since permanent degradation of the fibers or laminates has occurred. Hence, when loading is reapplied, acoustic energy is not emitted until the stress in the material exceeds the previous level.

Due to this irreversible nature, acoustic emission can be used nondestructively to determine structural degradation in fiber reinforced composites. Composite panels which have been subjected to high energy impulse electric current loading and as a result have suffered internal fiber or structural weakening were expected to emit such acoustic type stress waves at a much lower loading than an undamaged panel. Hence, it was suggested that by comparing the acoustic emission of degraded and non-degraded panels at stress levels far below the ultimate failure threshold of the composite, structural degradation

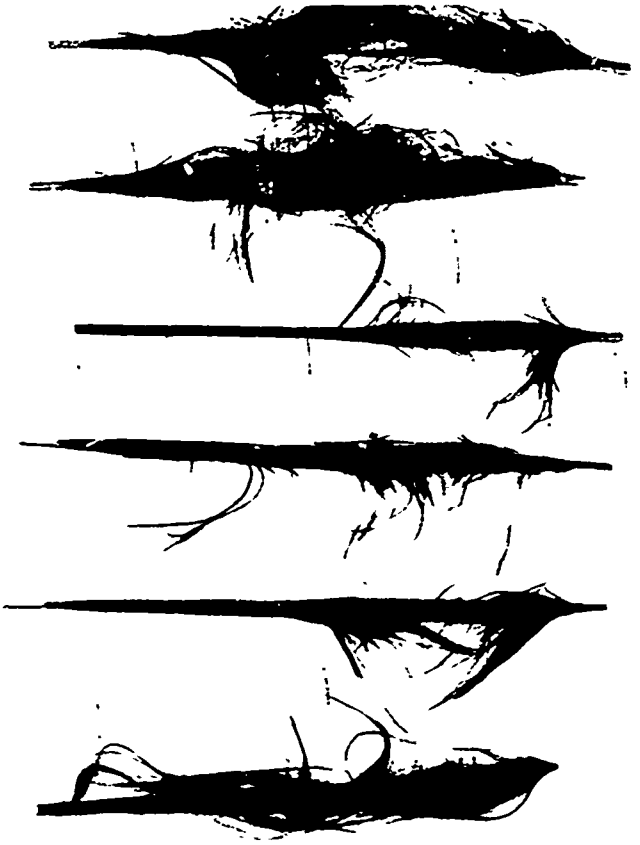

FIGURE 26. EFFECT OF HIGH INTENSITY ELECTRIC CURRENT FLOW ON MODMOR II/EPOXY COMPOSITES (3 x 26μSEC WAVEFORM)

Specimens have been exposed to current levels from 46×10^4 to 66×10^4 amps/cm^2 of filament cross-sectional area.

in the damaged panel could be characterized or identified as to degree of degradation. This then would represent a useful non-destructive research tool. Such a tool might prove useful in order to non-destructively evaluate composite panels that are suspected of being damaged due to high intensity electric currents from lightning strikes.

For this investigation a series of unidirectional boron filament epoxy composite flexural specimens were prepared. The specimens were prepared in the conventional autoclave cure manner using the 3M SP-272 boron filament epoxy tape with 104 glass scrim cloth spearating each layer of the 0.004 in. diameter boron filaments. Each specimen was 0.5 in. wide by 0.1 in. thick by 6 in. in length. To provide electrical contact, the ends of each specimen were scarfed, vapor honed, and nickel plated. Also, to prevent electrical flashover along the cut specimen edges where filaments are exposed, the edges were coated with epoxy resin.

As shown in Table VI of the Appendix, five groups of flexural specimens were so prepared. One group was not electrically exposed to serve as a control. The other four groups, respectively, were exposed to current intensities of 5.7×10^4, 8×10^4, 10×10^4, and 12×10^4 amps per cm^2 of filament cross-section with a waveform shape of 3 x 24 microseconds (rise time x tail time). Prior to acoustic emission tests, one specimen of each group was tested in flexure to determine if damage in fact had been created. All flexural test results are also shown in Table VI of the Appendix. The acoustic emission test results are summarized in Table X in the Appendix. All specimens were loaded in three point bending over a span of 3.75 in. with a contact radius of 0.125 in. The head speed was 0.20 in./min. One specimen from each electric current exposure level and two control specimens were unloaded and reloaded to failure. The significance of these experiments are discussed later. The acoustic emission transducer was taped to the three point bending fixture; silicone grease was used to insure good acoustic coupling. Total acoustic emission, acoustic emission count rate, and load were recorded for each test. The acoustic emissions were measured with a Dunegan Research Corporation Acoustic Emission Instrumentation System. The acoustic measurements were made by representatives of General Research Corporation, Effects Technology Inc. Subsidiary.

The acoustic emission as a function of percentage of flexure strength is plotted for each specimen tested in Figures 1 through 5 in the Appendix. The results are summarized in Figure 27 to show the range of acoustic emission as a function of electric current exposure and stress. The considerable scatter in the data is probably due mostly to material variation. Although there is overlap between the ranges of data for the two lowest current exposures and the unexposed material, the results definitely show acoustic emission occurring at lower applied stress as the current exposure is increased. The material strength is strongly affected by current exposure; however, the total acoustic emission to failure is not a strong function of current exposure.

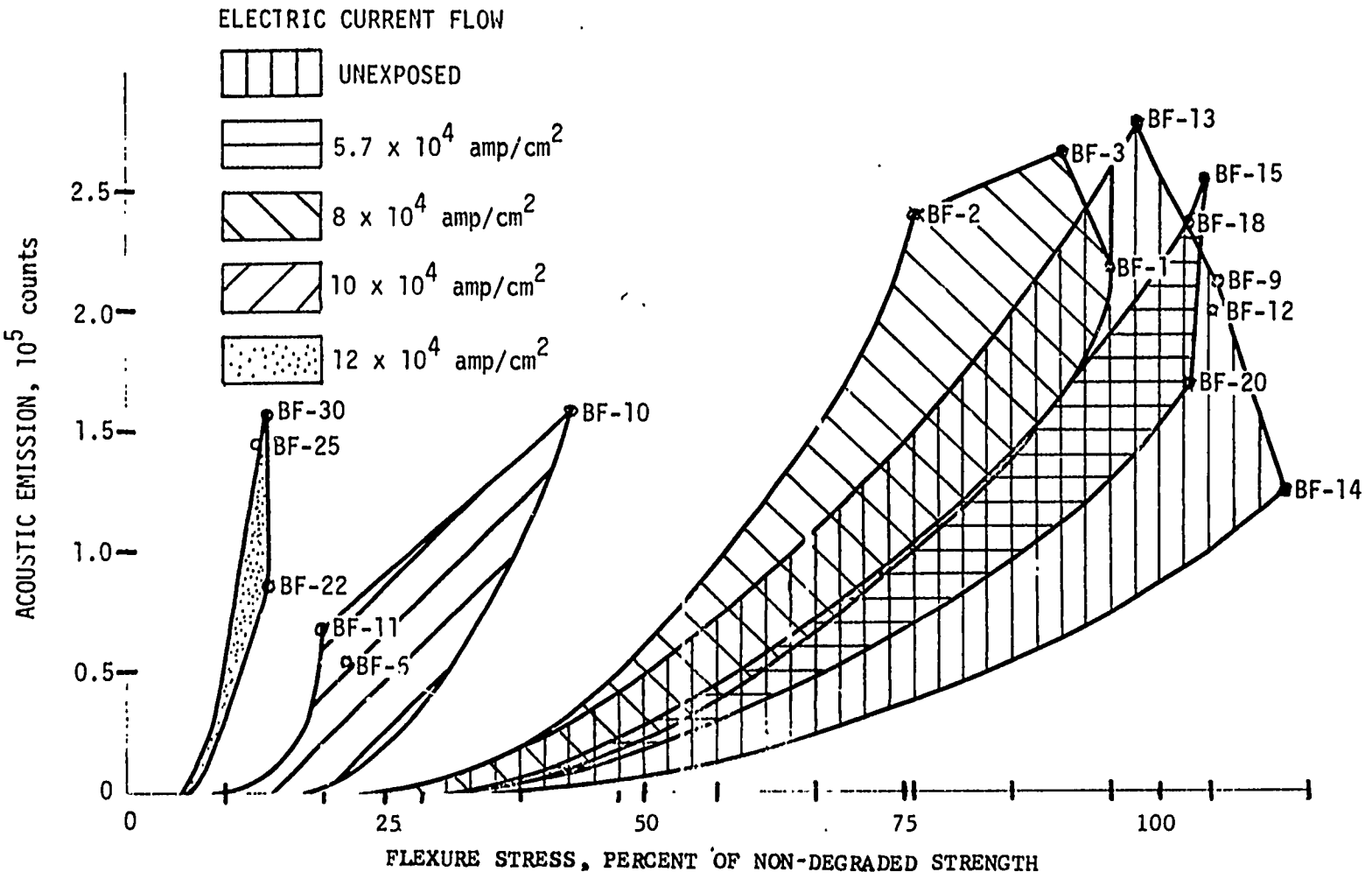

FIGURE 27. SUMMARY OF ACOUSTIC EMISSION OF BORON EPOXY COMPOSITES EXPOSED TO INTENSE ELECTRIC CURRENT FLOW

As can be seen from Figure 27, the specimens exposed to a current intensity of 5.7×10^4 amps/cm^2 did not show any more loss in tensile strength or change in acoustic emission as compared to the unexposed control specimens. The specimens exposed to an 8×10^4 amps/cm^2 current intensity, however, showed slightly reduced flexure strength and slightly increased acoustic emission at lower stress levels. It is then apparent that the threshold for boron filament damage had been exceeded at the 8×10^4 amps/cm^2 exposure level. This fact checks out with previous data reported in this program. As can also be seen, the 10×10^4 and 12×10^4 amps/cm^2 exposures produced degraded composites with even lower flexure strengths and even higher acoustic emissions at lower stress levels.

There was considerably more scatter in the acoustic emission count rate data than in the total acoustic emission data. Thus, no correlation could be found between the acoustic emission count rate and the current exposure level with the limited amount of data from this study.

A control specimen and one specimen from each current exposure level was unloaded prior to failure and then reloaded to failure. Another control sample was unloaded and reloaded several times prior to failure. In each case the "Kaiser effect" was displayed, wherein no new acoustic emission was observed until the load was returned to the point of unloading. This is shown by the horizontal lines in Figures 1 through 5 in the Appendix. In some cases a slight change was noted in the curvature of the acoustic emission versus bending load after reloading.

In conclusion, the objectives of this limited testing program were achieved. The acoustic emission activity of the boron epoxy composites was strongly influenced by the current exposure level and degree of resulting filament degradation. Thus, a structure could be evaluated for possible degradation caused by intense current flow by monitoring the acoustic emission at low applied loads. By comparison of the data with "calibration" data as from this testing program, the degree of degradation could be determined without loading the structure to failure. Further work would be needed, however, to ascertain the utility of monitoring the acoustic emission count rate as an additional indicator of the material property degradation.

2.8 TASK VIII - INVESTIGATION OF DEGRADATION LIMITING TECHNIQUES

Lightweight composite materials offer many advantages to an aircraft designer and as confidence in their reliability are established their use will become more commonplace. However, their vulnerability to lightning strike damage must be eliminated or circumvented before such reliability can be established. Two obvious protective devices (electrically conductive coatings and metallic wire screens) have shown considerable promise in minimizing the electrical current induced damage. One disadvantage of an external coating is that the protection afforded could be effective to only a single lightning strike, i.e., if the current were of sufficient magnitude, rupture and vaporization

of the protective coating would leave the composite unprotected in the case of multiple strokes or a later lightning strike. Therefore, it was decided to investigate the protective effects of an aluminum wire mesh screen (incorporated into a boron composite) which was present not only in the external composite surface but was also embedded within the center of the composite thickness.

Ninety conventional 7 in. length boron filament composite tensile specimens were fabricated from 3M's SR-272 boron filament epoxy prepreg and thin aluminum wire mesh screen as follows:

(1) Thirty specimens were composed of four plies of boron filament epoxy with one ply of aluminum screen on the surface of the composite.

(2) Thirty specimens were composed of four plies of boron filament epoxy with one ply of aluminum screen in the middle of the composite.

(3) Thirty specimens were composed of four plies of boron filament epoxy with one ply of aluminum screen in the middle of the composite.

The aluminum screen consisted of 0.0021 diameter 5056 aluminum wire which was woven into a twilled weave 200 x 200 mesh screen (Pacific Wire Products, Seattle, Washington). The screen was preimpregnated with 3M's PR-279 resin system (35% by weight) which is the same resin system that 3M uses in their SR-272 boron/epoxy prepreg. After the conventional vacuum bag 350°F cure cycle, the composite was cut into 7 in. x 0.1 in. x 0.025 in. tensile specimens. Each specimen was then edge coated with an epoxy system (Epibond 122/952) in order to prevent current flashover along the exposed boron filaments on the specimen edges during electrical testing.

The specimens were subjected by the General Electric Co. to high intensity electric current exposure to stipulated current levels based on the specimen cross-section area. The current levels which were investigated and the specimen test results are given in Appendix Table XI. The current injection levels selected for investigation were 3.8×10^4 amps/cm^2, 5.3×10^4 amps/cm^2, and 8.0×10^4 amps/cm^2 based on the specimen (not the filament) cross-sectional area. Unprotected boron filament epoxy composites are usually degraded at current intensities of 3-4 amps per cm^2 of specimen cross-section with the 3 x 24μsec. waveform used in these tests. The test results show that the introduction of aluminum wire mesh screen on the surface or within the boron composite is an effective method of enhancing the composite resistance to damage caused by the passage of electrical current as none of the specimens with aluminum wire mesh showed any strength degradation. Figure 28 presents cross-sectional views of these protected composites which incorporate aluminum wire mesh screen. The cracks which appear in

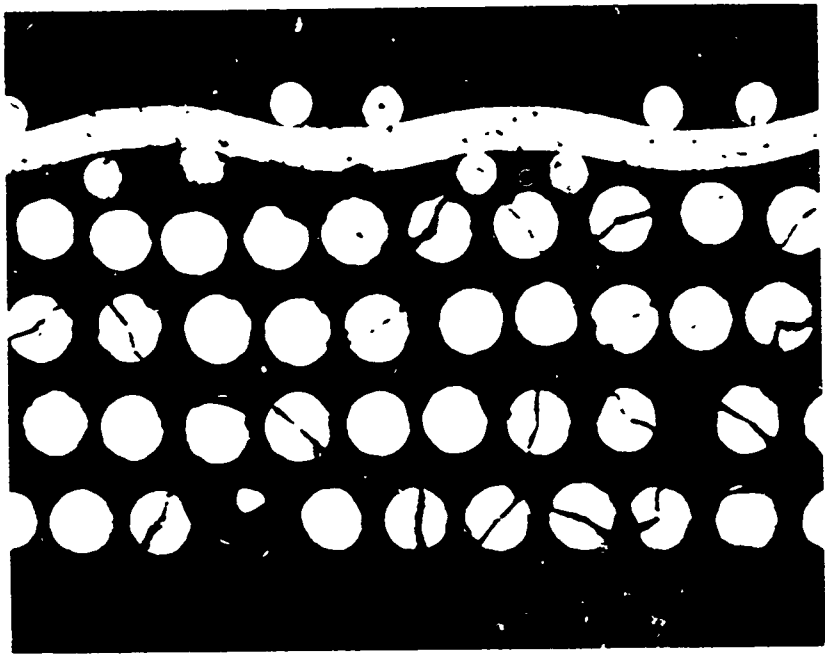

A. ALUMINUM SCREEN ON SURFACE OF COMPOSITE (100X)

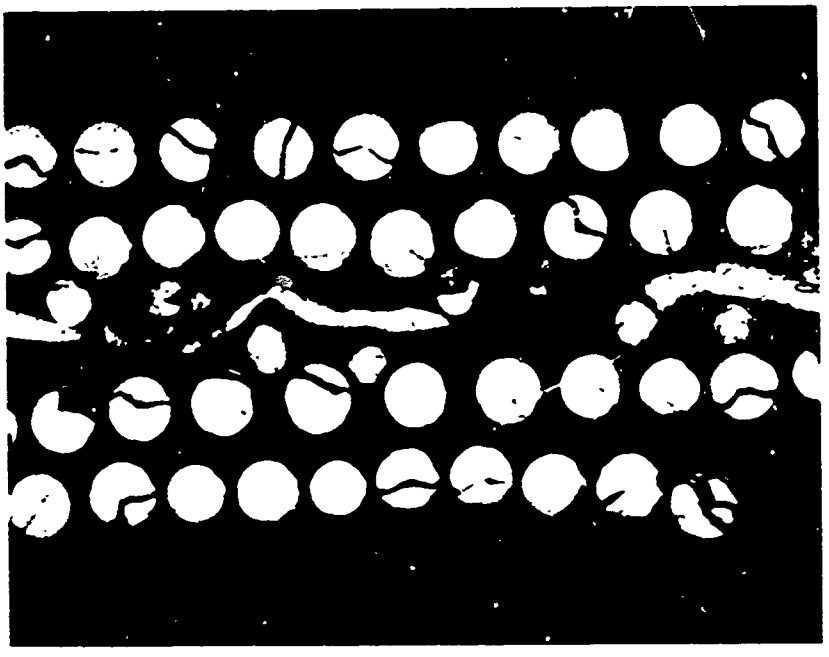

B. ALUMINUM SCREEN IN MIDDLE OF COMPOSITE (100X)

FIGURE 28. BORON FILAMENT EPOXY COMPOSITES WITH INCLUDED ALUMINUM SCREEN AFTER ELECTRICAL EXPOSURE TO 16.0 X 10^4 AMPS/CM^2 OF FILAMENT CROSS-SECTIONAL AREA (8 X 10^4 AMPS/CM^2 OF SPECIMEN AREA) 3 X 24μSEC. WAVEFORM (continued on page 2-64)

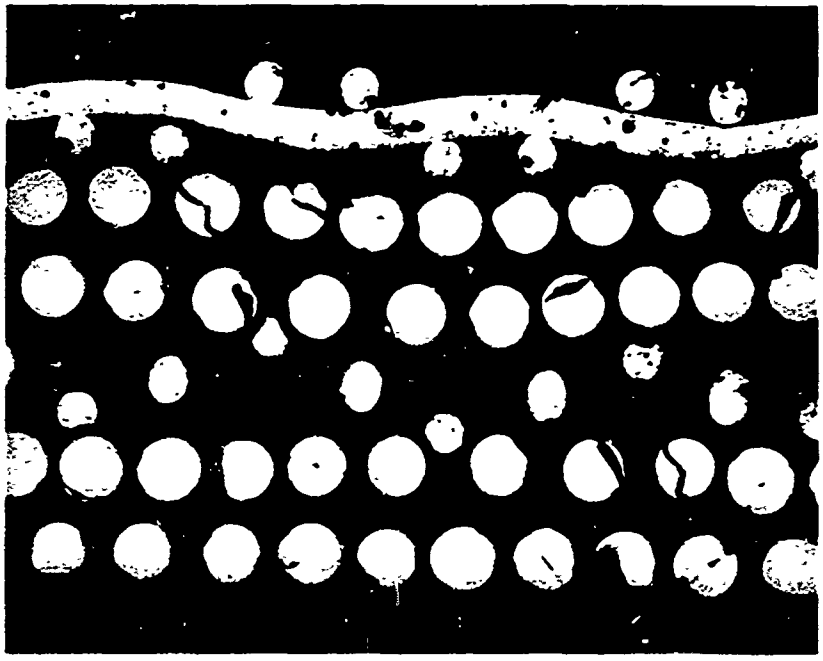

C. ALUMINUM SCREEN ON SURFACE AND IN THE MIDDLE OF COMPOSITE (100X)

FIGURE 28. BORON FILAMENT EPOXY COMPOSITES WITH INCLUDED ALUMINUM SCREEN AFTER ELECTRICAL EXPOSURE TO 16.0 X 10^4 AMPS/CM^2 OF FILAMENT CROSS-SECTIONAL AREA (8 X 10^4 AMPS/CM^2 OF SPECIMEN AREA) 3 X 24μSEC. WAVEFORM

the boron filaments in the photograph are believed to be entirely caused by the polishing technique used in the preparation of the specimen. Comparisons of the exposed with unexposed control specimens do not indicate any loss in tensile strength due to electrical exposure, Appendix Table XI. However, the introduction of the protective aluminum screen in a boron filament composite does of course decrease the tensile strength in the range of 24%. This is because of the increased specimen thickness because of the screen, or in other words, for a given thickness the screen replaces the stronger boron filaments thereby reducing the strength on a pounds per unit cross-sectional area basis.

2.9 TASK IX - ELECTRICAL CURRENT FLOW PATHS IN MULTIORIENTED BORON AND GRAPHITE FILAMENT COMPOSITES

Multi-oriented ply composite panels of boron and graphite filaments have been fabricated in which alternate plies of the reinforcement have been directionally oriented varying from 0° to 90°. The fabrication of the panels utilized 3M SP-272 boron filament/PR-279 epoxy composition and Modmor II filament/Whittaker 1004 epoxy resin composition and were laminated and cured according to the same autoclave techniques used throughout this program. The panels of both the boron filament and graphite filament composites were machined to the configurations shown in Figure 29. The reasons for selection of these configurations will be discussed in detail later; however, the purpose was to place cutouts so that the effect of the current flow to different points could be measured as a function of the number of non-interrupted filament conduction paths. Each point of electrical contact was nickel plated for that purpose.

The specific panel filament orientation scheme and current injection levels to which the composite panels were exposed are given in Appendix Table VIII. Two current injection levels were selected for each panel. The first level was of a low nondegrading magnitude to evaluate current flow paths in the absence of degradation due to current flow. The second was of a higher current level to induce composite damage in order to study relative locations of such damage. Current was injected at the prescribed levels through one contact point (No. 1) and the emitted current was measured at the other three contact sites. Resistivity of each composite was measured both before and after each current level injection test. Each specimen was first exposed to the lower level and then to the higher level. A total of 42 composite panels were prepared (21 of boron and 21 of graphite) with identification as follows:

First letter	B = boron, G = graphite
Second letter	A, B, C, or D = specimen configuration as shown in Figure 29
Third number	1 or 2 = ply orientation as given in Table VIII of the Appendix
Fourth letter	a, b, or c - individual specimen number

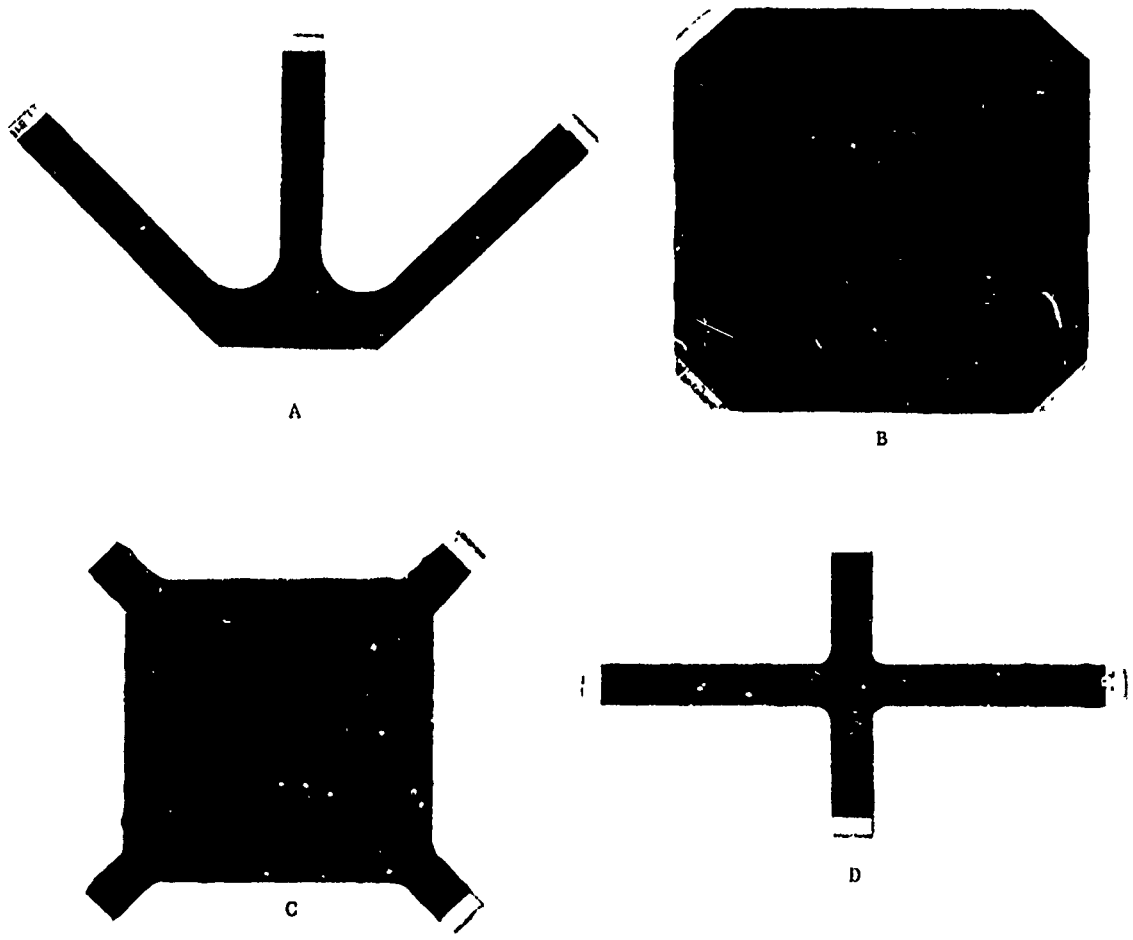

FIGURE 29. FOUR TYPES OF CONFIGURATIONS OF MULTIORIENTED PLY COMPOSITE TEST SPECIMENS FOR ELECTRICAL CURRENT FLOW PATH EVALUATIONS

Only one specimen of each configuration (A, B, C, or D) of both the graphite filament and boron filament composites were exposed to electrical currents. After electrical exposure the panels were dissected and flexural specimens were taken from various locations in order to determine areas of electric current damage. To determine percent loss in strength due to the electrical exposures an identical panel of each material and configuration was dissected and flexural specimens from identical locations tested. The degradation at each location then was expressed as a percentage reduction in flexural strength from the three point bending flexural test. The span for the flexural tests was sixteen times the specimen thickness.

The following paragraphs present a summary of the test results.

2.9.1 BORON FILAMENT COMPOSITE CURRENT FLOW INVESTIGATION

The boron filament composite panels electrically exposed are illustrated in Figures 30-36. In each point No. 1 is the point of current injection. Of each specimen, points No. 2, 3, and 4 were connected to ground. The amplitude of current injected to point No. 1 and exiting points 2, 3, and 4 was measured. A current waveform of 3 x 24 microseconds was utilized. The locations of the flexural specimens taken are drawn on the panel configurations, and the percent degradation as measured for each specimen is noted within the rectangle that denotes each specimen. Also noted in each figure is the level of current injected at the low and at the high level, also provided is the measured current exiting from points 2, 3, and 4. Also, after the low and after the high level of current injection, the resistance between the point of current injection (No. 1) and points 2, 3, and 4 was measured. It had been previously determined[1] that increased resistivity of boron filament composites after current injection is a good indicator of boron filament damage. Resistance was also measured prior to either level of current injection.

In Figure 30 specimen BA-1a has 12 plies with fiber directions of 0°, +45°, -45°, and 90° in that order. As shown, the panel is cut out to permit current flow in only the -45°, 0°, and +45° directions (1-2, 1-3, and 1-4). The slight resistance decreasing after the low level exposure simply means that the epoxy resin at the electrical contact points has dielectrically broken down. The significant increase in the resistances after the high level exposure is indicative of the gross filament damage that occurred, as further illustrated by the percent decrease in flexural strengths (54-63%) of the 1-2, 1-3, and 1-4 legs of the specimen.

Specimen BA-2a as shown in Figure 31 was identical to the specimen in Figure 30 except that the filament ply sequence was altered. The same number of plies of filaments in each direction are present; however, the front and back surface plies are of -45° and +45° orientation instead of 0° and 90° as in Figure 30. This was done because it was expected that

Panel BA-1a

Plies 12

Orientation 0, +45, -45, 90°

Filaments Boron

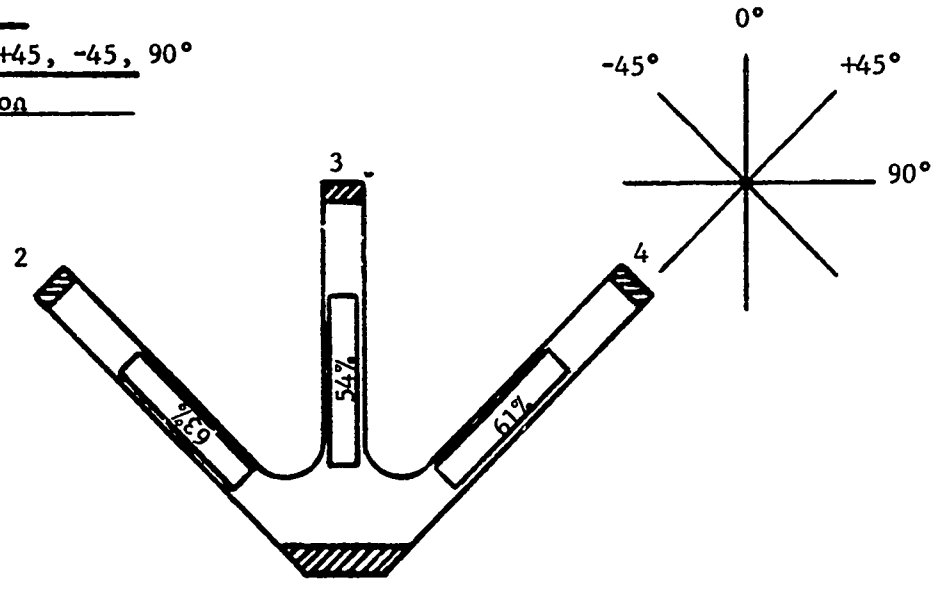

(point of current injection)

Low level current level (100%) 3,570 amps

High level current level (100%) 13,000 amps

	Current Flow in Percent			
	Term 1	Term 2	Term 3	Term 4
Low Level	100	34.7	32.8	32.5
High Level	100	38.4	No oscillogram	

	Resistance in Ohms Between		
	1-2	1-3	1-4
Before low level current injection	1.57	1.41	1.49
Between low and high levels	1.15	1.07	1.18
After high level current injection	53,800	46,800	49,900

FIGURE 30. PANEL BA-1a

Panel BA-2a

Plies 12

Orientation -45, 90, 0, +45°

Filaments Boron

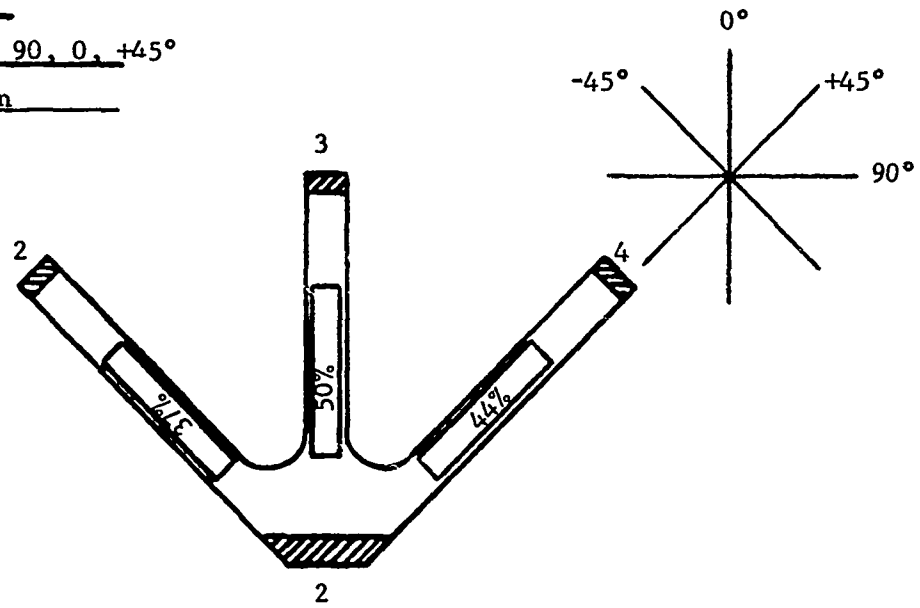

(point of current injection)

Low level current level (100%) 3,360 amps

High level current level (100%) ~~10,750 amps~~

	Current Flow in Percent			
	Term 1	Term 2	Term 3	Term 4
Low Level	100	42	29	29
High Level	100	33.3	34.2	32.5

	Resistance in Ohms Between		
	1-2	1-3	1-4
Before Low Level Current Injection	1.82	1.419	1.428
Between Low and High Levels	1.410	1.146	1.144
After High Level Current Injection	149.6	4,086	99.79

FIGURE 31. PANEL BA-2a

Panel BB-1a

Plies 12

Orientation 0, +45, -45, 90

Filaments Kevlar

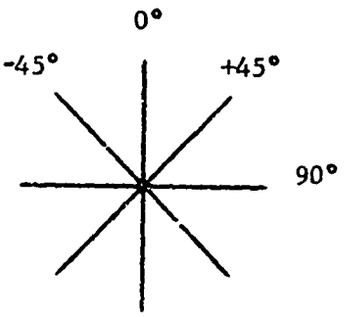

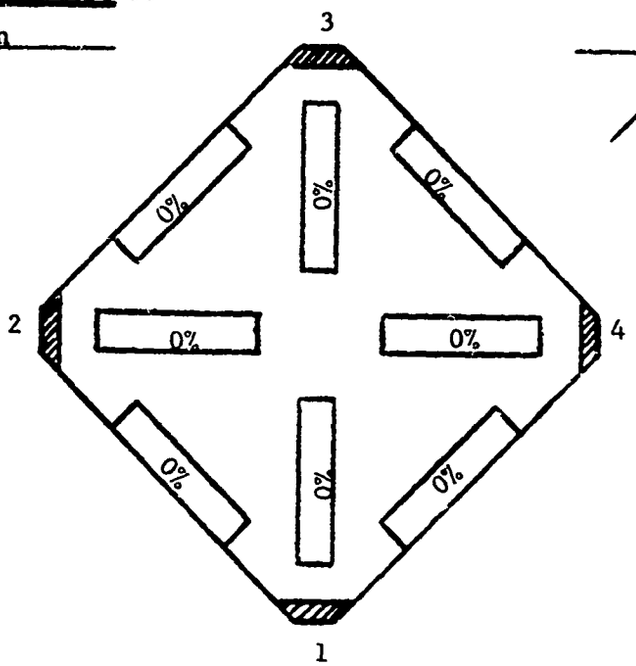

(point of current injection)

Low level current level (100%) 2,520 amps

High level current level (100%) 13,500 amps

	Current Flow in Percent			
	Term 1	Term 2	Term 3	Term 4
Low Level	100	35.4	32.2	32.4
High Level	100	37.5	31.5	31.0

	Resistance in Ohms Between		
	1-2	1-3	1-4
Before Low Level Current Injection	0.449	0.452	0.490
Between Low and High Levels	0.450	0.459	0.496
After High Level Current Injection	0.516	0.547	0.536

FIGURE 32. PANEL BB-1a

Panel BB-2a

Plies 12

Orientation 0, 90, 0, 90°

Filaments Boron

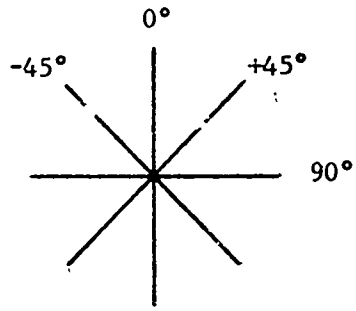

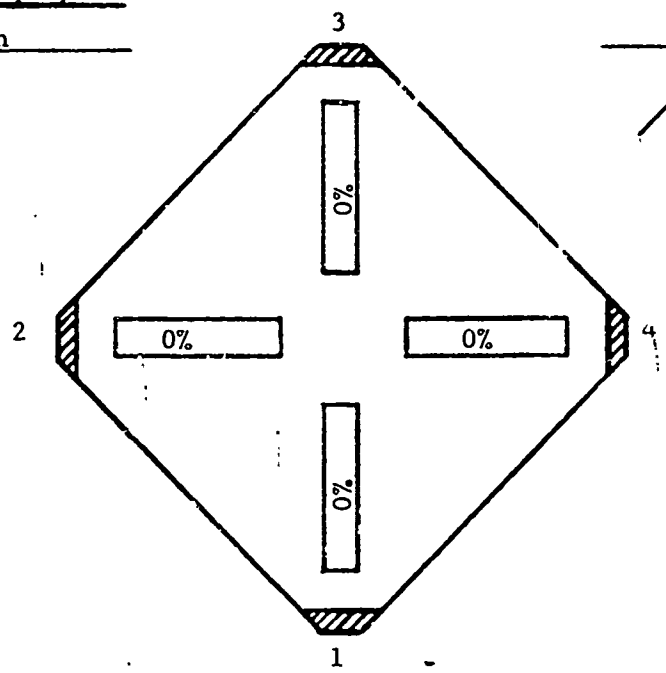

(point of current injection)

Low level current level (100%) 2,670 amps

High level current level (100%) 5,116 amps

	Current Flow in Percent			
	Term 1	Term 2	Term 3	Term 4
Low Level	100	5.5	90.0	4.5
High Level	100	20.8	61.5	17.7

	Resistance in Ohms Between		
	1-2	1-3	1-4
Before Low Level Current Injection	800K	0.461	800K
Between Low and High Levels	17.5K	0.473	17.5K
After High Level Current Injection	1.5K	0.443	1.5K

FIGURE 33. PANEL BB-2a

Panel BC-1a

Plies 12

Orientation 0, 45, -45, 90°

Filaments Boron

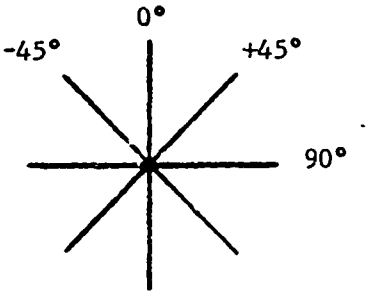

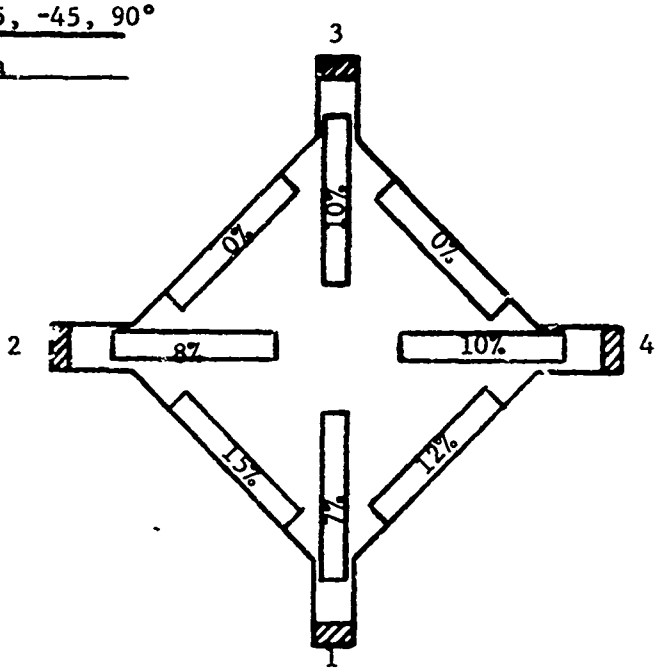

(point of current injection)

Low level current level (100%) 816 amps

High level current level (100%) 3,060 amps

	Current Flow in Percent			
	Term 1	Term 2	Term 3	Term 4
Low Level	100	0	100	0
High Level	100	30.8	43.5	25.7

	Resistance in Ohms Between		
	1-2	1-3	1-4
Before Low Level Current Injection	1.2×10^6	2.894	1.2×10^6
Between Low and High Levels	25K	1.923	25K
After High Level Current Injection	4.5K	13.29	4.5K

FIGURE 34. PANEL BC-1a

Panel BC-2a

Plies 12

Orientation 0, 90, 0, 90°

Filaments Boron

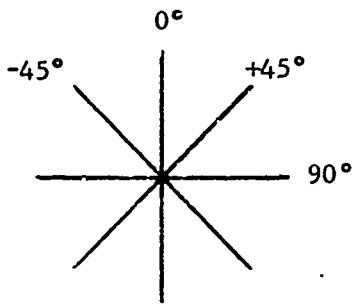

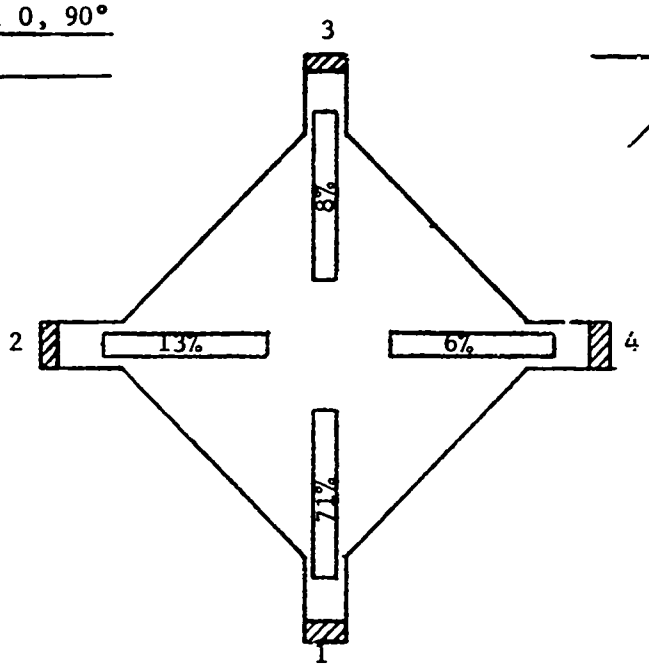

(point of current injection)

Low level current level (100%) 1,980 amps

High level current level (100%) 6,000 amps

	Current Flow in Percent			
	Term 1	Term 2	Term 3	Term 4
Low Level	100	6.4	88.2	5.4
High Level	100	23	54.5	22.5

	Resistance in Ohms Between		
	1-2	1-3	1-4
Before Low Level Current Injection	750K	1.089	750K
Between Low and High Levels	12K	0.799	12K
After High Level Current Injection	250	10.70	250

FIGURE 35. PANEL BC-2a

Panel BD-1a

Plies 12

Orientation 0, 90, 0, 90°

Filaments Boron

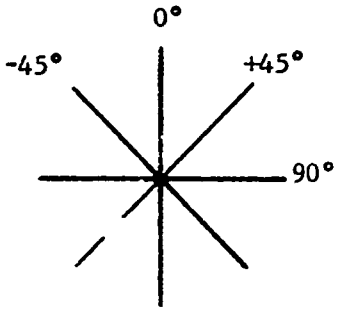

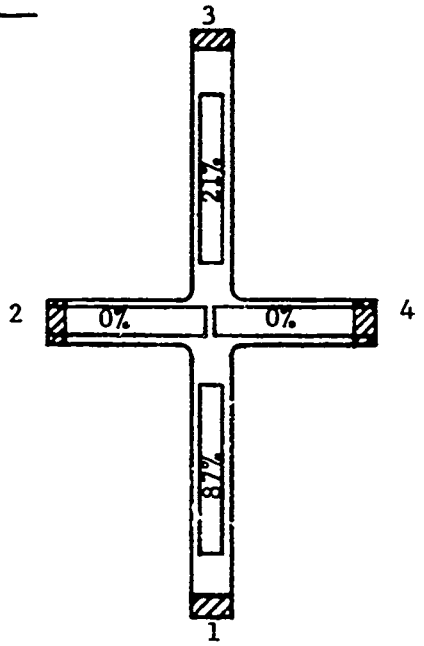

(point of current injection)

Low level current level (100%) 1,920 amps

High level current level (100%) 5,350 amps

	Current Flow in Percent			
	Term 1	Term 2	Term 3	Term 4
Low Level	100	7	90	3
High Level	100	31.3	39	29.7

	Resistance in Ohms Between		
	1-2	1-3	1-4
Before Low Level Current Injection	250 x 10^6	0.907	250 x 10^6
Between Low and High Levels	3K	0.799	3K
After High Level Current Injection	90	8.68	90

FIGURE 36. PANEL BD-1a

surface plies in the direction of conduction would be more severely degraded. If so, specimens from the -45° (1-2) and +45° (1-4) legs would have lower flexural strengths than the 1-3 leg in the Figure 31 case and the 1-3 leg in the Figure 30 case would be the most degraded. This is because flexural strength is slightly dependent on the strength of the external plies where the stress is highest. So, specimens with external plies in the current flow direction (1-3 in Figure 30 and 1-2/1-4 in Figure 31) should have the highest degradation in strength. This appeared to be so in the case of the 1-3 specimen in Figure 30 as well as for the 1-2 and 1-4 specimens of Figure 31. In both Figures 30 and 31 there was equal current flow in the 1-2, 1-3, and 1-4 legs as would be expected since 25% of the filaments were in each of those three directions.

The boron filament composite panel in Figure 32 (BB-1a) had the same filament ply orientation as BA-1a in Figure 30. In the case of Figure 32, as shown, the portions of the panels between the 1-2, 1-3, and 1-4 paths of conduction were not removed. This distinction was made to determine if dielectric breakdown of interply resin layers would come into play and permit dispersion of current over greater panel area, which perhaps would reduce current intensities and resulting degradation. As noted in Figure 32, the high level of current injection was 13,500 amps, slightly higher than in Figure 30; however, there was no degradation in flexural strength at any location. This lack of strength degradation is corroborated by the fact that there was not a significant increase in resistance. It is then concluded that the current flow did not confine itself precisely to the 1-2, 1-3, and 1-4 paths but did in fact dielectrically break down the epoxy resin films and disperse over greater panel area, which kept current intensities to a low level that did not produce filament damages. As in Figure 30 and 31, the current flows shown in Figure 32 were nearly equal in the 1-2, 1-3, and 1-4 directions.

The panel shown in Figure 33 was identical to that shown in Figure 32 except that the +45° and -45° filament plies were replaced with additional 0° and 90° plies. The purpose of this panel was to determine the extent of dielectric breakdown of the epoxy resin and dispersal of current flow to other filament plies. Specifically, in Figure 33, there are no +45° or -45° filament plies so there are no filaments to provide paths of conduction between the 1-2 and 1-4 electrical contact points; therefore, current should not flow between points 1-2 and between points 1-4 unless the current dielectrically breaks down the resin and begins flowing in the 90° filament plies as well. To some extent this did occur. As noted in Figure 33, 20.8% of the current flowed between 1-2; 17.7% of the current flowed between 1-4; and 61.6% of the current flowed between 1-3 where there were direct filament paths to provide conduction. From the resistances measured it is obvious that the 1-3 path is much less resistive as expected. The extent of dielectric breakdown of the epoxy resin that permitted current flow in the 90° filament plies is indicated by the much reduced resistance of the 1-2 and 1-4 paths

after even the low level of current injection and the further reduction in resistance after the high level of current injection. In Figure 33 the current exposure level was not sufficiently high to produce filament damage and strength degradation.

The filament ply orientation of panel BC-1a in Figure 34 is the same as that of panel BB-1a in Figure 32. The panel in Figure 34 was cut so as to geometrically remove the direct filament ply paths in the +45° (1-4) and -45° (1-2) paths between electrical contact points. As shown there, the greatest amount of current (43.5%) did flow in the 1-3 path where there were direct filament paths for conduction. Also, as shown, 30.8% and 25.7% of the current flowed between points 1-2 and between points 1-4. This is further indication that dielectric breakdown of epoxy resin does occur to permit dispersement of the electrical current over more ply layers than just those connecting points of current entry and exit. In the Figure 34 case dielectric breakdown enabled current to flow in both the +45, -45, and 90° filament paths which bridged around the geometric restrictions (cutouts) that eliminated the direct filament paths between points 1-2 and between points 1-4. As noted by the fact that there was no current flow at the low level between the 1-2 and 1-4 points, the dielectric breakdown occurred only at the high level of current injection. Also, as indicated by the slight flexural strength degradation, there was slight filament damage produced by the higher level current injection.

Panel BC-2a in Figure 35 is the same as the panel shown in Figure 34 except that in BC-2a the +45 and -45° filament ply layers were replaced by additional 0° and 90° filament ply layers. In this case, not only is the panel geometrically restricted (cutouts) but the only way that current could flow between points 1-2 and between points 1-4 would be for the dielectric breakdown of the epoxy resin to permit current flow in the 90° filament ply layers. This means that there should be somewhat less current flow to points 2 and 4 in Figure 35 than occurred with the panel shown in Figure 34. As shown, the percent of current flow to points 2 and 4 is in fact less in Figure 35 at the high current injection level than was shown in Figure 34 where +45° and -45° filament ply layers were present. The degradation of flexural strength is greater (71%) in the specimen nearest the point of current injection in the 1-3 path. In the same path but nearest point No. 3 the degradation was much less (8%). This is apparently because the current divided in the exact center of the specimen with a portion of the current then flowing in the 90° filament layers to points 2 and 4. The intensity of current flow from the center to point No. 3 was then reduced and so was the degradation of the composite in that half of the 1-3 path.

Panel BD-1a in Figure 36 was prepared to ascertain that current flowing in the 0° filament direction between two points (1-3) will dielectrically break down the epoxy resin and a portion of the current begin flowing in 90° filament paths to other points, such as No. 2 and No. 4. As noted in the previous paragraph discussion of Figure 35, this division of the current

was thought to have occurred in the exact center of the panel where the 2-4 and 1-3 paths (0° and 90°) intersect. Again, in Figure 36, the strength degradation was greatest from the point of current injection (No. 1) to the center of the panel and somewhat less from the center of the panel to point No. 2. Further indication that the current divided at the intersection of the 2-4 and 1-3 flow paths is the amount of current flowing out of points No. 2 and No. 4 noted in Figure 36. The current flow out of points No. 2 and No. 4 is a higher percentage for the panel in Figure 36 than for the panel shown in Figure 35 because the conduction paths from the panel center to points No. 2 and No. 4 are less in the panel shown in Figure 36.

In the panels illustrated in Figures 35 and 36 there was current flow to points No. 2 and No. 4 even at the low level of current injection. This is probably because of the current dividing only at the center of the panel at the cross-over of the 1-3 and 2-4 paths. This then creates a path of high electrical stress which more readily result in dielectric breakdown of the epoxy resin, thereby permitting current to flow to points No. 2 and No. 4 at lower current levels.

2.9.2 GRAPHITE FILAMENT COMPOSITE CURRENT FLOW INVESTIGATION

Panels of Modmor II graphite filament reinforced Whittaker Corp. 1004 epoxy were fabricated into configurations identical to those discussed for the boron filament epoxy composites in Section 2.9.1. Each was exposed, as in the boron filament panels, first to a low non-damaging level of electric current injection and then to a higher level of current injection. The results are summarized in Figures 37 through 42. As can be seen, it was discovered that electric current flow in graphite filament composites is independent of filament ply orientation. In other words, for the various panel configurations and ply orientations, the current injected into point No. 1 always appeared to flow from points No. 2, 3, and 4 in nearly equal quantities. This observation appears to indicate that current injected into graphite filament epoxy composites rapidly disperses over the whole panel. This then means that electric current flow does not prefer to remain in the conductive paths of fibers that intersect the point of current injection as occur to a degree in boron filament epoxy composites. This phenomena then results in an almost instantaneous reduction of current intensity as the current spreads over the entire panel and accounts for the fact that very little damage resulted from even the high level of current injection in this series of tests. The high level of current injection was calculated to cause damage if this unexpected current dispersal phenomena had not occurred.

In the boron filament composites the plies of filaments are separated by epoxy resin layers of 0.0005 to 0.0015 in. In the graphite filament epoxy composites, however, the filaments are of much smaller diameter than the boron filaments (0.0003 in. compared to 0.004 in.) and are separated by

Panel GA-1a

Plies 8

Orientation 0, +45, -45, 90°

Filaments Modmor II Graphite

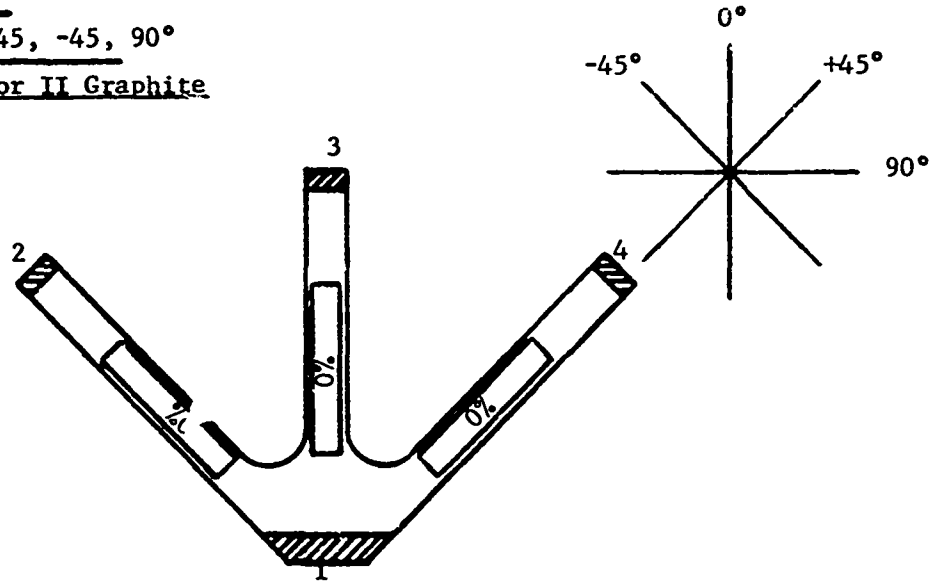

(point of current injection)

Low level current level (100%) 23,700 amps

High level current level (100%) 35,200 amps

	Current Flow in Percent			
	Term 1	Term 2	Term 3	Term 4
Low Level	100	32	36.5	31.5
High Level	100	31.6	37.6	30.8

	Resistance in Ohms Between		
	1-2	1-3	1-4
Before Low Level Current Injection	0.320	0.230	0.284
Between Low and High Levels	0.350	0.257	0.356
After High Level Current Injection	0.338	0.234	0.650

FIGURE 37. PANEL GA-1a

Panel GA-2a

Plies 8

Orientation -45, 90, 0, +45°

Filaments Modmor II Graphite

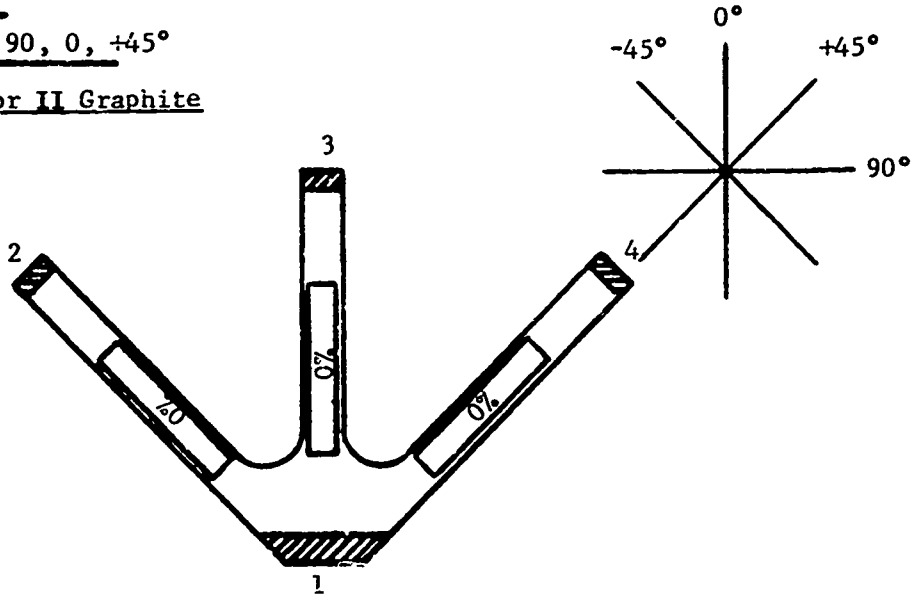

(point of current injection)

Low level current level (100%) 15,300 amps

High level current level (100%) 36,700 amps

	Current Flow in Percent			
	Term 1	Term 2	Term 3	Term 4
Low Level	100	36.7	No Oscillogram	
High Level	100	24	No Oscillogram	

	Resistance in Ohms Between		
	1-2	1-3	1-4
Before Low Level Current Injection	0.282	0.270	0.281
Between Low and High Levels	0.276	0.304	0.296
After High Level Current Injection	0.247	0.249	0.256

FIGURE 38. PANEL GA-2a

Panel GB-1a

Plies 8

Orientation 0, 90, 0, 90°

Filaments Modmor II Graphite

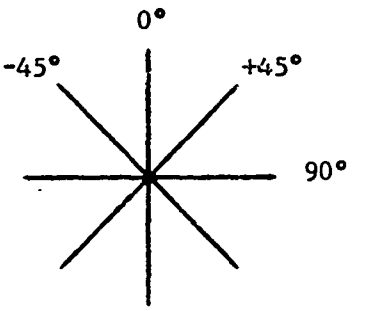

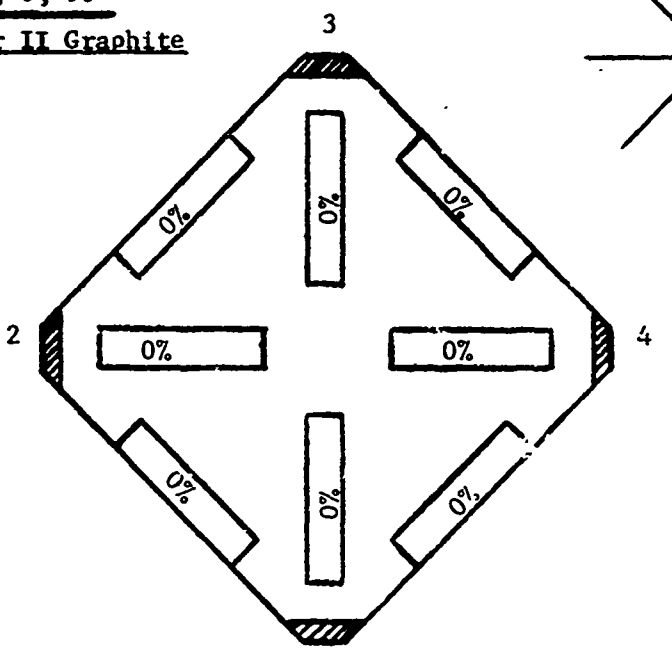

(point of current injection)

Low level current level (100%) 15,300 amps

High level current level (100%) 36,000 amps

	Current Flow in Percent			
	Term 1	Term 2	Term 3	Term 4
Low Level	100	29.9	36.1	34
High Level	100	28.2	33.8	38

	Resistance in Ohms Between		
	1-2	1-3	1-4
Before Low Level Current Injection	0.179	0.117	0.153
Between Low and High Levels	0.122	0.104	0.109
After High Level Current Injection	0.233	0.285	0.244

FIGURE 39. PANEL GB-1a

Panel GB-2a

Plies 8

Orientation 0, 90, 0, 90°

Filaments Modmor II Graphite

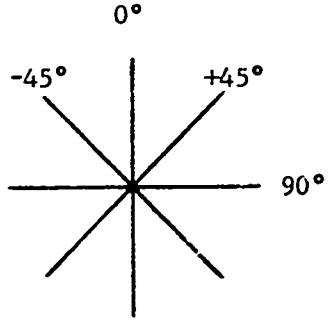

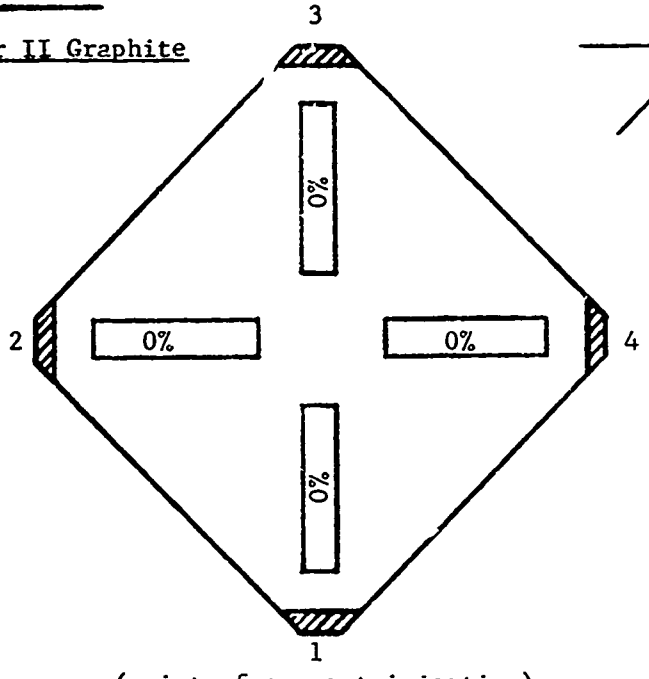

(point of current injection)

Low level current level (100%) 8,130 amps

High level current level (100%) 35,200 amps

	Current Flow in Percent			
	Term 1	Term 2	Term 3	Term 4
Low Level	100	34	35.1	30.9
High Level	100	28.4	38	33.6

	Resistance in Ohms Between		
	1-2	1-3	1-4
Before Low Level Current Injection	0.120	0.173	0.203
Between Low and High Levels	0.097	0.159	0.100
After High Level Current Injection	3.100	2.72	3.91

FIGURE 40. PANEL GB-2a

Panel GC-2a

Plies 8

Orientation 0, 90, 0, 90°

Filaments Modmor II Graphite

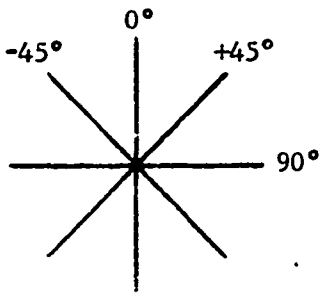

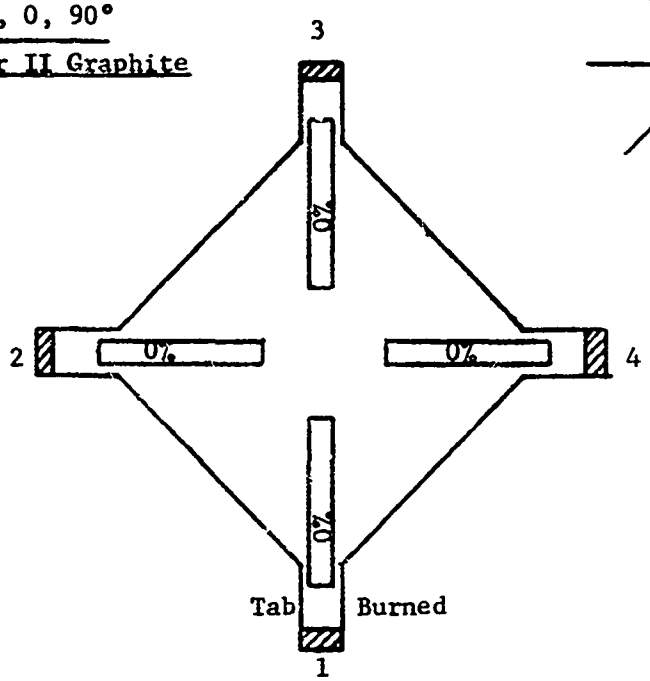

(point of current injection)

Low level current level (100%) 10,400 amps

High level current level (100%) 36,800 amps

	Current Flow in Percent			
	Term 1	Term 2	Term 3	Term 4
Low Level	100	30	34.2	35.8
High Level	100	29	34.2	36.8

	Resistance in Ohms Between		
	1-2	1-3	1-4
Before Low Level Current Injection	0.243	0.503	0.256
Between Low and High Levels	0.243	0.256	0.284
After High Level Current Injection	0.618	0.638	0.623

FIGURE 41. PANEL GC-2a

Panel GD-1a

Plies 8

Orientation 0, 90, 0, 90°

Filaments Modmor II Graphite

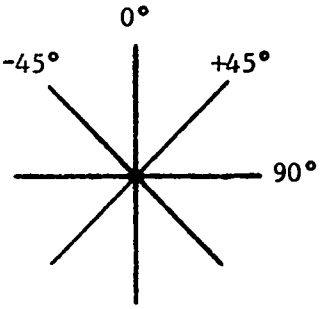

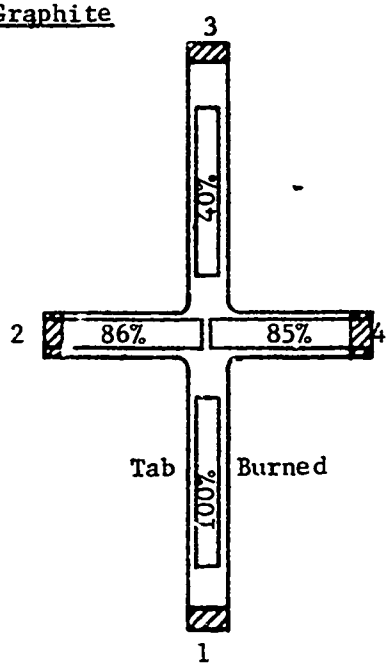

(point of current injection)

Low level current level (100%) 10,100 amps

High level current level (100%) 33,700 amps

	Current Flow in Percent			
	Term 1	Term 2	Term 3	Term 4
Low Level	100	34	31.2	34.8
High Level	100	28.4	30.3	41.3

	Resistance in Ohms Between		
	1-2	1-3	1-4
Before Low Level Current Injection	0.556	0.373	0.323
Between Low and High Levels	0.383	0.326	0.250
After High Level Current Injection	1.480	1.555	1.494

FIGURE 42. PANEL GB-1a

epoxy resin films of only 0.0001 in., typically. Such thin films only require approximately 40 volts to dielectrically break down.[1] The thicker epoxy resin films in the boron filament composites require 200-600 volts before dielectric breakdown occurs to permit current flow from one ply of filaments across the epoxy resin gap to another ply. This then accounts for the relative ease with which electric current disperses in graphite filament epoxy composites. As previously reported,[1] the graphite filament epoxy composites are basically more resistant to damage by electric current flow (due to their lower resistivity) than are boron filaments. This current dispersal phenomena then adds even more advantage to the graphite filament composites since it has long been recognized[1] that a key damage limiting technique is to provide means of dispersal of electric current over a greater area of the composite to thereby reduce current intensities in any one area.

The No. 1 tab (point of current injection) on the two panels shown in Figures 41 and 42 were severely burned, as shown in Figures 43 and 44. It is significant that no burning and delamination occurred beyond the tab where current dispersal and reduction in current intensity occurred. In the panel shown in Figure 42 (GD-1a) the strength of the other three tabs was degraded, apparently because the current intensity was still high enough to produce slight pyrolysis, although not to a degree that gross delamination was produced as in tab No. 1.

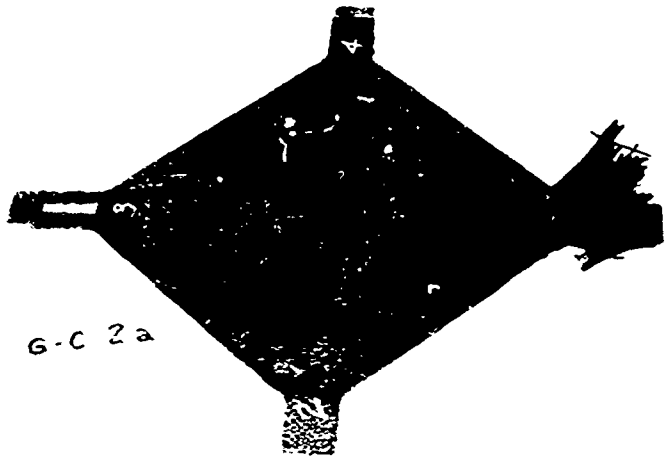

FIGURE 43. PANEL GC-2a

FIGURE 44. PANEL GD-1a

REFERENCES

1. Penton, A. P., Perry, J. L., and Lloyd, K. J., "The Effects of High Intensity Electrical Currents on Advanced Composite Materials," 15 Sept. 1970, Report U-4866.

2. Rudy, E. and St. Windisch, "Ternary Phase Equilibrium in Transition Metal-Boron-Carbon-Silicon Systems," AFML-TR-65-2, Part I, Vol. III, July 1965.

3. Klug, H. P., Alexander, L. E., X-Ray Diffraction Procedures, John Wiley & Sons, p. 512-517.

4. Steward, E. G. and Davidson, H. W., "Graphitization Processes in Relation to Carbon Black," Industrial Carbon and Graphite Conference, London, 1957. Papers of Society of Chem. Industry, p. 207-215.

5. Mering, J. and Maire, J. J., Chem. Phys. 57, 803 '60, Proc. of 4th Conference on Carbon, Buffalo, 1959, Pergamon Press, N.Y., 1960, p. 345.

6. Franklin, R. E., Acta Cryst 4, p. 253 (1951).

SECTION 3

CONCLUSIONS

(1) Investigations have verified that the substitution of a carbon monofilament for the tungsten wire commonly used as a substrate for the manufacture of boron filaments does not significantly affect the damage mechanisms or threshold of damage resulting from high intensity electric current flow. In the boron filament manufacturing process the boron is deposited onto the substrate and the substrate becomes an integral part of the filament. Whether manufactured using a tungsten wire or a carbon monofilament substrate, the electrical conduction of the boron filaments is still via the substrate core, due to the extremely low conductivity of the boron so deposited.[1]

(2) The energy relationship models originally developed have been verified through exposures of boron and graphite filament composites to electric current flow using a variety of combinations of current amplitude and waveform duration. The controlling factor in the degree of degradation of the composites is the total energy that is resistively dissipated within the composites. In other words, the same degree of degradation can be produced by low current amplitude, long duration current waveforms as was produced by very high current amplitude, short duration current waveforms.

(3) The mechanism of degradation of graphite filament composites that was mathematically modeled previously[1] has been experimentally verified through the use of high speed motion photography. At the threshold of such degradation the graphite filaments, due to electric current flow, become so hot that the pyrolysis of the epoxy resin surrounding the filaments is initiated. At

current intensities of higher amplitude or longer waveform than at the threshold, the filaments become so hot that the epoxy resin pyrolysis is so extensive that the gases formed by the pyrolysis rupture or explode the composite due to internal pressure buildup. At the instant the rupturing occurs, air coming into contact with the pyrolysis gases and the hot filaments results in burning and visible flames.

(4) Neither mass spectrographic nor electron microprobe analyses identified any chemical impurities or variations in any balance of chemical constituents that could explain apparent variations that have been noted in boron filament conductivity. Scanning electron microscope studies of the end condition of boron filaments as result from normal machining operations have yielded clues as to the reason for the variations in conductivity. Due to the highly brittle nature of the fine boron filaments, a clean cut surface is not produced on the ends of boron filaments when boron filament composites are either milled or sawed. The filament ends are chipped in an irregular fashion. The substrate core is exposed on some filament ends more than on others, and on the ends of some filaments the core is actually broken off back inside of the filament end. Since the electrical conduction of a boron filament is through the substrate core, it is therefore concluded that the current can more readily enter the filament ends with the more exposed substrate core. This is because the dielectric air gap to those filament ends would be less.

(5) Electric current injection tests were performed on single boron filaments that were encapsulated in plastic to study crack frequency as a function of the severity of the current injection. At damage threshold levels of current injections the radial cracks in boron filaments are localized, probably in weaker areas of the filaments. At higher levels the radial cracks become more severe in number at any one location on the length of filament and cracks are perpetuated throughout the length of filament so exposed.

(6) Controlled experiments with carbonaceous or graphite filaments manufactured using different levels of temperature of processing were accomplished. Graphite or carbonaceous filaments are manufactured by the thermal conversion of synthetic filaments such as rayon or polyacrylonitrile (PAN). The most significant factor controlling the conductivity of the filaments so manufactured was the maximum temperature used in the thermal conversion process. Filaments manufactured at higher temperatures are more conductive than filaments manufactured at lower temperatures. This appears true even in lower temperature ranges where the filaments so produced have no ordered or graphitic structure as can be identified through X-ray diffraction analysis.

(7) Two additional types of graphite filaments, Union Carbide Thornel 75S and Whittaker-Morgan Modmor II, were characterized as to damage mechanisms and threshold of degradation when used in composite construction and exposed to high intensity electric current flow. It was found that the mechanisms of degradation determined in the previous program[1] for Courtaulds HM-S and HITCO HMG-50 graphite filaments, and as verified in (3), held true for the two additional types of graphite filaments. The degradation thresholds differed slightly, however, but were of the same order of magnitude.

(8) It was determined that measurements of acoustic emissions can be used as a non-destructive tool to assess the level of degradation in boron filament composites that have been exposed to high intensity electric current flow. Such composites can be stressed to low levels and the total acoustic emissions at those low levels (short of structural failure) can be accurately correlated with the degree of reduction of the ultimate strength of the boron filament composite due to the high intensity current.

(9) It was determined that fine aluminum wires can be incorporated within boron filament epoxy composites to act as primary electric current conductors. Because the aluminum wires are substantially more conductive than the boron filaments, current is directed from flowing through the filaments. Initial experiments have indicated that the degradation threshold for such boron filament composites can at least be doubled by this technique. More work, however, is needed to determine what the upper limits of this technique are, and what minimum amount of incorporated aluminum wire is required before the effect is lost. The incorporation of fine aluminum wire should be to a minimum because its incorporation effectively serves to displace a certain amount of the lower density and stronger boron filaments; therefore, it is essential that the practical limits of this technique should be determined through further experimentation.

(10) Initial studies of the effect of filament orientation on current flow processes in composites were initiated. The studies performed to date were with both boron and graphite filament composites with several combinations of filament orientations and composite panel geometries. It has been determined that in boron filament epoxy composites the electric current will flow predominantly in the boron filaments that intersect the point where the current is introduced into the panel. If electrical stress (potential difference between filaments or plies of filaments) is high between successive plies or filaments, the resin film separating the plies will be dielectrically broken down and at least a portion of the current will begin to flow in the filament

plies that do not intersect the point of current entry. With respect to such observations, they do tend to verify the current flow process model presented in the previous program.[1] In that model, the composite can be represented as a complex electrical circuit wherein the filaments and insulating resin films that separate the filaments are in effect a complex array of resistors. The circuit model, however, is subject to dynamic change as the resin films suffer dielectric breakdown at zones of highest electrical stress.

(11) The studies of the effect of filament orientation summarized in (10) for boron filament epoxy composites were also conducted, in an identical manner, for graphite filament epoxy composites. The results, however, produced quite different conclusions. Electric current flow in graphite filament epoxy composites appears to be isotropic in that equal flow is independent of filament orientation. In other words, flow will proceed to several ground contact points independent of whether or not there are filaments in the direction of the current flow. The proposed current flow model,[1] however, is still considered to apply to graphite filament composites. The filaments of graphite are much finer than boron filaments. Also, the epoxy resin films surrounding the filaments is much more thin than in boron filament composites. Therefore, the resin film in graphite filament composites will dielectrically break down at a much reduced level of electrical stress (potential difference between filaments or plies of filaments). The net result of this, as was demonstrated, is that current introduced into a graphite filament composite will instantaneously disperse itself over a wide area of the panel. Since the current does not then flow predominantly in a restricted path of filaments, the current intensity at any one point is reduced. Because of this current dispersion effect and resulting reduced current intensities, graphite filament composite panels can be exposed to higher current flow levels than otherwise would be possible without damage. This advantage relative to graphite filament epoxy composites is added to the inherent superior resistance to such damage that they possess, as compared to boron filament epoxy composites. It has been previously identified by unidirectional composite specimens (where the current dispersion phenomena is not possible) that graphite filament epoxy composites can survive current intensity levels of a given waveform 3-7 times higher (depending on type of graphite filament) than boron filament epoxy composites can survive.

APPENDIX

TABLE I

FIBER AND FILAMENT ELECTRICAL EXPOSURE RESULTS (1)

Specimen	Current Crest		Resistivity, ohm-cm Before-After Exposure	Tensile Strength, Lbs	Observation and/or Approximate Peak Temperature During Exposure
	Actual Current Applied, Amps	Current Applied Per Unit Cross Sectional Area, Amps/cm^2			
Boron / Tungsten Core					
1BW8	4	4.94×10^4	10.8×10^{-3} - ∞		
10BW8	4.25	5.25×10^4	$7.7 - 4.3 \times 10^{-3}$		
2BW2	4.37	5.4×10^4	$8.6 - 4.4 \times 10^{-3}$		
5BW4	4.37	5.4×10^4	$6.4 - 4.1 \times 10^{-3}$		
9BW6	4.37	5.4×10^4	$9.5 - 7.9 \times 10^{-3}$		
4BW1 (2)	3	3.71×10^4	$4.7 - 6.2 \times 10^{-3}$		
16BW1 (2)	3	3.71×10^4	$7.6 - 4.6 \times 10^{-3}$		
3BW3 (2)	3.05	3.77×10^4	$10.8 - 4.2 \times 10^{-3}$		
8BW1 (2)	3.05	3.77×10^4	$33.0 - 30.3 \times 10^{-3}$		

TABLE I (cont'd)

Specimen	Current Crest		Resistivity, ohm-cm Before-After Exposure	Tensile Strength, Lbs	Observation and/or Approximate Peak Temperature During Exposure
	Actual Current Applied, Amps	Current Applied Per Unit Cross Sectional Area, Amps/cm^2			
7BW1 (2)	4.9	6.05×10^4	$17.8 - 4.4 \times 10^{-3}$		
14BW1 (2)	5	6.18×10^4	$10.2 - 4.4 \times 10^{-3}$		
Heat Treated Graphite					
HTG21-a	580	11.5×10^4	$1.4 - 1.4 \times 10^{-3}$		$T < 130°F$
HTG21-b	632	12.5×10^4	$1.4 - 1.4 \times 10^{-3}$		$T < 130°F$
HTG22-a	632	12.5×10^4	$1.3 - 1.3 \times 10^{-3}$		$T < 130°F$
HTG22-b	632	12.5×10^4	$1.3 - 1.3 \times 10^{-3}$		$130 < T < 140°F$
HTG23-a	632	12.5×10^4	$1.2 - 1.2 \times 10^{-3}$		$T < 130°F$
HTG23-b	632	12.5×10^4	$1.2 - 1.2 \times 10^{-3}$		$T < 130°F$
HTG24-a	632	12.5×10^4	$1.1 - 1.1 \times 10^{-3}$		$T < 130°F$
HTG24-b	675	13.4×10^4	$1.1 - 1.1 \times 10^{-3}$		$T < 130°F$

TABLE I (Cont'd.)

Specimen	Current Crest: Actual Current Applied, Amps	Current Crest: Current Applied Per Unit Cross Sectional Area, Amps/cm^2	Resistivity, ohm-cm Before-After Exposure	Tensile Strength, Lbs	Observation and/or Approximate Peak Temperature During Exposure
Boron/Carbon Core					
BC-21	0	0	Not Exposed	2.3	
-4	0	0	Not Exposed	2.6	
			AVG	2.45	
BC-16	3.0	3.71×10^4	$17.1\text{-}17.4 \times 10^{-3}$	1.9	
-3	3.0	3.71×10^4	$24.6\text{-}16.5 \times 10^{-3}$		
BC-12	4.6	5.6×10^4	$18.18 - 18.3 \times 10^{-3}$		
-13	4.6	5.6×10^4	$18.15 - 17.45 \times 10^{-3}$	3.4	
BC-2	6.4	7.91×10^4	$16.6 - 16.8 \times 10^{-3}$	4.55	
-1	6.8	8.41×10^4	$21.9 \times 10^{-3} - \infty$	4.0	End of Filament Fractured

TABLE I (Cont'd.)

Specimen	Current Crest		Resistivity, ohm-cm Before-After Exposure	Tensile Strength, Lbs	Observation and/or Approximate Peak Temperature During Exposure
	Actual Current Applied, Amps	Current Applied Per Unit Cross Sectional Area, Amps/cm^2			
BC-18	8.0	9.9×10^4	$27.4 - 20.2 \times 10^{-3}$	1.95	
-9	8.?	10.1×10^4	$31.4 - 35.8 \times 10^{-3}$	4.3	
BC-5	12.0	14.79×10^4	$19.6 \times 10^{-3} - \infty$		Disintegrated
BC-19	"	14.80×10^4	$18.4 \times 10^{-3} - \infty$		"
BC-20	"	"	$16.6 \times 10^{-3} - \infty$		"
-11	13.0	16.0×10^4	$25.65 - 10.35 \times 10^{-3}$	3.75	
BC-10	6.2/7.0/9.0	$(7.6/8.6/11.1) \times 10^4$	$30.35 \times 10^{-3} - \infty$		
MII - 11	-	-	-	62.0	
- 12	-	-	-	69.0	
			AVG	65.5	
MII - 4	61	1.21×10^4		-	
- 5	61	1.21×10^4		-	
- 1	58	1.15×10^4		71.3	
- 2	61	1.21×10^4		71.5	
- 3	61	1.21×10^4		65.8	
			AVG	69.5	
MII - 9	100	1.99×10^4		-	
- 10	"	"		-	
- 6	"	"		77.0	
- 7	"	"		74.5	
- 8	100	1.99×10^4		65.6	
			AVG	72.4	

TABLE I (Cont'd)

Specimen	Current Crest		Resistivity, ohm-cm Before-After Exposure	Tensile Strength, Lbs	Observation and/or Approximate Peak Temperature During Exposure
	Actual Current Applied, Amps	Current Applied Per Unit Cross Sectional Area, Amps/cm^2			
MII - 16	3800	75.3×10^4	$11.48 - 20.0 \times 10^{-4}$		Brilliant Glow (Flame)
MII - 17	"	"	$11.73 - * \times 10^{-4}$		
MII - 18	"	"	$11.68 - 20.3 \times 10^{-4}$	3.5	
MII - 23	"	"	$11.62 - 19.7 \times 10^{-4}$	5.6	
MII - 25	"	"	$11.1 - 19.62 \times 10^{-4}$	14.9	Brilliant Glow (Flame)
				8.0	
*Ends of specimen blown apart.					

TABLE I (cont'd)

Specimen	Current Crest: Actual Current Applied, Amps	Current Crest: Current Applied Per Unit Cross Sectional Area, Amps/cm^2	Resistivity, ohm-cm Before-After Exposure	Tensile Strength, Lbs	Observation and/or Approximate Peak Temperature During Exposure
Thornel 75S (Control Specimens)					
WYJ-11	0	0	Not Exposed	9.6	
WYJ-12	"	"	"	9.8	
WYJ-13	"	"	"	9.9	
			AVG	9.8	
Thornel 75S (Control Specimens)					
WYJ-4	63	15.75×10^4	$0.905\text{-}0.911 \times 10^{-3}$		
WYJ-2	"	"	$0.882\text{-}0.876 \times 10^{-3}$	5.5	
WYJ-3	"	"	$0.851\text{-}0.844 \times 10^{-3}$	9.5	
WYJ-5	"	"	$0.85\text{-}0.844 \times 10^{-3}$	8.4	
WYJ-6	63	15.75×10^4	$0.866\text{-}0.858 \times 10^{-3}$	9.3	
			AVG	8.2	
Thornel 75S (Control Specimens)					
WYJ-8	98.5	24.6×10^4	$1.0\text{-}1.0 \times 10^{-3}$		
WYJ-1	90	22.5×10^4	$1.595\text{-}0.975 \times 10^{-3}$	6.7	
WYJ-9	98.5	24.6×10^4	$0.95\text{-}0.978 \times 10^{-3}$	10.0	
WYJ-10	102	25.5×10^4	$0.85\text{-}0.85 \times 10^{-3}$	10.0	Puff of Smoke
WYJ-7	115	28.8×10^4	$0.93\text{-}0.855 \times 10^{-3}$	6.5	Puff of Smoke
			AVG	8.3	

(1) t_f = 8 μ sec. and t_t = 24 μ sec.

(2) Tested in a parallel circuit arrangement

TABLE (Cont'd)

Specimen	Current Crest		Resistivity, ohm-cm Before-After Exposure	Tensile Strength, Lbs	Observation and/or Approximate Peak Temperature During Exposure
	Actual Current Applied, Amps	Current Applied Per Unit Cross Sectional Area, Amps/cm^2			
WYJ-25	382	95.5×10^4	$0.875 - 0.95 \times 10^{-4}$		
WYJ-24	283	95.5×10^4	$0.82 - 0.877 \times 10^{-4}$		
WYJ-23	382	95.5×10^4	$0.84 - 0.937 \times 10^{-4}$	.7	
WYJ-22	435	109×10^4	$0.85 - 0.912 \times 10^{-4}$	1.7	
WYJ-21	474	118.5×10^4	$0.869 - 0.995 \times 10^{-4}$	3.1	
			AVG	1.8	

TABLE II

CURRENT INJECTION TEST RESULTS FOR BORON/EPOXY COMPOSITES EXPOSED TO VARYING CURRENT WAVEFORMS

Specimen	T_f	T_t	Filament Volume Content %	CURRENT CREST: Actual Current Applied, AMPS	CURRENT CREST: Current Applied Per Unit Cross Sectional Area Of Filament, AMP/CM^2	CURRENT CREST: Current Applied Per Cross Sectional Area Of Specimen, AMP/CM^2	Current Applied Per Filament, AMPS	Resistivity, OHM-CM Before-After Exposure	Tensile Strength, KSI-Modulus PSI x 10^{-6}	Approx Peak Temperature During Exposure
BT-4	0	0	50	0	0	0	0	Not Exposed	156.9-34.3	0
BT-10	"	"	"	"	"	"	"	"	175.5-33.3	"
BT-102	"	"	"	"	"	"	"	"	160.8-34.9	"
BT-107	0	0	50	0	0	0	0	Not Exposed	165.1-34.5	0
								AVG	164.6-34.3	
BT27	1	10	50	356	5.04×10^4	2.52×10^4	4.09	$7.2\text{-}5.32 \times 10^{-3}$		T<100°F
BT57	"	"	"	356	5.04×10^4	2.52×10^4	4.09	$5.08\text{-}3.6 \times 10^{-3}$		"
BT17	"	"	"	343	4.86×10^4	2.43×10^4	3.94	$5.66\text{-}4.07 \times 10^{-3}$	164.5	"
BT83	"	"	"	343	5.04×10^4	2.52×10^4	4.09	$5.56\text{-}4.22 \times 10^{-3}$	147.6	"
BT65	"	"	"	358	5.08×10^4	2.54×10^4	4.12	$5.05\text{-}3.85 \times 10^{-3}$	168.7-33.0	"
BT38	1	10	50	360	5.12×10^4	2.56×10^4	4.15	$7.17\text{-}4.6 \times 10^{-3}$	188.1-31.9	T<100°F
								AVG	167.2-32.5	
BT91	1	10	50	535	7.6×10^4	3.8×10^4	6.16	$5.0\text{-}3.72 \times 10^{-3}$		T<100°F
BT41	"	"	"	535	7.6×10^4	3.8×10^4	6.16	$4.51\text{-}3.63 \times 10^{-3}$		"
BT86	"	"	"	526	7.46×10^4	3.73×10^4	6.05	$6.28\text{-}4.27 \times 10^{-3}$	173.6-34.9	"
BT71	"	"	"	535	7.6×10^4	3.8×10^4	6.16	$5.1\text{-}3.72 \times 10^{-3}$	185.6	"
BT67	"	"	"	535	7.6×10^4	3.8×10^4	6.16	$7.18\text{-}4.19 \times 10^{-3}$	151.3	"
BT43	1	10	50	535	7.6×10^4	3.8×10^4	6.16	$9.15\text{-}5.25 \times 10^{-3}$	134.5	T<100°F
								AVG	161.3-34.9	
BT79	1	10	50	535	7.6×10^4	3.8×10^4	6.16	$5.57\text{-}4.15 \times 10^{-3}$		100<T<110°F
BT55	1	10	50	535	7.6×10^4	3.8×10^4	6.16	$5.92\text{-}4.24 \times 10^{-3}$	155.2-33.9	110<T<120°F
								AVG	155.2-33.9	

TABLE II (cont'd)

Specimen	T_f	T_t	Filament Volume Content %	CURRENT CREST: Actual Current Applied, AMPS	CURRENT CREST: Current Applied Per Unit Cross Sectional Area Of Filament, AMP/CM^2	CURRENT CREST: Current Applied Per Cross Sectional Area Of Specimen, AMP/CM^2	Current Applied Per Filament, AMPS	Resistivity, OHM-CM Before-After Exposure	Tensile Strength, KSI-Modulus PSI x 10^{-6}	Approx Peak Temperature During Exposure
BT85	3	10	50	356	5.04×10^4	2.52×10^4	4.09	$5.38\text{-}3.97 \times 10^{-3}$		T<130°F
BT36	"	"	"	"	"	"	"	$5.23\text{-}4.1 \times 10^{-3}$		"
BT73	"	"	"	"	"	"	"	$6.19\text{-}4.09 \times 10^{-3}$	181.9	"
BT32	"	"	"	356	5.04×10^4	2.52×10^4	4.09	$5.36\text{-}4.03 \times 10^{-3}$	190.6	"
BT81	"	"	"	362	5.14×10^4	2.57×10^4	4.17	$6.5\text{-}4.36 \times 10^{-3}$	164.5-33.2	"
BT31	3	10	50	388	5.50×10^4	2.75×10^4	4.46	$5.38\text{-}4.31 \times 10^{-3}$	170.7	T<130°F
								AVG	176.9-33.2	
BT23	3	10	50	530	7.52×10^4	3.76×10^4	6.10	$4.82\text{-}3.8 \times 10^{-3}$		100<T<110°F
BT92	"	"	"	"	"	"	"	$5.06\text{-}3.6 \times 10^{-3}$		T<100°F
BT54	"	"	"	"	"	"	"	$5.44\text{-}3.99 \times 10^{-3}$	171.9-34.1	T<100°F
BT96	"	"	"	"	"	"	"	$6.33\text{-}4.31 \times 10^{-3}$	127.5	100<T<110°F
BT89	"	"	"	"	"	"	"	$5.44\text{-}3.87 \times 10^{-3}$	168.1	"
BT68	3	10	50	530	7.52×10^4	3.76×10^4	6.10	$5.85\text{-}4.35 \times 10^{-3}$	174.2	100<T<110°F
								AVG	160.4-34.1	
BT50	3	24	50	356	5.04×10^4	2.52×10^4	4.09	$4.75\text{-}4.11 \times 10^{-3}$		T<130°F
BT69	"	"	"	356	5.04×10^4	2.52×10^4	4.09	$7.92\text{-}4.24 \times 10^{-3}$		"
BT74	"	"	"	344	4.88×10^4	2.44×10^4	3.96	$6.14\text{-}4.24 \times 10^{-3}$	163.0	"
BT72	"	"	"	356	5.04×10^4	2.52×10^4	4.09	$5.57\text{-}4.11 \times 10^{-3}$	188.3	"
BT48	"	"	"	356	5.04×10^4	2.52×10^4	4.09	$5.64\text{-}3.8 \times 10^{-3}$	166.3	"
BT82	3	24	50	382	5.42×10^4	2.71×10^4	4.40	$5.71\text{-}4.08 \times 10^{-3}$	181.7-34.7	T<130°F
								AVG	174.8-34.7	

TABLE II (cont'd)

Specimen	T_f	T_t	Filament Volume Content %	CURRENT CREST: Actual Current Applied, AMPS	CURRENT CREST: Current Applied Per Unit Cross Sectional Area Of Filament, AMP/CM^2	CURRENT CREST: Current Applied Per Cross Sectional Area Of Specimen, AMP/CM^2	Current Applied Per Filament, AMPS	Resistivity, OHM-CM Before-After Exposure	Tensile Strength, KSI-Modulus PSI x 10^{-6}	Approx Peak Temperature During Exposure
BT16	3	24	50	532	7.56×10^4	3.78×10^4	6.13	$5.58\text{-}4.31 \times 10^{-3}$		T<130°F
BT87	"	"	"	532	7.56×10^4	3.78×10^4	6.13	$5.96\text{-}4.56 \times 10^{-3}$		130<T<140°F
BT75	"	"	"	529	7.50×10^4	3.75×10^4	6.08	$6.69\text{-}4.55 \times 10^{-3}$	147.8-31.9	130<T<140°F
BT29	"	"	"	532	7.56×10^4	3.78×10^4	6.13	$5.58\text{-}4.31 \times 10^{-3}$	135.3	130<T<140°F
BT62	"	"	"	532	7.56×10^4	3.78×10^4	6.13	$6.39\text{-}5.26 \times 10^{-3}$	146.4	T<130°F
BT93	3	24	50	532	7.56×10^4	3.78×10^4	6.13	$5.9\text{-}4.55 \times 10^{-3}$	160.7	130<T<140°F
								AVG	147.6-31.9	
BT70	3	50	50	178	2.52×10^4	1.26×10^4	2.04	$5.34\text{-}3.97 \times 10^{-3}$		T<130°F
BT100	"	"	"	178	2.52×10^4	1.26×10^4	2.04	$5.64\text{-}4.5 \times 10^{-3}$		"
BT99	"	"	"	172	2.44×10^4	1.22×10^4	1.98	$6.37\text{-}4.01 \times 10^{-3}$	158.5	"
BT80	"	"	"	178	2.52×10^4	1.26×10^4	2.04	$5.05\text{-}3.84 \times 10^{-3}$	163.5	"
BT53	"	"	"	178	2.52×10^4	1.26×10^4	2.04	$5.85\text{-}4.24 \times 10^{-3}$	195.6	"
BT35	3	50	50	184	2.60×10^4	1.30×10^4	2.27	$6.84\text{-}4.32 \times 10^{-3}$	171.0-33.0	T<130°F
								AVG	172.2-33.0	
BT37	3	50	50	264	3.74×10^4	1.87×10^4	3.03	$6.28\text{-}4.31 \times 10^{-3}$		T<130°F
BT25	"	"	"	"	"	"	"	$5.24\text{-}4.02 \times 10^{-3}$		"
BT40	"	"	"	"	"	"	"	$5.64\text{-}4.32 \times 10^{-3}$	176.5	"
BT61	"	"	"	"	"	"	"	$5.54\text{-}4.31 \times 10^{-3}$	166.0	"
BT98	"	"	"	"	"	"	"	$7.06\text{-}4.72 \times 10^{-3}$	166.7	"
BT39	3	50	50	264	3.74×10^4	1.87×10^4	3.03	$5.85\text{-}4.54 \times 10^{-3}$	153.9-33.1	T<130°F
								AVG	165.8-33.1	

TABLE II (cont'd)

Specimen	T_f	T_t	Filament Volume Content %	CURRENT CREST: Actual Current Applied, AMPS	CURRENT CREST: Current Applied Per Unit Cross Sectional Area Of Filament, AMP/CM^2	CURRENT CREST: Current Applied Per Cross Sectional Area Of Specimen, AMP/CM^2	Current Applied Per Filament, AMPS	Resistivity, OHM-CM Before-After Exposure	Tensile Strength, KSI-Modulus PSI x 10^{-6}	Approx Peak Temperature During Exposure
BT-19	3	50	50	350	4.96×10^4	2.48×10^4	4.02	$5.5\text{-}3.81 \times 10^{-3}$		T<130°F
BT33	"	"	"	350	4.96×10^4	2.48×10^4	4.02	$5.79\text{-}4.2 \times 10^{-3}$		"
BT51	"	"	"	345	4.88×10^4	2.44×10^4	3.96	$6.62\text{-}4.32 \times 10^{-3}$	168.5-34.1	T<130°F
BT52	"	"	"	350	4.96×10^4	2.48×10^4	4.02	$7.65\text{-}5.94 \times 10^{-3}$	156.0	130<T<140°F
BT46	"	"	"	"	"	"	"	$6.93\text{-}4.72 \times 10^{-3}$	168.1	T<130°F
BT66	3	50	50	350	4.96×10^4	2.48×10^4	4.02	$6.06\text{-}3.67 \times 10^{-3}$	164.0	T<130°F
								AVG	164.2-34.1	
BT-1	0	0	50	0	0	0	0	Not Exposed	185.2-29.6	
BT-2	"	"	"	"	"	"	"	" "	182.4-28.2	
BT-3	"	"	"	"	"	"	"	" "	194.9-30.0	
BT-5	0	0	50	0	0	0	0	Not Exposed	174.6-29.4	
								AVG	184.3-29.3	
BT18	3	10	50	712	10.10×10^4	5.05×10^4	8.19	$5.56\text{-}3.99 \times 10^{-3}$		120<T<140°F
BT24	"	"	"	"	"	"	"	$6.56\text{-}4.9 \times 10^{-3}$		"
BT94	"	"	"	"	"	"	"	$4.68\text{-}3.97 \times 10^{-3}$	174.2-30.4	"
BT20	"	"	"	712	10.10×10^4	5.05×10^4	8.19	$11.58\text{-}5.72 \times 10^{-3}$	136.1	"
BT84	"	"	"	717	10.16×10^4	5.08×10^4	8.24	$7.1\text{-}4.47 \times 10^{-3}$	176.7	"
BT34	3	10	50	750	10.64×10^4	5.32×10^4	8.63	$5.62\text{-}4.03 \times 10^{-3}$	150.8-29.3	120<T<140°F
								AVG	159.5-29.9	
BT78	3	24	50	670	9.50×10^4	4.75×10^4	7.70	$5.53\text{-}4.66 \times 10^{-3}$		180<T<200°F
BT26	"	"	"	730	10.34×10^4	5.17×10^4	8.39	$5.58\text{-}8.35 \times 10^{-3}$		"
BT49	"	"	"	725	10.28×10^4	5.14×10^4	8.34	$6.56\text{-}19.8 \times 10^{-3}$	66.7	"
BT88	"	"	"	740	10.50×10^4	5.25×10^4	8.52	$5.6\text{-}10.32 \times 10^{-3}$	87.2	"
BT30	"	"	"	740	10.50×10^4	5.25×10^4	8.52	$5.42\text{-}9.82 \times 10^{-3}$	87.5-19.9	180<T<200°F
BT63	3	24	50	788	11.18×10^4	5.59×10^4	9.07	$6.03\text{-}93.7 \times 10^{-3}$	28.8	220<T<240°F
								AVG	67.6-19.9	

TABLE II (Cont'd.)

Specimen	T_f	T_t	Filament Volume Content %	Actual Current Applied, AMPS	Current Applied Per Unit Cross Sectional Area Of Filament, AMP/CM^2	Current Applied Per Cross Sectional Area Of Specimen, AMP/CM^2	Current Applied Per Filament, AMPS	Resistivity, OHM-CM Before-After Exposure	Tensile Strength KSI Modulus PSI x 10^{-6}	Approx Peak Temperature During Exposure
BT47	3	50	50	562	7.96×10^4	3.98×10^4	6.46	$6.01\text{-}6.43 \times 10^{-3}$		220<T<240°F
BT56	"	"	"	562	7.96×10^4	3.98×10^4	6.46	$5.9\text{-}8.37 \times 10^{-3}$		"
BT44	"	"	"	540	7.66×10^4	3.83×10^4	6.21	$7.78\text{-}21.2 \times 10^{-3}$	66.3 - 22.5	"
BT28	"	"	"	562	7.96×10^4	3.98×10^4	6.46	$6.18\text{-}9.88 \times 10^{-3}$	102.5	"
BT42	"	"	"	562	7.96×10^4	3.98×10^4	6.46	$6.46\text{-}19.3 \times 10^{-3}$	82.8 - 22.7	220<T<240°F
BT97	3	50	50	562	7.96×10^4	3.98×10^4	6.46	$5.69\text{-}30.4 \times 10^{-3}$	70.7	T>180°F
								AVG	80.6 - 22.6	
BT90	3	50	50	712	10.10×10^4	5.05×10^4	8.19	$6.72\text{-}100 \times 10^{-3}$		300<T<320°F
BT22	"	"	"	"	"	"	"	$5.81\text{-}107.1 \times 10^{-3}$		"
BT95	"	"	"	"	"	"	"	$6.34\text{-}208.7 \times 10^{-3}$	22.2	"
BT60	"	"	"	"	"	"	"	$6.76\text{-}140.5 \times 10^{-3}$	26.6	"
BT76	"	"	"	"	"	"	"	$4.97\text{-}169 \times 10^{-3}$	38.4 - 18.1	"
BT45	3	50	50	712	10.10×10^4	5.05×10^4	8.19	$5.57\text{-}244 \times 10^{-3}$	30.4 - 20.3	300<T<320°F
								AVG	29.4 - 19.2	
BT7	1	10	50	4420	62.8×10^4	31.4×10^4	50.9	$5.03 \times 10^{-3}\text{-}2.24$		200<T<220°F
BT103	"	"	"	"	"	"	"	$5.65 \times 10^{-3}\text{-}3.95$		"
BT106	"	"	"	"	"	"	"	$6.86 \times 10^{-3}\text{-}1.03$	8.6	220<T<240°F
BT108	"	"	"	4500	63.8×10^4	31.9×10^4	51.7	$5.05 \times 10^{-3}\text{-}5.64$	11.7	240<T<260°F
BT110	"	"	"	"	"	"	"	$5.1 \times 10^{-3}\text{-}4.22$	7.2	"
BT6	"	"	"	4700	66.8×10^4	33.4×10^4	54.2	$6.4 \times 10^{-3}\text{-}1.39$	12.9	T>180°F
								AVG	10.1	

TABLE II (Cont'd)

Specimen	T_f	T_t	Filament Volume Content %	CURRENT CREST: Actual Current Applied, AMPS	CURRENT CREST: Current Applied Per Unit Cross Sectional Area Of Filament, AMP/CM^2	CURRENT CREST: Current Applied Per Cross Sectional Area Of Specimen, AMP/CM^2	Current Applied Per Filament, AMPS	Resistivity, OHM-CM Before-After Exposure	Tensile Strength Tensile-Modulus, PSI x 10^{-6}	Approx Peak Temperature During Exposure
BT15	3	10	50	424C	60.2×10^4	30.1×10^4	48.8	∞.82x10^{-3}-0.837		200<T<220°F
BT14	"	"	"	4310	61.2×10^4	30.6×10^4	49.6	7.28x10^{-3}-0.825		240<T<260°F
BT13	"	"	"	"	"	"	"	∞.95x10^{-3}-0.381	12.2	"
BT12	"	"	"	"	"	"	"	∞.47x10^{-3}-1.62	11.4	220<T<240°F
BT11	"	"	"	"	"	"	"	∞.13x10^{-3}-5.34	10.9 - 6.5	180<T<200°F
BT9	"	"	"	4320	61.30×10^4	30.65×10^4	49.7	∞.79x10^{-3}-0.587	9.2 ___	220<T<240°F
								AVG	10.9 - 6.5	
BT109	3	50	50	1920	27.2×10^4	13.6×10^4	22.1	∞.16x10^{-3} - ∞		
BT111	"	"	"	1990	28.2×10^4	14.1×10^4	22.9	7.06x10^{-3}-0.69		
BT8	"	"	"	2000	28.4×10^4	14.2×10^4	23.0	∞.42x10^{-3} - ∞	7.4	
BT104	"	"	"	"	"	"	"	∞.24x10^{-3}-0.966	8.9	
BT105	"	"	"	2010	29.8×10^4	14.9×10^4	24.2	∞.27x10^{-3}-0.527	8.8 - 5.9	
BT101	"	"	"	2200	31.2×10^4	15.6×10^4	25.3	∞.54x10^{-3}-0.926	8.5 ___	
								AVG	8.4 - 5.9	

TABLE III

CURRENT INJECTION TEST RESULTS FOR GRAPHITE/EPOXY COMPOSITES EXPOSED TO VARYING CURRENT WAVEFORMS

Specimen	T_f	T_t	Filament Volume Content %	CURRENT CREST: Actual Current Applied, AMPS	CURRENT CREST: Current Applied Per Unit Cross Sectional Area Of Filament, AMP/CM^2	CURRENT CREST: Current Applied Per Cross Sectional Area Of Specimen, AMP/CM^2	Current Applied Per Filament Bundle, Amps	Resistivity, OHM-CM Before-After Exposure	Tensile Strength, KSI-Modulus PSI x 10^{-6}	Approx Peak Temperature During Exposure
HMG50T										
-3	0	0	55	0	0	0	0	Not Exposed	155.9-33.3	
-4	"	"	"	"	"	"	"	" "	148.7	
-7	"	"	"	"	"	"	"	" "	150.7-33.2	
-14	0	0	55	0	0	0	0	Not Exposed	139.4	
								AVG	148.7-33.3	
HMG50T										
-40	1	10	55	1585	20.45×10^4	11.25×10^4	108.71	$1.038\text{-}1.038 \times 10^{-3}$		T<100°F
-49	"	"	"	1585	20.45×10^4	11.25×10^4	108.71	$1.18\text{-}1.197 \times 10^{-3}$		"
-85	"	"	"	1530	19.73×10^4	10.85×10^4	104.88	$0.975\text{-}0.975 \times 10^{-3}$	136.3-30.1	"
-80	"	"	"	1585	20.45×10^4	11.25×10^4	108.71	$0.998\text{-}0.992 \times 10^{-3}$	140.5	"
-88	"	"	"	1630	21.00×10^4	11.55×10^4	111.64	$0.957\text{-}0.96 \times 10^{-3}$	137.5	"
-73	1	10	55	1710	22.02×10^4	12.11×10^4	117.06	$0.95\text{-}0.957 \times 10^{-3}$	168.0-31.6	T<100°F
								AVG	145.6-30.9	
HMG50T										
-23	1	10	55	2480	32.0×10^4	17.6×10^4	170.1	$0.927\text{-}0.935 \times 10^{-3}$		100<T<120°F
-20	"	"	"	2400	30.9×10^4	17.0×10^4	164.3	$1.015\text{-}1.022 \times 10^{-3}$		120<T<140°F
-51	"	"	"	2300	29.6×10^4	16.3×10^4	157.4	$0.943\text{-}0.934 \times 10^{-3}$	144.4	100<T<120°F
-66	"	"	"	2330	30.04×10^4	16.52×10^4	159.69	$0.965\text{-}0.961 \times 10^{-3}$	151.9	100<T<120°F
-46	1	10	55	2360	30.40×10^4	16.72×10^4	161.61	$1.02\text{-}1.02 \times 10^{-3}$	129.2	100<T<120°F

TABLE III (cont'd)

Specimen	T_f	T_t	Filament Volume Content %	CURRENT CREST: Actual Current Applied, AMPS	CURRENT CREST: Current Applied Per Unit Cross Sectional Area Of Filament, AMP/CM^2	CURRENT CREST: Current Applied Per Cross Sectional Area Of Specimen, AMP/CM^2	Current Applied Per Filament Bundle, Amps	Resistivity, OHM-CM Before-After Exposure	Tensile Strength, KSI-Modulus PSI x 10^{-6}	Approx Peak Temperature During Exposure
HMG50T -75	(contd) 1	10	55	2550	32.9×10^4	18.1×10^4	174.9	$0.934 \pm 0.934 \times 10^{-3}$	148.6-31.7	100<T<140°F
								AVG	143.5-31.7	
HMG50T -17	3	10	55	1630	21.00×10^4	11.55×10^4	111.64	$0.965 \pm 0.99 \times 10^{-3}$		T<100°F
-55	"	"	"	"	"	"	"	$0.935 \pm 0.942 \times 10^{-3}$		"
-44	"	"	"	"	"	"	"	$0.95 \pm 0.949 \times 10^{-3}$	137.4-33.2	"
-65	"	"	"	"	"	"	"	$1.005 \pm 0.988 \times 10^{-3}$	135.2	"
-25	"	"	"	"	"	"	"	$0.93 \pm 0.935 \times 10^{-3}$	148.4	"
-92	3	10	55	1630	21.00×10^4	11.55×10^4	111.64	$1.005 \pm 0.965 \times 10^{-3}$	137.1	T<100°F
								AVG	139.5-33.2	
HMG50T -71	3	10	55	2430	31.36×10^4	17.25×10^4	166.71	$1.061 \pm 1.061 \times 10^{-3}$		140<T<160°F
-91	"	"	"	2430	31.36×10^4	17.25×10^4	166.71	$1.003 \pm 1.003 \times 10^{-3}$		"
-64	"	"	"	2420	31.3×10^4	17.2×10^4	166.4	$1.13 \pm 1.132 \times 10^{-3}$	126.5-33.7	140<T<160°F
-61	"	"	"	2420	31.3×10^4	17.2×10^4	166.4	$1.163 \pm 1.163 \times 10^{-3}$	136.9	160<T<180°F
-48	"	"	"	2430	31.36×10^4	17.25×10^4	166.71	$0.942 \pm 0.935 \times 10^{-3}$	159.2	140<T<160°F
-45	3	10	55	2430	31.36×10^4	17.25×10^4	166.71	$0.932 \pm 0.935 \times 10^{-3}$	150.0	140<T<160°F
								AVG	143.2-33.7	

TABLE III (cont'd)

Specimen	T_f	T_r	Filament Volume Content %	CURRENT CREST: Actual Current Applied, AMPS	CURRENT CREST: Current Applied Per Unit Cross Sectional Area Of Filament, AMP/CM^2	CURRENT CREST: Current Applied Per Cross Sectional Area Of Specimen, AMP/CM^2	Current Applied Per Filament Bundle, Amps	Resistivity, OHM-CM Before-After Exposure	Tensile Strength, KSI-Modulus PSI x 10^{-6}	Approx Peak Temperature During Exposure
HMG50T										
-33	3	24	55	1660	21.36×10^4	11.75×10^4	113.55	$0.97 \underset{-3}{-} 0.975 \times 10$		180<T<200°F
-21	"	"	"	"	"	"	"	$0.974 \underset{-3}{-} 0.988 \times 10$		180<T<200°F
-60	"	"	"	"	"	"	"	$0.988 \underset{-3}{-} 0.996 \times 10$	138.5-30.8	T>140°F
-89	"	"	"	"		"	"	$0.945 \underset{-3}{-} 0.957 \times 10$	143.5-30.5	200<T<240°F
-57	"	"	"	"		"		$1.16 \underset{-3}{-} 1.169 \times 10$	146.1	T>240°F
-68	3	24	55	1660	21.36×10^4	11.75×10^4	113.55	$0.941 \underset{-3}{-} 0.941 \times 10$ AVG	156.4 146.1-30.7	180<T<200°F
HMG50T										
-29	3	24	55	2480	32.0×10^4	17.6×10^4	170.1	$1.201 \underset{-3}{-} 1.218 \times 10$		240<T<280°F
-42	"	"	"	2480	32.0×10^4	17.6×10^4	170.1	$0.973 \underset{-3}{-} 0.98 \times 10$		200<T<240°F
-39	"	"	"	2300	29.6×10^4	16.3×10^4	157.4	$0.933 \underset{-3}{-} 0.947 \times 10$	145.3	180<T<200°F
-82	"	"	"	2420	31.3×10^4	17.2×10^4	166.4	$1.149 \underset{-3}{-} 1.161 \times 10$	143.2	200<T<240°F
-38	"	"	"	2420	31.3×10^4	17.2×10^4	166.4	$1.035 \underset{-3}{-} 1.015 \times 10$	110.7-28.8	180<T<200°F
-53	3	24	55	2550	32.9×10^4	18.1×10^4	174.9	$0.991 \underset{-3}{-} 0.997 \times 10$ AVG	107.4-29.7 126.7-29.3	180<T<200°F

TABLE III (Cont'd)

Specimen	T_f	T_t	Filament Volume Content %	CURRENT CREST: Actual Current Applied, AMPS	CURRENT CREST: Current Applied Per Unit Cross Sectional Area Of Filament, AMP/CM^2	CURRENT CREST: Current Applied Per Cross Sectional Area Of Specimen, AMP/CM^2	Current Applied Per Filament Bundle, Amps	Resistivity, OHM-CM Before-After Exposure	Tensile Strength KSI Modulus PSI x 10^{-6}	Approx Peak Temperature During Exposure
HMG50-T										
-77	3	10	55	3360	43.27×10^4	23.8×10^4	230.02	$0.928\text{-}0.942 \times 10^{-3}$		T>270°F
-41	"	"	"	3240	41.82×10^4	23.0×10^4	222.32	$1.012\text{-}1.21 \times 10^{-3}$		320<T<340°F
-50	"	"	"	"	"	"	"	$0.936\text{-}0.96 \times 10^{-3}$	151.0-31.9	270<T<300°F
-58	"	"	"	"	"	"	"	$1.062\text{-}1.075 \times 10^{-3}$	121.7	300<T<320°F
-19	"	"	"	"	"	"	"	$0.95\text{-}0.958 \times 10^{-3}$	150.9	220<T<250°F
-31	3	10	55	3240	41.82×10^4	23.0×10^4	222.32	$1.042\text{-}1.082 \times 10^{-3}$	129.2	270<T<300°F
								AVG	138.2-31.9	
HMG50-T										
-36	3	24	55	3490	45.00×10^4	24.75×10^4	239.22	$0.947\text{-}1.02 \times 10^{-3}$		T>380°F
-90	"	"	"	3420	44.00×10^4	24.2×10^4	233.90	$0.916\text{-}0.96 \times 10^{-3}$		400<T<420°F
-78	"	"	"	3240	41.82×10^4	23.0×10^4	222.32	$0.928\text{-}0.965 \times 10^{-3}$	102.9-29.7	380<T<400°F
-28	"	"	"	"	"	"	"	$0.965\text{-}0.99 \times 10^{-3}$	84.8	380<T<400°F
-63	"	"	"	"	"	"	"	$1.005\text{-}1.155 \times 10^{-3}$	41.7	400<T<420°F
-27	3	24	55	3240	41.82×10^4	23.0×10^4	222.32	$0.99\text{-}1.045 \times 10^{-3}$	91.6	380<T<400°F
								AVG	80.3 - 29.7	

TABLE III (cont'd)

Specimen	T_f	T_t	Filament Volume Content %	CURRENT CREST: Actual Current Applied, AMPS	CURRENT CREST: Current Applied Per Unit Cross Sectional Area Of Filament, AMP/CM^2	CURRENT CREST: Current Applied Per Cross Sectional Area Of Specimen, AMP/CM^2	Current Applied Per Filament Bundle, Amps	Resistivity, OHM-CM Before-After Exposure	Tensile Strength, KSI-Modulus PSI x 10^{-6}	Approx Peak Temperature During Exposure
HMG50T										
-56	3	50	55	815	10.51×10^4	5.78×10^4	55.87	$0.995_{-3}^{-}0.987 \times 10^{-3}$		100<T<110°F
-47	"	"	"	815	10.51×10^4	5.78×10^4	55.87	$0.953_{-3}^{-}0.953 \times 10^{-3}$		"
-84	"	"	"	805	10.4×10^4	5.7×10^4	55.3	$0.999_{-3}^{-}0.992 \times 10^{-3}$	110.8	"
-18	"	"	"	815	10.51×10^4	5.78×10^4	55.87	$1.081_{-3}^{-}1.081 \times 10^{-3}$	123.2	100<T<110°F
-37	"	"	"	817	10.5×10^4	5.8×10^4	55.8	$1.156_{-3}^{-}1.156 \times 10^{-3}$	142.4-32.2	100<T<140°F
-52	3	50	55	842	10.85×10^4	5.97×10^4	57.68	$0.965_{-3}^{-}0.974 \times 10^{-3}$ AVG	159.6 134.0-32.2	100<T<110°F
HMG50T										
-69	3	50	55	1210	15.62×10^4	8.59×10^4	83.04	$0.975_{-3}^{-}0.975 \times 10^{-3}$		120<T<140°F
-35	"	"	"	"	"	"	"	$0.966_{-3}^{-}0.967 \times 10^{-3}$		120<T<140°F
-67	"	"	"	"	"	"	"	$0.933_{-3}^{-}0.933 \times 10^{-3}$	149.2-29.5	100<T<140°F
-87	"	"	"	"	"	"	"	$1.191_{-3}^{-}1.162 \times 10^{-3}$	103.8	120<T<140°F
-43	"	"	"	"	"	"	"	$0.974_{-3}^{-}0.974 \times 10^{-3}$	152.9	120<T<140°F
-79	3	50	55	1210	15.62×10^4	8.59×10^4	83.04	$0.961_{-3}^{-}0.961 \times 10^{-3}$ AVG	148.2 138.5-29.5	120<T<140°F

TABLE III (cont'd)

Specimen	T_f	T_t	Filament Volume Content %	CURRENT CREST: Actual Current Applied, AMPS	CURRENT CREST: Current Applied Per Unit Cross Sectional Area Of Filament, AMP/CM^2	CURRENT CREST: Current Applied Per Cross Sectional Area Of Specimen, AMP/CM^2	Current Applied Per Filament Bundle, Amps	Resistivity, OHM-CM Before-After Exposure	Tensile Strength, KSI-Modulus PSI x 10^{-6}	Approx Peak Temperature During Exposure
HMG50T										
-24	3	50	55	1610	20.75×10^4	11.41×10^4	110.31	$0.982_{-3}0.984 \times 10^{-3}$		220<T<240°F
-62	"	"	"	1610	20.75×10^4	11.41×10^4	110.31	$1.405_{-3}1.41 \times 10^{-3}$		220<T<240°F
-32	"	"	"	1630	21.00×10^4	11.55×10^4	111.64	$1.052_{-3}1.062 \times 10^{-3}$	106.6-29.3	220<T<260°F
-72	"	"	"	1630	21.00×10^4	11.55×10^4	111.64	$0.995_{-3}0.995 \times 10^{-3}$	141.1	T<200°F
-86	"	"	"	1630	21.00×10^4	11.55×10^4	111.64	$1.189_{-3}1.156 \times 10^{-3}$	161.5	220<T<240°F
-54	3	50	55	1680	21.6×10^4	11.9×10^4	114.8	$1.152_{-3}1.164 \times 10^{-3}$ AVG	147.5 139.2-29.3	220<T<240°F
HMG50-T										
-1	0	0	55	0	0	0	0	Not Exposed	136.2-32.1	
-2	"	"	"	"	"	"	"	"	138.3-32.2	
-5	"	"	"	"	"	"	"	"	135.1-32.0	
-6	0	0	55	0	0	0	0	Not Exposed	149.6-32.1	
								AVG	139.8-32.1	

TABLE III (Cont'd)

Specimen	T_f	T_t	Filament Volume Content %	Current Crest: Actual Current Applied, AMPS	Current Crest: Current Applied Per Unit Cross Sectional Area Of Filament, AMP/CM^2	Current Crest: Current Applied Per Cross Sectional Area Of Specimen, AMP/CM^2	Current Applied Per Filament Bundle, Amps	Resistivity, OHM-CM Before-After Exposure	Tensile Strength, PSI-Modulus, PSI x 10^{-6}	Approx Peak Temperature During Exposure
HMG50T										
-8	3	10	55	8930	115.1×10^4	63.3×10^4	611.9	$0.93\text{-}0.976 \times 10^{-3}$		T>360°F
-10	"	"	"	"	"	"	"	$0.924\text{-}0.953 \times 10^{-3}$	126.4	340<T<360°F
-11	"	"	"	"	"	"	"	$0.954\text{-}0.982 \times 10^{-3}$	135.5	"
								AVG	131.0	
HMG50T										
-16	3	50	55	1620	21.07×10^4	11.59×10^4	112.0	$0.968\text{-}0.994 \times 10^{-3}$	116.9	280<T<300°F
-13	"	"	"	1640	21.13×10^4	11.62×10^4	112.3	$1.14\text{-}1.17 \times 10^{-3}$	160.2	T>280°F
-22	"	"	"	1720	22.18×10^4	12.2×10^4	117.9	$1.0\text{-}1.045 \times 10^{-3}$		300<T<320°F
								AVG	138.6	
HMG50T										
-12	3	50	55	3330	42.9×10^4	23.6×10^4	228.1	$0.953\text{-}1.63 \times 10^{-3}$		Brief Flame
-9	"	"	"	"	"	"	"	$1.125\text{-}1.93 \times 10^{-3}$		Glowed Red
-15	"	"	"	4340	56.0×10^4	30.8×10^4	297.7	$1.02\text{-}2.48 \times 10^{-3}$		Brief Flame
GY69C	3	24	55	1330	17.16×10^4	9.44×10^4	91.2	$2.64\text{-}2.68 \times 10^{-3}$		240<T<260°F
GY70B	"	"	"	1420	19.09×10^4	10.5×10^4	101.5	$2.79\text{-}2.91 \times 10^{-3}$	62.8 - 22.1	"
GY70A	"	"	"	1500	19.33×10^4	10.63×10^4	102.8	$2.59\text{-}2.8 \times 10^{-3}$	63.7	260<T<280°F
GY69A	"	"	"	1630	21.04×10^4	11.57×10^4	111.8	$2.37\text{-}2.46 \times 10^{-3}$		T>280
GY70C	"	"	"	"	"	"	"	$2.85\text{-}3.17 \times 10^{-3}$	48.8	"
GY69B	"	"	"	1730	22.4×10^4	12.3×10^4	119.1	$2.28\text{-}2.32 \times 10^{-3}$	82.3 - 22.6	260<T<280°F
GY71A	"	"	"	2330	30.05×10^4	16.53×10^4	159.7	$3.2\text{-}3.55 \times 10^{-3}$		Flamed
GY71B	"	"	"	"	"	"	"	$3.23\text{-}3.78 \times 10^{-3}$	67.9 - 21.0	280<T<300°F
GY71C	"	"	"	"	"	"	"	$3.87\text{-}4.66 \times 10^{-3}$	65.2	"
								AVG		
GY42	3		55	8420	17.91×10^4	9.85×10^4	95.2			Film 2
GY3	"	"	"	11700	24.9×10^4	13.7×10^4	132.4			Film 3
GY30	"	"	"	13800	29.36×10^4	16.15×10^4	156.1			Film 4

TABLE III (Cont'd)

Specimen	T_f	T_t	Filament Volume Content %	CURRENT CREST: Actual Current Applied, AMPS	CURRENT CREST: Current Applied Per Unit Cross Sectional Area Of Filament, AMP/CM^2	CURRENT CREST: Current Applied Per Cross Sectional Area Of Specimen, AMP/CM^2	Current Applied Per Filament Bundle, Amps	Resistivity, OHM-CM Before-After Exposure	Tensile Strength KSI Modulus PSI x 10^{-6}	Approx Peak Temperature During Exposure
HMG50-T										
-74	3	50	55	2500	32.18×10^4	17.7×10^4	171.07	$1.08\text{-}1.16 \times 10^{-3}$		T>300°F
-70	"	"	"	2440	31.45×10^4	17.3×10^4	167.21	$0.988\text{-}1.735 \times 10^{-3}$		T>300°F
-59	"	"	"	"	"	"	"	$0.985\text{-}1.03 \times 10^{-3}$	95.9-25.4	T>300°F
-81	"	"	"	"	"	"	"	$0.959\text{-}1.03 \times 10^{-3}$	70.0-26.6	T>380°F
-76	"	"	"	"	"	"	"	~~$1.07\text{-}1.172 \times 10^{-3}$~~	~~13.5~~	~~T>420°F~~
-26	3	50	55	2440	31.45×10^4	17.3×10^4	167.21	$1.16\text{-}1.33 \times 10^{-3}$	25.9	
								AVG	51.3-26.0	
HMG50-T										
-9	3	50	55	3330	42.9×10^4	23.6×10^4	228.1	$1.13\text{-}1.93 \times 10^{-3}$		GLOWED RED
-12	3	50	55	3330	42.9×10^4	23.6×10^4	228.1	$0.95\text{-}1.63 \times 10^{-3}$	30.3	BRIEF FLAME
-15	3	50	55	4340	56.0×10^4	30.8×10^4	297.7	$1.02\text{-}2.48 \times 10^{-3}$	17.4	"
								AVG	23.9	

TABLE IV

CURRENT INJECTION TEST RESULTS FOR THORNEL 75S/EPOXY COMPOSITES

Specimen	T_f	T_t	Filament Volume Content %	CURRENT CREST: Actual Current Applied, AMPS	CURRENT CREST: Current Applied Per Unit Cross Sectional Area Of Filament, AMP/CM^2	CURRENT CREST: Current Applied Per Cross Sectional Area Of Specimen, AMP/CM^2	Current Applied Per Filament Bundle, Amps	Resistivity, OHM-CM Before-After Exposure	Tensile Strength, KSI-Modulus PSI x 10^{-6}	Approx Peak Temperature During Exposure
T-75-T										
-39	0	0	55	0	0	0	0	Not Exposed	170.5-38.9	
-42	"	"	"	"	"	"	"	" "	170.3-39.7	
-43	"	"	"	"	"	"	"	" "	185.7	
-44	0	0	55	0	0	0	0	Not Exposed	183.2	
								AVG	177.4-39.3	
T-75-T										
-26	3	22	55	1460	18.82×10^4	10.35×10^4	76.48	$1.038 \text{-} 1.042 \times 10^{-3}$		120<T<140°F
-28	"	"	"	"	"	"	"	$1.26 \text{-} 1.205 \times 10^{-3}$		120<T<140°F
-10	"	"	"	"	"	"	"	$1.14 \text{-} 1.125 \times 10^{-3}$	183.1	120<T<140°F
-4	"	"	"	"	"	"	"	$1.34 \text{-} 1.134 \times 10^{-3}$	159.0	T>140°F
-27	"	"	"	1460	$18.82\ 10^4$	10.35×10^4	76.48	$1.075 \text{-} 1.078 \times 10^{-3}$	177.8	120<T<140°F
-3	3	22	55	1530	19.73×10^4	10.85×10^4	80.18	$1.098 \text{-} 1.092 \times 10^{-3}$	172.4-41.3	120<T<140°F
								AVG	173.1-41.3	
T-75-T										
-25	3	22	55	1850	23.8×10^4	13.1×10^4	96.7	$1.26 \text{-} 1.23 \times 10^{-3}$		160<T<180°F
-18	"	"	"	"	"	"	"	$1.117 \text{-} 1.148 \times 10^{-3}$		160<T<180°F
-8	"	"	"	"	"	"	"	$1.242 \text{-} 1.23 \times 10^{-3}$	163.4	160<T<180°F
-9	3	22	55	1850	23.8×10^4	13.1×10^4	96.7	$1.197 \text{-} 1.218 \times 10^{-3}$	162.5	140<T<160°F

TABLE IV (cont'd)

Specimen	T_f	T_t	Filament Volume Content %	CURRENT CREST: Actual Current Applied, AMPS	CURRENT CREST: Current Applied Per Unit Cross Sectional Area Of Filament, AMP/CM^2	CURRENT CREST: Current Applied Per Cross Sectional Area Of Specimen, AMP/CM^2	Current Applied Per Filament Bundle, Amps	Resistivity, OHM-CM Before-After Exposure	Tensile Strength, KSI-Modulus PSI x 10^{-6}	Approx Peak Temperature During Exposure
T-75-T (cont'd)										
-6	3	22	55	1850	23.8×10^4	13.1×10^4	96.7	$1.122 \overline{-} 1.115 \times 10^{-3}$	172.3-38.9	140<T<160°F
-24	3	22	55	1850	23.8×10^4	13.1×10^4	96.7	$1.172 \overline{-} 11.7 \times 10^{-3}$ AVG	149.0-36.2 161.8-37.6	160<T<180°F
T-75-T										
-30	3	22	55	2220	28.64×10^4	15.75×10^4	116.39	$1.202 \overline{-} 1.195 \times 10^{-3}$		180<T<200°F
-11	"	"	"	2220	28.64×10^4	15.75×10^4	116.39	$1.12 \overline{-} 1.133 \times 10^{-3}$		180<T<200°F
-15	"	"	"	2170	28.0×10^4	15.4×10^4	113.8	$1.188 \overline{-} 1.188 \times 10^{-3}$	174.7	180<T<200°F
-22	"	"	"	2220	28.64×10^4	15.75×10^4	116.39	$1.228 \overline{-} 1.243 \times 10^{-3}$	161.4	T>200°F
-20	"	"	"	2220	28.64×10^4	15.75×10^4	116.39	$1.07 \overline{-} 1.092 \times 10^{-3}$	169.8	160<T<180°F
-2	3	22	55	2290	29.5×10^4	16.2×10^4	119.9	$1.122 \overline{-} 1.116 \times 10^{-3}$ AVG	170.6-40.1 169.1-40.1	180<T<200°F

TABLE IV (cont'd)

Specimen	T_f	T_t	Filament Volume Content %	CURRENT CREST: Actual Current Applied, AMPS	CURRENT CREST: Current Applied Per Unit Cross Sectional Area Of Filament, AMP/CM^2	CURRENT CREST: Current Applied Per Cross Sectional Area Of Specimen, AMP/CM^2	Current Applied Per Filament Bundle, Amps	Resistivity, OHM-CM Before-After Exposure	Tensile Strength, KSI-Modulus PSI x 10^{-6}	Approx Peak Temperature During Exposure
T-75-T										
-23	3	22	55	2960	38.2×10^4	21.0×10^4	155.2	$1.355 \frac{-3}{-3} 1.355 \times 10$		200<T<220°F
-1	"	"	"	2960	38.2×10^4	21.0×10^4	155.2	$1.069 \frac{-3}{-3} 1.069 \times 10$		220<T<240°F
-19	"	"	"	2900	37.5×10^4	20.6×10^4	152.4	$1.202 \frac{-3}{-3} 1.275 \times 10$	166.9-38.9	"
-29	"	"	"	2960	38.2×10^4	21.0×10^4	155.2	$1.218 \frac{-3}{-3} 1.275 \times 10$	182.4	"
-14	"	"	"	2960	38.2×10^4	21.0×10^4	155.2	$1.312 \frac{-3}{-3} 1.349 \times 10$	136.4	"
-13	3	22	55	2960	38.2×10^4	21.0×10^4	155.2	$1.15 \frac{-3}{-3} 1.26 \times 10$ AVG	164.6 162.6-38.9	220<T<240°F
T-75-T										
-21	3	22	55	3720	48.0×10^4	26.4×10^4	195.1	$1.23 \frac{-3}{-3} 1.315 \times 10$		280<T<300°F
-16	"	"	"	"	"	"	"	$1.316 \frac{-3}{-3} 1.388 \times 10$		280<T<300°F
-17	"	"	"	"	"	"	"	$1.074 \frac{-3}{-3} 1.062 \times 10$	185.5	280 <T<300°F
-5	"	"	"	3720	48.0×10^4	26.4×10^4	195.1	$1.187 \frac{-3}{-3} 1.187 \times 10$	138.2	300<T<320°F
-12	"	"	"	3760	48.5×10^4	26.7×10^4	197.1	$1.195 \frac{-3}{-3} 1.242 \times 10$	145.5	280<T<300°F
-7	3	22	55	3880	50.0×10^4	27.5×10^4	203.2	$1.26 \frac{-3}{-3} 1.245 \times 10$ AVG	146.7-37.9 154.0-37.9	280<T<300°F

TABLE IV (Cont'd)

Specimen	T_f	T_t	Filament Volume Content %	CURRENT CREST: Actual Current Applied, AMPS	CURRENT CREST: Current Applied Per Unit Cross Sectional Area Of Filament, AMP/CM^2	CURRENT CREST: Current Applied Per Cross Sectional Area Of Specimen, AMP/CM^2	Current Applied Per Filament Bundle, Amps	Resistivity, OHM-CM Before-After Exposure	Tensile Strength, KSI-Modulus PSI x 10^{-6}	Approx Peak Temperature During Exposure
T-75-T										
-36	3	26	55	3310	42.72×10^4	23.5×10^4	173.6	$1.21\text{-}1.35 \times 10^{-3}$	21.0	Flames
-37	3	26	55	3380	43.64×10^4	24.0×10^4	177.4	$1.11\text{-}1.16 \times 10^{-3}$	12.9	Flames
								AVG	17.0	
T-75-T										
-33	3	26	55	4850	62.55×10^4	34.4×10^4	254.2	$1.09\text{-}1.49 \times 10^{-3}$	11.0	Flames
T-75-T										
-49	3	26	55	7400	95.45×10^4	52.5×10^4	387.9	$1.07 \times 10^{-3} - \infty$	0	Flames
-46	3	26	55	8170	105.5×10^4	58.0×10^4	428.8	$1.15 \times 10^{-3} - \infty$	0	Flames

TABLE V

CURRENT INJECTION TEST RESULTS FOR MODMOR II/1004 COMPOSITES

Specimen	T_f	T_t	Filament Volume Content %	CURRENT CREST: Actual Current Applied, AMPS	CURRENT CREST: Current Applied Per Unit Cross Sectional Area Of Filament, AMP/CM^2	CURRENT CREST: Current Applied Per Cross Sectional Area Of Specimen, AMP/CM^2	Current Applied Per Filament Bundle, Amps	Resistivity, OHM-CM Before-After Exposure	Tensile Strength, KSI-Modulus PSI x 10^{-6}	Approx Peak Temperature During Exposure
MOD II/1004										
-39	0	0	55	0	0	0	0	Not Exposed	182.2-21.2	
-41	"	"	"	"	"	"	"	" "	208.6-21.0	
-42	"	"	"	"	"	"	"	" "	140.3	
-44	0	0	55	0	0	0	0	Not Exposed	175.8	
								AVG	176.7-21.1	
MOD II/1004										
-30	3	22	55	1460	18.82×10^4	10.35×10^4	946.02	$1.562 \overline{-3} 1.558 \times 10$		140<T<160°F
-10	"	"	"	"	"	"	"	$1.515 \overline{-3} 1.53 \times 10$		"
-12	"	"	"	"	"	"	"	$1.568 \overline{-3} 1.592 \times 10$	228.3	"
-1	"	"	"	"	"	"	"	$1.52 \overline{-3} 1.52 \times 10$	166.7	"
-8	"	"	"	"	"	"	"	$1.578 \overline{-3} 1.52 \times 10$	171.0	140<T<160°F
-20	3	22	55	1460	18.82×10^4	10.35×10^4	946.02	$1.498 \overline{-3} 1.47 \times 10$	191.1-21.5	T>140°F
								AVG	189.3-21.5	
MOD II/1004										
-3	3	22	55	1850	23.8×10^4	13.1×10^4	1196.35	$1.49 \overline{-3} 1.472 \times 10$		T<160°F
-28	"	"	"	"	"	"	"	$1.468 \overline{-3} 1.435 \times 10$		180<T<200°F
-13	"	"	"	"	"	"	"	$1.52 \overline{-3} 1.538 \times 10$	167.3	"
-7	3	22	55	1850	23.8×10^4	13.1×10^4	1196.35	$1.618 \overline{-3} 1.77 \times 10$	187.3	180<T<200°F

TABLE V (cont'd)

Specimen	T_f	T_t	Filament Volume Content %	CURRENT CREST: Actual Current Applied, AMPS	CURRENT CREST: Current Applied Per Unit Cross Sectional Area Of Filament, AMP/CM^2	CURRENT CREST: Current Applied Per Cross Sectional Area Of Specimen, AMP/CM^2	Current Applied Per Filament Bundle, Amps	Resistivity, OHM-CM Before-After Exposure	Tensile Strength, KSI-Modulus PSI x 10^{-6}	Approx Peak Temperature During Exposure
MOD II/ (contd)										
-26	3	22	55	1850	23.8×10^4	13.1×10^4	1196.35	$1.6\text{-}1.585 \times 10^{-3}$	173.1	180<T<200°F
-11	3	22	55	1850	23.8×10^4	13.1×10^4	1196.35	$1.692\text{-}1.59 \times 10^{-3}$ AVG	184.9-21.9 178.2-21.9	180<T<200°F
MOD II/1004										
-19	3	22	55	2230	29.6×10^4	16.3×10^4	1487.9	$1.65\text{-}1.608 \times 10^{-3}$		220<T<240°F
-25	"	"	"	2230	29.6×10^4	16.3×10^4	1487,9	$1.52\text{-}1.518 \times 10^{-3}$		220<T<240°F
-14	"	"	"	2220	28.6×10^4	15.75×10^4	1437.6	$1.515\text{-}1.515 \times 10^{-3}$	119.2-21.4	T>220°F
-15	"	"	"	2220	28.6×10^4	15.75×10^4	1437.6	$1.69\text{-}1.645 \times 10^{-3}$	207.2	220<T<240°F
-6	"	"	"	2230	29.6×10^4	16.3×10^4	1487.9	$1.645\text{-}1.755 \times 10^{-3}$	205.3	220<T<240°F
-2	3	22	55	2230	29.6×10^4	16.3×10^4	1487.9	$1.46\text{-}1.442 \times 10^{-3}$ AVG	184.6 179.1-21.4	220<T<240°F
MOD II/1004										
-16	3	22	55	2960	38.2×10^4	21.0×10^4	1920.2	$1.662\text{-}1.577 \times 10^{-3}$		300<T<320°F
-5	"	"	"	"	"	"	"	$1.74\text{-}1.71 \times 10^{-3}$		300<T<320°F
-22	"	"	"	"	"	"	"	$2.2\text{-}2.139 \times 10^{-3}$	123.9	320<T<340°F
-4	"	"	"	"	"	"	"	$1.71\text{-}1.71 \times 10^{-3}$	129.7	300<T<320°F
-21	"	"	"	"	"	"	"	$1.583\text{-}1.528 \times 10^{-3}$	145.0	300<T<320°F
-23	3	22	55	2960	38.2×10^4	21.0×10^4	1920.2	$1.8\text{-}1.782 \times 10^{-3}$ AVG	201.2-21.8 150.0-21.8	T>300°F

TABLE V (cont'd)

Specimen	T_f	T_t	Filament Volume Content %	CURRENT CREST: Actual Current Applied, AMPS	CURRENT CREST: Current Applied Per Unit Cross Sectional Area Of Filament, AMP/CM^2	CURRENT CREST: Current Applied Per Cross Sectional Area Of Specimen, AMP/CM^2	Current Applied Per Filament Bundle, Amps	Resistivity, OHM-CM Before-After Exposure	Tensile Strength, KSI-Modulus PSI x 10^{-6}	Approx Peak Temperature During Exposure
MOD II/1004										
-24	3	22	55	3720	47.5×10^4	26.4×10^4	2387.7	$1.588-1.551 \times 10^{-3}$		380<T<400°F
-17	"	"	"	"	"	"	"	$1.53-1.515 \times 10^{-3}$		"
-18	"	"	"	"	"	"	"	$1.76-1.645 \times 10^{-3}$	204.1	"
-9	"	"	"	"	"	"	"	$1.53-1.705 \times 10^{-3}$	224.5	"
-27	"	"	"	"	"	"	"	$1.577-1.578 \times 10^{-3}$	233.1	"
-29	3	22	55	3720	47.5×10^4	26.4×10^4	2387.7	1.691	184.3-21.7	380<T<400°F
								AVG	211.5-21.7	
MOD II/1004										
-38	3	26	55	3450	44.55×10^4	24.5×10^4	2239	$1.59-2.44 \times 10^{-3}$	25.2	Flames
-45	"	"	"	3570	46.18×10^4	25.4×10^4	2321	$1.63-3.12 \times 10^{-3}$	14.2	"
-40	3	26	55	3700	47.64×10^4	26.2×10^4	2395	$1.55-3.07 \times 10^{-3}$	29.7	Flames
								AVG	23.0	
MOD II/1004										
-49	3	26	55	3960	51.09×10^4	28.1×10^4	2568	$1.56-2.28 \times 10^{-3}$	21.3	Flames
-52	3	26	55	4080	52.55×10^4	28.9×10^4	2642	$1.58-2.63 \times 10^{-3}$	14.8	Flames
								AVG	18.1	
MOD II/1004										
-36	3	26	55	5100	65.82×10^4	36.82×10^4	3309	$1.48-2.47 \times 10^{-3}$	16.1	Flames

TABLE VI

CURRENT INJECTION TEST DATA FOR BORON/EPOXY COMPOSITES

Specimen	T_f	T_t	Filament Volume Content %	CURRENT CREST: Actual Current Applied, AMPS	CURRENT CREST: Current Applied Per Unit Cross Sectional Area Of Filament, AMP/CM^2	CURRENT CREST: Current Applied Per Cross Sectional Area Of Specimen, AMP/CM^2	Current Applied Per Filament, AMPS	Resistivity, OHM-CM Before-After Exposure	Flexural Strength, KSI	Approx Peak Temperature During Exposure
BF-7	0	0	50	0	0	0	0	Not Exposed	230	
BF-8	"	"	"	"	"	"	"	"	223	
BF-9	"	"	"	"	"	"	"	"	225	
BF-12	"	"	"	"	"	"	"	"	223	
BF-13	"	"	"	"	"	"	"	"	208	
BF-14	"	"	"	"	"	"	"	"	238	
									225	
BF-20	3	24	50	9150	5.70×10^4	2.85×10^4	4.62	$7.17\text{-}4.75 \times 10^{-3}$	220	160<T<180°F
BF-18	"	"	"	"	"	"	"	$6.21\text{-}4.75 \times 10^{-3}$	221	"
BF-15	"	"	"	"	"	"	"	$6.9\text{-}5.28 \times 10^{-3}$	223	"
BF-27	3	24	50	9200	5.72×10^4	2.86×10^4	4.64	$6.92\text{-}4.6 \times 10^{-3}$	221	"
									221	
BF-3	3	24	50	12400	7.72×10^4	3.86×10^4	6.26	$7.9\text{-}6.67 \times 10^{-3}$	193	180<T<200°F
BF-4	"	"	"	12600	7.84×10^4	3.92×10^4	6.36	$6.84\text{-}5.15 \times 10^{-3}$	186	200<T<250°F
BF-2	"	"	"	12750	7.94×10^4	3.97×10^4	6.44	$6.73\text{-}5.11 \times 10^{-3}$	162	200<T<220°F
BF-1	"	"	"	13000	8.08×10^4	4.04×10^4	6.55	$7.64\text{-}5.02 \times 10^{-3}$	203	180<T<200°F
									186	
BF-2	3	24	50	16500	10.28×10^4	5.14×10^4	8.27	$8.3\text{-}138.5 \times 10^{-3}$	46	280<T<300°F
BF-10	"	"	"	15320	9.54×10^4	4.77×10^4	7.63	$6.98\text{-}3.86 \times 10^{-3}$	92	240<T<260°F
BF-11	"	"	"	16500	10.28×10^4	5.14×10^4	8.27	$7.45\text{-}88 \times 10^{-3}$	41	260<T<280°F
BF-5	"	"	"	"	"	"	"	$8.19\text{-}434 \times 10^{-3}$	67	240<T<260°F
									62	
BF-30	3	24	50	18600	11.58×10^4	5.79×10^4	9.39	$4.98\text{-}5.06 \times 10^{-3}$	29	320<T<340°F
BF-29	"	"	"	19400	12.08×10^4	6.04×10^4	9.80	$7.2 \times 10^{-3}\text{-}4.23$	32	T>360°F
BF-25	"	"	"	19800	12.32×10^4	6.16×10^4	9.99	$7.43 \times 10^{-3}\text{-}14.9$	27	340<T<360°F
BF-22	"	"	"	20400	12.70×10^4	6.35×10^4	10.30	$6.75 \times 10^{-3}\text{-}55.5$	29	T>300°F
									29	

TABLE VII

EFFECT OF HIGH INTENSITY CURRENT FLOW THROUGH BORON AND GRAPHITE COMPOSITES ON THE TENSILE AND FLEXURAL STRENGTHS

Specimen	T_f	T_t	Current Applied Per Cross Sectional Area Of Filament, AMP/CM^2	Tensile Strength Degradation %	VISUAL OBSERVATIONS
HMG 50T	1	10	21.0×10^4	0	No Visual Defects
"	1	10	31.0×10^4	0	"
HMG 50T	3	10	21.0×10^4	0	No Visual Defects
"	3	10	31.4×10^4	0	"
"	3	10	41.9×10^4	0	"
HMG 50T	3	24	21.4×10^4	0	No Visual Defects
"	3	24	32.0×10^4	0	"
"	3	24	42.0×10^4	100	Delaminated and Resin Pyrolysis
HMG 50T	3	50	10.5×10^4	0	No Visual Defects
"	3	50	15.6×10^4	0	"
"	3	50	21.0×10^4	0	
"	3	50	31.6×10^4	100	Delaminated and Resin Pyrolysis
"	3	50	47.3×10^4	100	"
BT	1	10	5.0×10^4	0	No Visual Defects
"	1	10	7.6×10^4	0	"
BT	3	10	5.1×10^4	0	"
"	3	10	7.6×10^4	0	"
BT	3	10	10.2×10^4	0	No Visual Defects
BT	3	24	5.2×10^4	0	No Visual Defects
"	3	24	7.6×10^4	13	"
"	3	24	10.6×10^4	60	"

TABLE VII

(Cont'd)

Specimen	T_f	T_t	Current Applied Per Cross Sectional Area Of Filament, AMP/CM^2	Tensile Strength Degradation %	VISUAL OBSERVATIONS
BT	3	50	2.5×10^4	0	No Visual Defects
"	3	50	3.7×10^4	0	"
"	3	50	5.0×10^4	0	"
"	3	50	8.0×10^4	53	"
"	3	50	10.0×10^4	83	"
T-75-T	3	22	18.8×10^4	0	No Visual Defects
"	3	22	23.8×10^4	0	"
"	3	22	28.6×10^4	0	"
"	3	22	38.2×10^4	0	"
"	3	22	49.0×10^4	0	"
T-75-T	3	26	42.0 43.0×10^4	100	Resin Pyrolysis and Varying Degrees of Delamination
"	3	26	62.6 62.6×10^4	100	"
"	3	26	100.5 100.5×10^4	100	"
MOD II/1004	3	22	18.8×10^4	0	No Visual Defects
"	3	22	23.8×10^4	0	"
"	3	22	29.0×10^4	0	"
"	3	22	38.2×10^4	0	"
"	3	22	47.5×10^4	0	"
MOD II/1004	3	26	46.2×10^4	100	Delaminated and Resin Pyrolysis
"	3	26	52.0×10^4	100	"
"	3	26	65.8×10^4	100	"

TABLE VII
(Cont'd)

Specimen	T_f	T_t	Current Applied Per Cross Sectional Area Of Filament, AMP/CM^2	Tensile Strength Degradation %	VISUAL OBSERVATIONS
BF	3	24	4.0×10^4	0 (1)	No Visual Defects
"	3	24	5.7×10^4	0 (1)	"
"	3	24	8.0×10^4	16 (1)	"
"	3	24	10.0×10^4	71 (1)	"
"	3	24	12.0×10^4	86 (1)	"

(1) = % Flexural Strength Degradation

TABLE VII

(Cont'd)

Specimen	T_f	T_t	Current Applied Per Cross Sectional Area Of Filament, AMP/CM^2	Tensile Strength Degradation %	VISUAL OBSERVATIONS
BT	1	10	64.0×10^4	94	No Visible Damage
"	3	10	61.0×10^4	94	No Visible Damage
"	3	50	29.0×10^4	95	Resin Pyrolysis Under ID Tag
HMG-50T	3	10	115.0×10^4	0	No Visible Damage
"	3	50	21.5×10^4	0	No Visible Damage
"	3	50	47.3×10^4	100	Resin Pyrolysis and Exfoliated
BTS (Aluminum Screen in Middle of Laminate)	3	24	7.5×10^4	0	No Visible Damage
"	3	24	10.4×10^4	0	No Visible Damage
"	3	24	16.3×10^4	0	No Visible Damage
BT-S (Aluminum Screen on Surface of Laminate)	3	24	7.6×10^4	0	No Visible Damage
"	3	24	10.7×10^4	0	No Visible Damage
"	3	24	15.6×10^4	0	No Visible Damage
BT-S (Aluminum Screens in Middle and on Surface of Laminate)	3	24	7.6×10^4	1	No Visible Damage
"	3	24	10.5×10^4	0	No Visible Damage
"	3	24	15.6×10^4	0	No Visible Damage

TABLE VIII

MULTI-ORIENTED BORON AND GRAPHITE PANEL FABRICATION AND CURRENT INJECTION LEVEL "ECI" SCHEME

PANEL CODE NO.	NO. OF PLIES	PLY ORIENTATION	NT FIBERS IN CRITICAL FLOW PATH	CURRENT INJECTION LEVEL, (1) 10 AMPS/CM - AMPERAGE LEVEL #1	LEVEL # 2
		BORON/EPOXY COMPOSITE			
BA-1a	12	0°, +45°, -45°, 90°	75	1.5 - 3,098	5 - 10,325
BA-1b	"	"			
BA-1c	"	"			
BA-2a	"	-45°,90°,0°,+45°	75	1.5 - 3,098	5 - 10,325
BA-2b	"	"			
BA-2c	"	"			
BB-1a	"	0°,+45°,-45°,90°	75	1.5 - 3,098	5 - 10,325
BB-1b	"	"			
BB-1c	"	"			
BB-2a	"	0°,90°,0°,90°	50	1.0 - 2,065	3.3 - 6,716
BB-2b	"	"			
BB-2c	"	"			
BC-1a	"	0°,+45°,-45°,90°	25	0.5 - 1,033	1.7 - 3,511
BC-1b	"	"			
BC-1c	"	"			
BC-2a	"	0°,90°,0°,90°	50	1.0 - 2,065	3.3 - 6,716
BC-2b	"	"			
bC-2c	"	"			
BO-1a	"	"	50	1.0 - 2,065	3.3 - 6.716
BD-1b	"	"			
BD-1c	12	0°,90°,0°,90°			

(1) BASED ON SPECIMEN CROSSECTIONAL AREA

TABLE VIII

MULTI-ORIENTED BORON AND GRAPHITE PANEL FABRICATION AND CURRENT INJECTION LEVEL TEST SCHEME

PANEL CODE NO.	NO. OF PLIES	PLY ORIENTATION	% OF FIBERS IN DIRECT FLOW PATH	CURRENT INJECTION LEVEL, (1) 10 AMPS/CM^2-AMPERAGE LEVEL #1	LEVEL # 2
		GRAPHITE/EPOXY COMPOSITE			
GA-1a	8	0°,+45°,-45°,90°	75	6 - 15,480	23 - 59,340
GA-1b	"	"			
GA-1c	"	"G			
GA-2a	"	-45°,90°,0°,+45°	75	6 - 15,480	23 - 59,340
GA-2b	"	"			
GA-2c	"	"			
GB-1a	"	0°,+45°,-45°,90°	75	6 - 15,480	23 - 59,340
GB-1b	"	"			
GB-1c	"	"			
GB-2a	"	0°,90°,0°,90°	50	4 - 10,320	15 - 38,700
GB-2b	"	"			
GB-2c					
GC-1a	"	0°,+45°,-45°,90°	25	2 - 5,160	7.5 - 19,350
GC-1b	"	"			
GC-1c	"	"			
GC-2a	"	0°,90°,0°,90°	50	4 - 10,320	15 - 38,700
GC-2b	"	"			
GC-2c	"	"			
GD-1a	"	"	50	4 - 10,320	15 - 38,700
GD-1b	"	"			
GD-1c	8	0°,90°,0°,90°			

(1) BASED ON SPECIMEN CROSSECTIONAL AREA

TABLE IX

ELECTRICAL TEST DATA FOR RESTRAINED ENCAPSULATED SINGLE BORON FILAMENTS

Specimen	Current Crest		Resistivity, ohm-cm Before-After Exposure	Tensile Strength, Lbs	Observation and/or Approximate Peak Temperature During Exposure
	Actual Current Applied, Amps	Current Applied Per Unit Cross Sectional Area, Amps/cm^2			
EB-4	1.4	1.73×10^4	$16.5 - 14.6 \times 10^{-3}$		
EB-1	1.6	1.98×10^4	$19.3 - 14.6 \times 10^{-3}$		
EB-13	1.6	1.98×10^4	$36.2 - 28 \times 10^{-3}$		
EB-11	1.64	2.03×10^4	$5.1 - 2.2 \times 10^{-3}$		
EB-10	1.7	2.1×10^4	$133.5 - 57 \times 10^{-3}$		
EB-2	1.7	2.1×10^4	$9.85 - 6.7 \times 10^{-3}$		
EB-5	3.26	4.02×10^4	$21.6 - 10.25 \times 10^{-3}$		
EB-7	3.3	4.07×10^4	$11.8 - 9.45 \times 10^{-3}$		
EB-18	3.3	4.07×10^4	$1.97 - 0.55 \times 10^{-3}$		
EB-17	3.5	4.32×10^4	$22.8 - 2.36 \times 10^{-3}$		
EB-16	3.5	4.32×10^4	$6.7 - 5.9 \times 10^{-3}$		
EB-15	3.5	4.32×10^4	$8.26 - 7.1 \times 10^{-3}$		
EB-8	4.0	4.95×10^4	$18.1 - 16.9 \times 10^{-3}$		
EB-22	"	"	$29.9 - 17.7 \times 10^{-3}$		
EB-21	"	"	$38.2 - 31.1 \times 10^{-3}$		
EB-20	"	"	$\infty - \infty$		
EB-19	4.2	5.19×10^4	$27.2 - 22.4 \times 10^{-3}$		
EB-11	6.3	7.78×10^4	$19.4 - 2.48 \times 10^{-3}$		
EB-10	6.4	7.9×10^4	$73 \times 10^{-3} - \infty$*		
EB-15	6.5	8.03×10^4	$13.75 - 2.24 \times 10^{-3}$		
EB-1	"	"	$34.2 - 2.13 \times 10^{-3}$		
EB-2	"	"	$39.3 - 18.3 \times 10^{-3}$		

TABLE IX (Continued)

Specimen	Current Crest		Resistivity, ohm-cm Before-After Exposure	Tensile Strength, Lbs	Observation and/or Approximate Peak Temperature During Exposure
	Actual Current Applied, Amps	Current Applied Per Unit Cross Sectional Area, Amps/cm^2			
EB-16	8.0	9.88×10^4	$\infty - \infty$		
EB-17	"	"	26.15×10^{-3} - *		
EB-5	8.1	10×10^4	14.25×10^{-3} - *		
EB-4	8.2	10.11×10^4	21×10^{-3} - *		
* No reading, filament broken					

TABLE X

ACOUSTIC EMISSION DURING THREE POINT BENDING OF BORON EPOXY COMPOSITES PREVIOUSLY EXPOSED TO INTENSE ELECTRIC CURRENT FLOWS

Specimen No.	Electric Current Flow (amp/cm^2)	Three Point Bending Loading Sequence (lb)	Failure Load Three Point Bending (lb)	Total Acoustic Emission to Failure (10^5 counts)	Acoustic Emission Count Rate at Failure (10^5 counts/min)
BF-8	Unexposed	0-Failure	220	-	-
BF-9	Unexposed	0-Failure	222	2.13	4.5
BF-12	Unexposed	0-Failure	220	2.00	3.0
BF-13	Unexposed	0-150-0-Failure	205	2.75	5.2
BF-14	Unexposed	0-50-0-100-0-150-0-200-0-Failure	235	1.26	2.5
BF-15	5.7×10^4	0-Failure	220	2.54	>3.0
BF-20	5.7×10^4	0-Failure	217	1.70	>3.0
BF-18	5.7×10^4	0-150-0-Failure	218	2.36	4.4
BF-1	8×10^4	0-Failure	200	2.18	4.2
BF-2	8×10^4	0-Failure	160	2.41	3.8
BF-3	8×10^4	0-125-0-Failure	190	2.66	6.0
BF-10	10×10^4	0-Failure	91	1.59	2.8
BF-11	10×10^4	0-Failure	40	0.70	4.7
BF-6	10×10^4	0-30-0-Failure	45	0.55	4.2
BF-25	12×10^4	0-Failure	27	1.45	0.9
BF-30	12×10^4	0-Failure	29	1.57	0.5
BF-22	12×10^4	0-20-0-Failure	29	0.86	1.0

TABLE XI

CURRENT INJECTION TEST RESULTS FOR BORON/EPOXY COMPOSITES CONTAINING ALUMINUM SCREEN AS AN INTEGRAL PART OF THE COMPOSITE

Specimen	T_f	T_t	Filament Volume Content %	CURRENT CREST: Actual Current Applied, AMPS	CURRENT CREST: Current Applied Per Unit Cross Sectional Area Of Filament, AMP/CM^2	CURRENT CREST: Current Applied Per Cross Sectional Area Of Specimen, AMP/CM^2	Current Applied Per Filament, AMPS	Resistivity, OHM-CM Before-After Exposure	Tensile Strength / Tensile Modulus, PSI x 10^{-6}	Approx Peak Temperature During Exposure
BT-S-57 BT-S-59 BT-S-62			Control specimens with aluminum screen (one ply) on the surface of the laminate.						110.7 - 27.6 141.5 102.6 ____ 118.3 - 27.6	
BT-S-51	3	24	50	535	7.6×10^4	3.8×10^4	6.2	$1.48\text{-}1.54 \times 10^{-4}$		
BT-S-43	"	"	"	"	"	"	"	$1.70\text{-}1.38 \times 10^{-4}$		T<120°F
BT-S-53	"	"	"	"	"	"	"	$1.71\text{-}105.5 \times 10^{-4}$	108.7	
BT-S-42	"	"	"	"	"	"	"	$1.47\text{-}1.59 \times 10^{-4}$	103.8	T<120°F
BT-S-45	"	"	"	"	"	"	"	$1.64\text{-}98.5 \times 10^{-4}$	128.3	
BT-S-37	3	24	50	535	7.6×10^4	3.8×10^4	6.2	$7.05\text{-}64.4 \times 10^{-4}$	133.2 - 26.7 118.5 - 26.7	T<120°F
BT-S-50	3	24	50	740	10.5×10^4	5.25×10^4	8.5	$3.13\text{-}1.35 \times 10^{-4}$		T<120°F
BT-S-32	"	"	"	"	"	"	"	$15.1\text{-}103 \times 10^{-4}$		T<120°F
BT-S-52	"	"	"	"	"	"	"	$3.82\text{-}66.3 \times 10^{-4}$	138.1	T<120°F
BT-S-34	"	"	"	"	"	"	"	$3.58\text{-}4.39 \times 10^{-4}$	120.2 - 26.8	*
BT-S-54	"	"	"	760	10.8×10^4	5.4×10^4	8.8	$2.39\text{-}1.40 \times 10^{-4}$	133.0	T<120°F
BT-S-39	"	"	"	800	11.3×10^4	5.67×10^4	9.2	$5.52\text{-}100.5 \times 10^{-4}$	119.3 ____ 127.7 - 26.8	T<120°F
BT-S-41	3	24	50	1040	14.8×10^4	7.38×10^4	12.0	$3.34\text{-}106.7 \times 10^{-4}$		**
BT-S-40	"	"	"	"	"	"	"	$5.02\text{-}51.2 \times 10^{-4}$		*
BT-S-55	"	"	"	"	"	"	"	$2.64\text{-}115 \times 10^{-4}$	123.7	*
BT-S-47	"	"	"	1100	15.6×10^4	7.8×10^4	12.7	$9.15\text{-}87 \times 10^{-4}$	115.1	**
BT-S-44	"	"	"	"	"	"	"	$4.74\text{-}62.5 \times 10^{-4}$	139.7	**
BT-S-38	"	"	"	1140	16.2×10^4	8.1×10^4	13.1	$2.27\text{-}6.03 \times 10^{-4}$	110.9 - 25.1 122.4 - 25.1	**

* Flash at both ends of sample.
** Flash at one end or sample.

TABLE XI (Cont'd)

Specimen	T_f	T_t	Filament Volume Content %	CURRENT CREST: Actual Current Applied, AMPS	CURRENT CREST: Current Applied Per Unit Cross Sectional Area Of Filament, AMP/CM^2	CURRENT CREST: Current Applied Per Cross Sectional Area Of Specimen, AMP/CM^2	Current Applied Per Filament, AMPS	Resistivity, OHM-CM Before-After Exposure	Flexural Strength - Modulus PSI x 10^{-6}	Approx Peak Temperature During Exposure
BT-S-87 BT-S-90 BT-S-92			Control specimens with one ply of aluminum screen on the surface and one ply in the middle of the laminate.						109.7 - 23.7 115.7 - 23.3 125.5 ____ 117.0 - 23.5	
BT-S-83	3	24	50	535	7.6×10^4	3.8×10^4	6.2	$0.802-0.818 \times 10^{-4}$		T<120°F
BT-S-68	"	"	"	"	"	"	"	$0.882-0.786 \times 10^{-4}$		T<120°F
BT-S-69	"	"	"	"	"	"	"	$0.859-0.739 \times 10^{-4}$	129.4	
BT-S-72	"	"	"	"	"	"	"	$0.865-0.707 \times 10^{-4}$	117.2 24.0	
BT-S-81	"	"	"	"	"	"	"	$0.937-0.785 \times 10^{-4}$	112.4	
BT-S-73	"	"	"	"	"	"	"	$0.882-0.739 \times 10^{-4}$	102.5 ____ 115.4 - 24.0	
BT-S-71	3	24	50	740	10.50×10^4	5.25×10^4	8.5	$0.81-0.762 \times 10^{-4}$		T<120°F
BT-S-78	"	"	"	"	"	"	"	$0.802-0.762 \times 10^{-4}$		
BT-S-77	"	"	"	"	"	"	"	$0.858-0.746 \times 10^{-4}$	112.2	
BT-S-76	"	"	"	"	"	"	"	$0.817-0.77 \times 10^{-4}$	128.3	
BT-S-75	"	"	"	"	"	"	"	$0.825-0.786 \times 10^{-4}$	113.9 - 24.4	
BT-S-67	"	"	"	"	"	"	"	$0.93-0.73 \times 10^{-4}$	100.0 ____ 113.6 - 24.4	
BT-S-64	3	24	50	1100	15.6×10^4	7.8×10^4	12.7	$0.746-0.73 \times 10^{-4}$		
BT-S-74	"	"	"	"	"	"	"	$0.764-0.70 \times 10^{-4}$		
BT-S-63	"	"	"	"	"	"	"	$0.81-0.739 \times 10^{-4}$	83.9	
BT-S-86	"	"	"	"	"	"	"	$0.755-0.691 \times 10^{-4}$	105.8	
BT-S-85	"	"	"	"	"	"	"	$0.913-0.913 \times 10^{-4}$	126.0	
BT-S-80	3	24	"	"	"	"	"	$0.913-0.73 \times 10^{-4}$	102.8 - 21.5 104.6 - 21.5	

TABLE XI (Cont'd)

Specimen	T_f	T_t	Filament Volume Content %	CURRENT CREST: Actual Current Applied, AMPS	CURRENT CREST: Current Applied Per Unit Cross Sectional Area Of Filament, AMP/CM^2	CURRENT CREST: Current Applied Per Cross Sectional Area Of Specimen, AMP/CM^2	Current Applied Per Filament, AMPS	Resistivity, OHM-CM Before-After Exposure	Tensile Strength PSI-Modulus PSI x 10^{-6}	Approx Peak Temperature During Exposure
BT-S-26 BT-S-29 BT-S-31			Control specimens with aluminum screen (one ply) in the middle of the laminate.						112.2 - 23.8 145.3 - 29.4 131.9 - 26.4 133.1 - 26.5	
BT-S-17	3	24	50	480	6.8×10^4	3.4×10^4	5.5	$1.37\text{-}1.33 \times 10^{-4}$		
BT-S-16	"	"	"	490	6.9×10^4		5.6	$1.24\text{-}1.22 \times 10^{-4}$		
BT-S-2	"	"	"	535	7.6×10^4	3.8×10^4	6.2	$1.24\text{-}1.28 \times 10^{-4}$	129.0 - 29.2	
BT-S-6	"	"	"	560	7.9×10^4	3.97×10^4	6.4	$1.18\text{-}1.19 \times 10^{-4}$	112.6	
BT-S-11	"	"	"	"	"	"	"	$1.37\text{-}1.22 \times 10^{-4}$	127.1	
BT-S-21	"	"	"	590	8.4×10^4	4.18×10^4	6.8	$1.24\text{-}1.22 \times 10^{-4}$	121.9 122.7 - 29.2	T<120°F
BT-S-18	3	24	50	720	10.2×10^4	5.1×10^4	8.3	$1.38\text{-}1.3 \times 10^{-4}$		T<120°F
BT-S-5	"	"	"	735	10.42×10^4	5.2×10^4	8.5	$1.30\text{-}1.23 \times 10^{-4}$		T<120°F
BT-S-10	"	"	"	"	"	"	"	$1.88\text{-}1.26 \times 10^{-4}$	93.7	T<120°F
BT-S-9	"	"	"	"	"	"	"	$1.51\text{-}1.24 \times 10^{-4}$	125.7 - 25.6	
BT-S-19	"	"	"	"	"	"	"	$1.45\text{-}1.26 \times 10^{-4}$	146.2	
BT-S-24	"	"	"	"	"	"	"	$1.41\text{-}1.30 \times 10^{-4}$	129.5 123.8 - 25.6	
BT-S-13	3	24	50	1140	16.2×10^4	8.1×10^4	13.1	$1.38\text{-}1.22 \times 10^{-4}$		
BT-S-20	"	"	"	"	"	"	"	$1.49\text{-}1.21 \times 10^{-4}$		
BT-S-7	"	"	"	"	"	"	"	$1.61\text{-}1.17 \times 10^{-4}$	147.1	
BT-S-12	"	"	"	"	"	"	"	$1.50\text{-}1.49 \times 10^{-4}$	135.5	
BT-S-4	"	"	"	"	"	"	"	$1.45\text{-}1.23 \times 10^{-4}$	114.3 - 27.0	
BT-S-15	"	"	"	1160	16.46×10^4	8.23×10^4	13.3	$1.57\text{-}1.41 \times 10^{-4}$	142.4 134.8 - 27.0	T<120°F

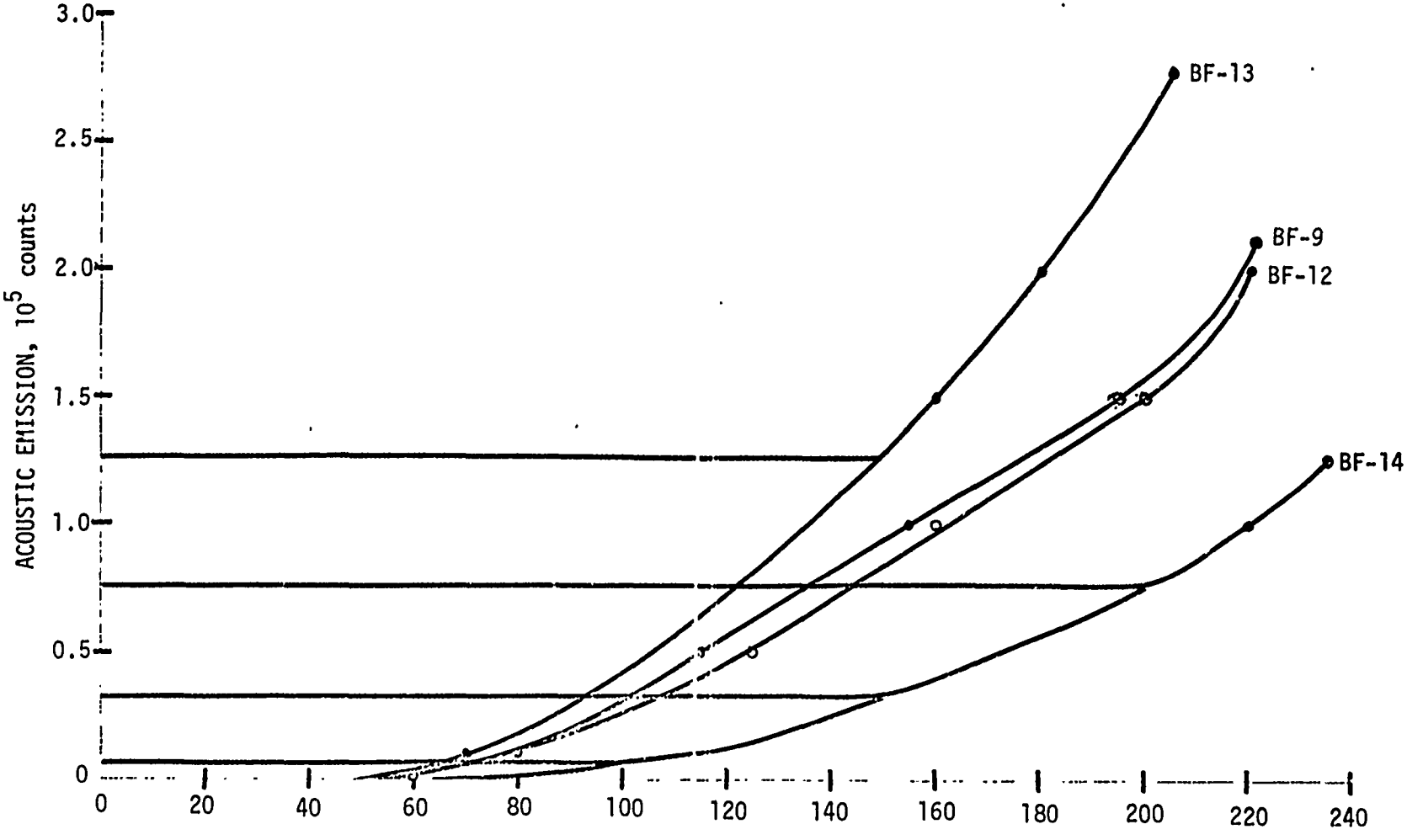

Figure 1. Acoustic Emission of Unexposed Boron Epoxy Composites.

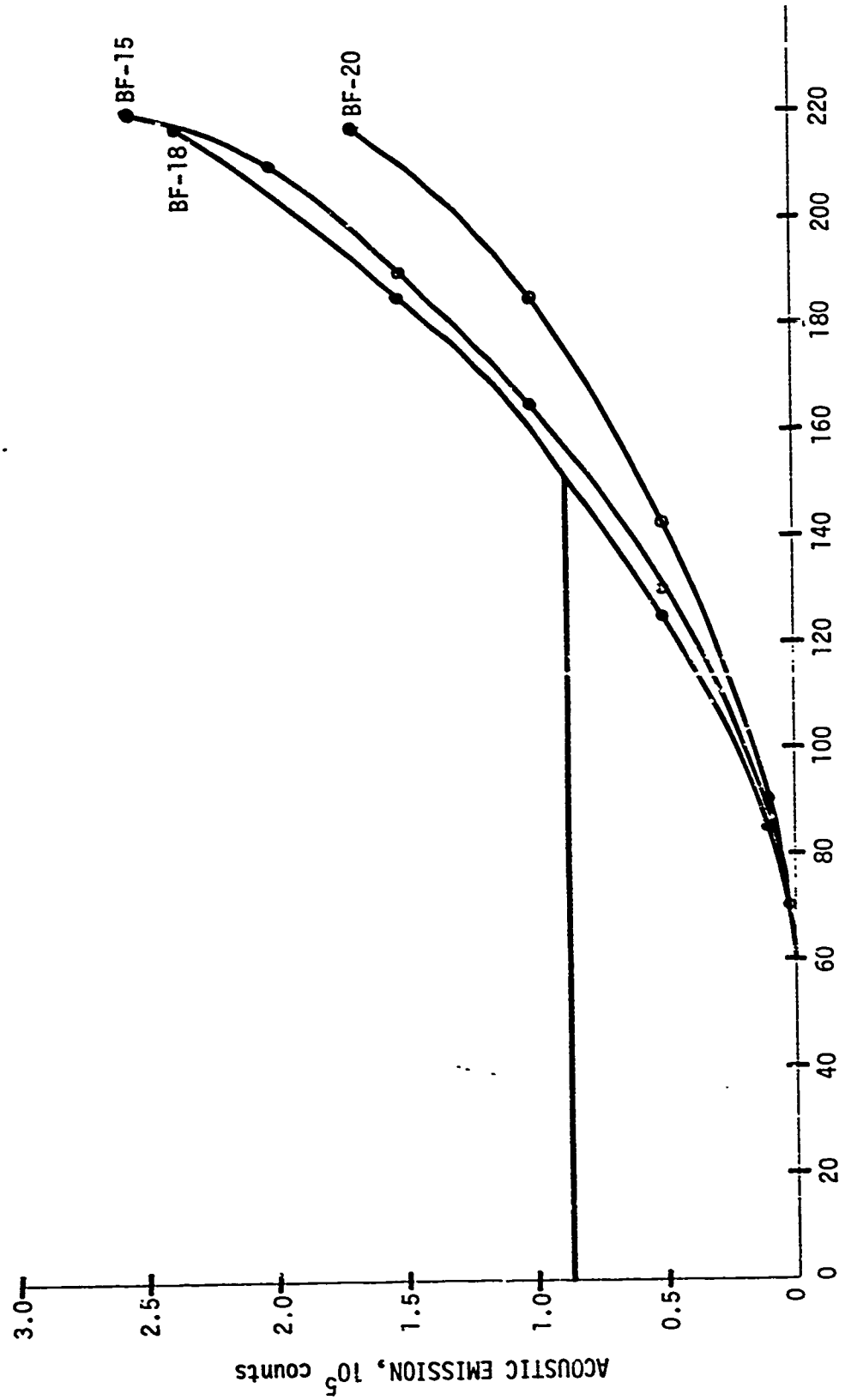

Figure 2. Acoustic Emission of Boron Epoxy Composites Exposed to 5.7×10^4 amp/cm^2 Electric Current Flow.

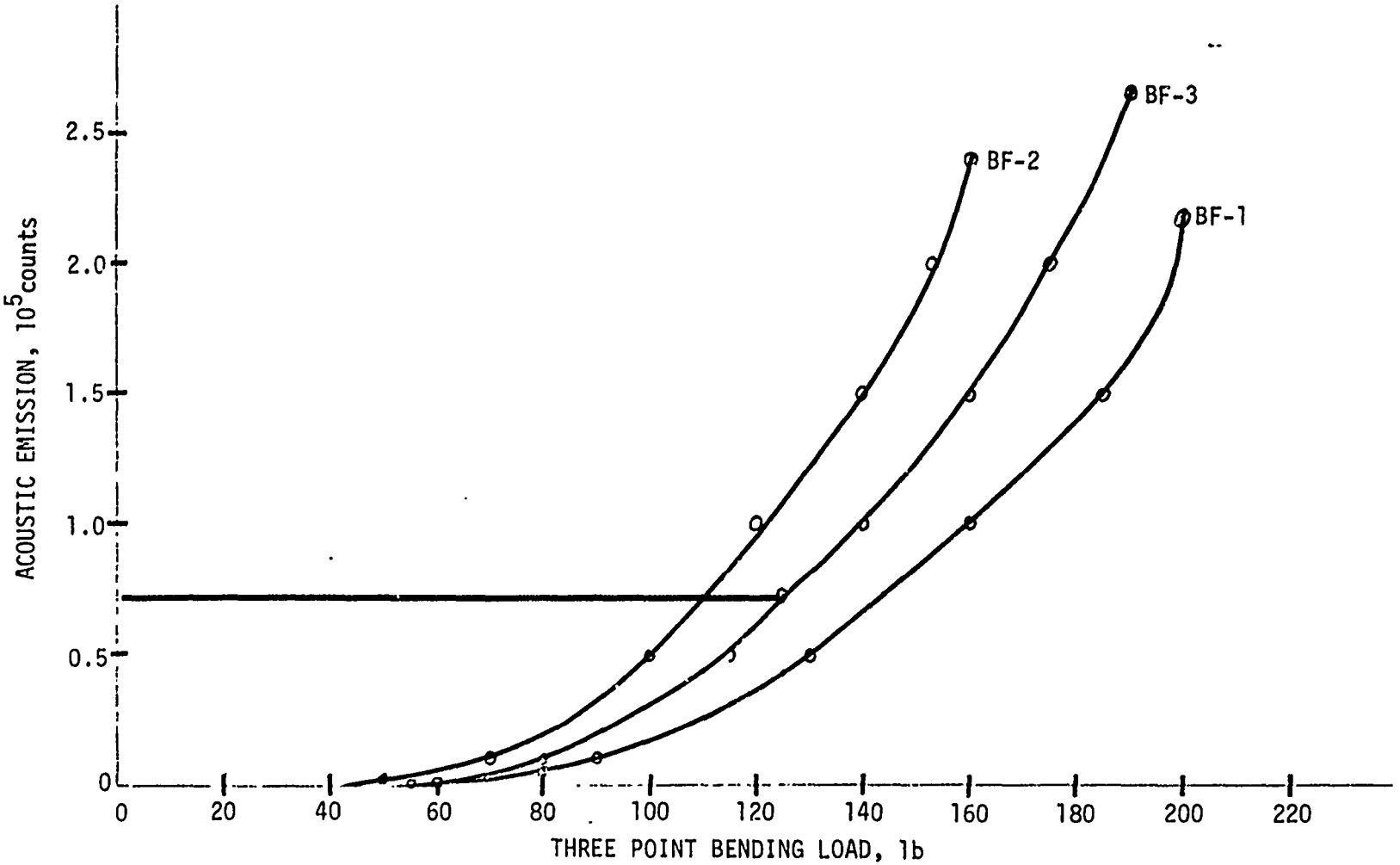

Figure 3. Acoustic Emission of Boron Epoxy Composites Exposed to 8×10^4 amp/cm^2 Electric Current Flow.

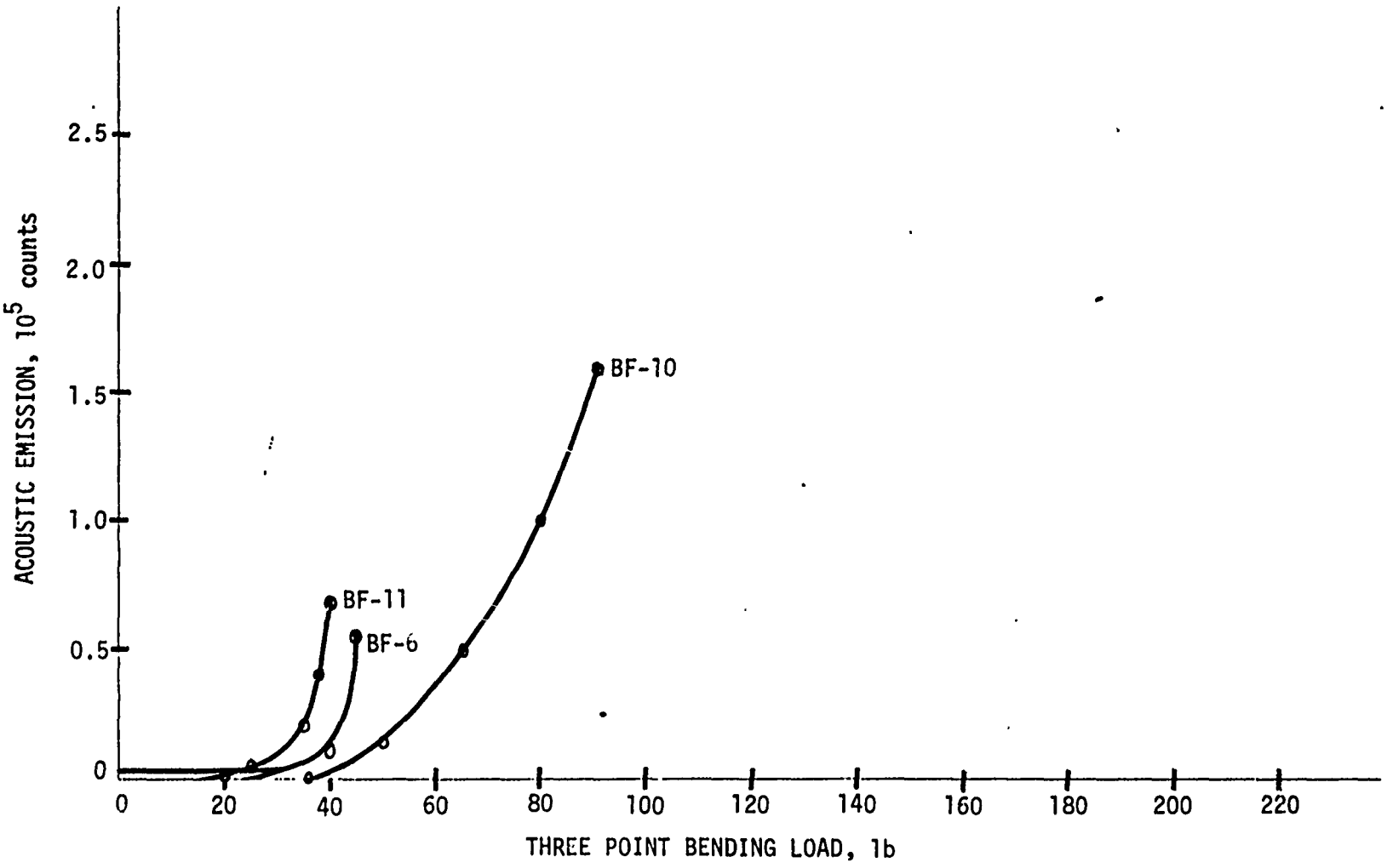

Figure 4. Acoustic Emission of Boron Epoxy Composites Exposed to 10×10^4 amp/cm^2 Electric Current Flow.

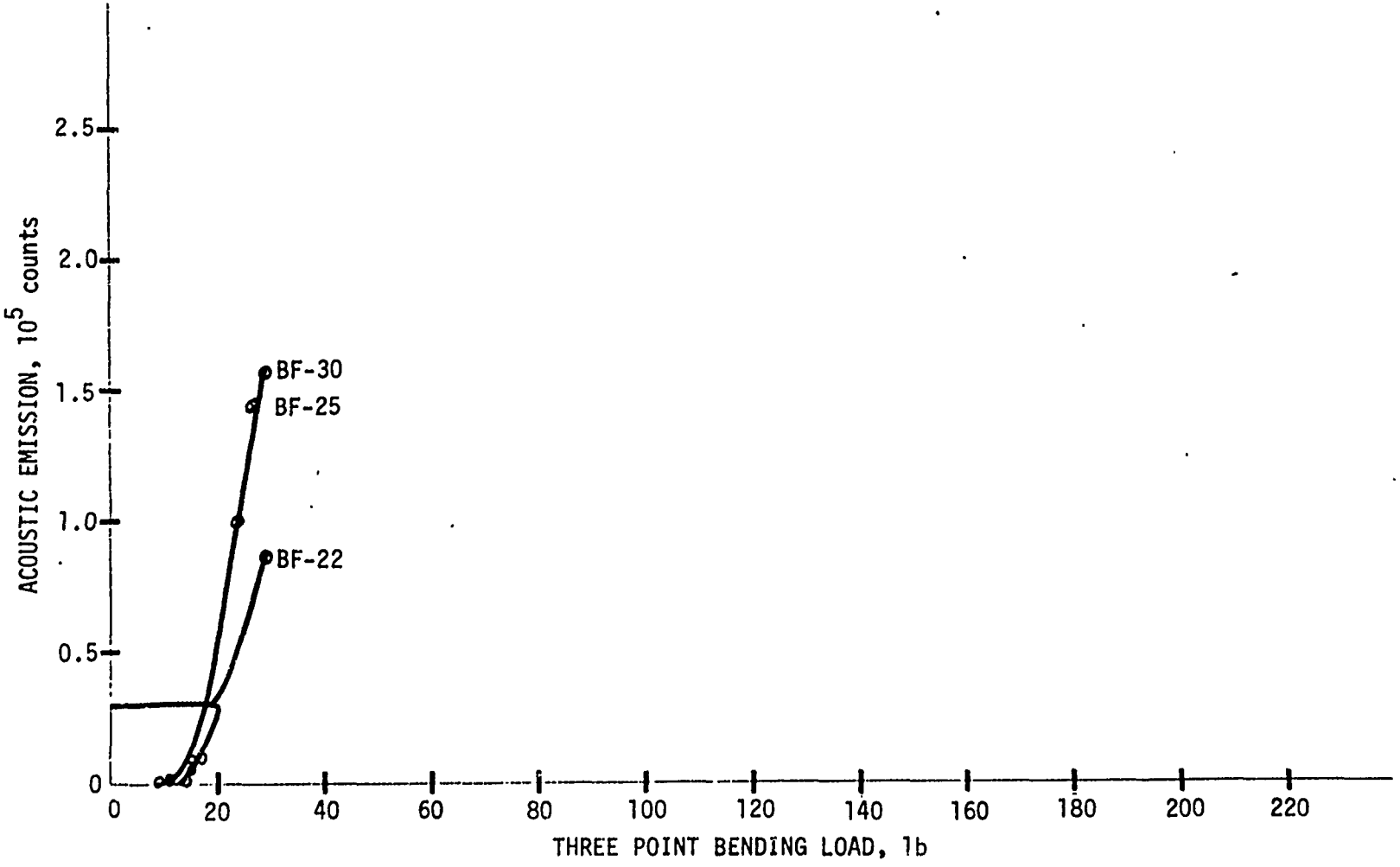

Figure 5. Acoustic Emission of Boron Epoxy Composites Exposed to 12×10^4 amp/cm^2 Electric Current Flow.